

2  
IITRI

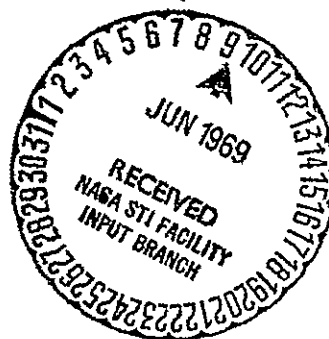
REPORT NO. X6910-F  
FINAL SCIENTIFIC REPORT

EMC STUDY OF SPACE APPLICATIONS  
REMOTE SENSORS

PREPARED BY  
RICHARD J. OTERO & WILLIAM C. WANBAUGH

UNDER  
CONTRACT NASw 17-29

FOR  
SPACE APPLICATIONS PROGRAM DIRECTORATE  
NATIONAL AERONAUTICS & SPACE ADMINISTRATION



IIT RESEARCH INSTITUTE  
SYSTEM SCIENCES RESEARCH DIVISION  
2024 WEST STREET  
ANNAPOLIS, MARYLAND 21401

MARCH 1969

Reproduced by the  
CLEARINGHOUSE  
for Federal Scientific & Technical  
Information Springfield, Vt. 01105

N69-38674  
(ACCESSION NUMBER)  
130  
(PAGES)  
PR-106088  
(NASA OR TMX OR AD NUMBER)  
(THRU)  
(CODE)  
07  
(CATEGORY)

FACILITY FORM 602

Distribution of this report is provided in the interest of information exchange and should not be construed as endorsement by NASA of the material presented. Responsibility for the contents resides with the organization that prepared it.

Report No. IITRI-X6910-F  
(Final Report)

EMC STUDY OF SPACE APPLICATIONS REMOTE SENSORS

April 1968 Through March 1969

CONTRACT NO. NASw 17-29  
IITRI Project No. X6910

Prepared by

RICHARD J. OTERO and WILLIAM C. WANBAUGH

of

IIT Research Institute  
Systems Sciences Research Division  
2024 West Street  
Annapolis, Maryland 21401

for

Space Applications Programs Directorate  
NASA Headquarters  
Washington, D.C.

IIT RESEARCH INSTITUTE

## FOREWORD

This final report, "EMC Study of Space Applications Remote Sensors" covers the research program conducted under Contract No. NASw 17-29 for the Office of the Operational Systems Support Program, NASA Headquarters, Washington, D.C. The objective of the program was to perform a study of the Electromagnetic Compatibility of Space Applications Remote Sensors.

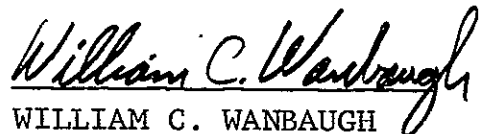
The cooperation, courtesy and technical assistance provided by the Contract Technical Monitor, Mr. John J. Kelleher, Operational Systems Support Program Manager, and other staff members of the Space Applications Programs Directorate were highly instrumental in the successful completion of the project. IITRI is also appreciative of the helpful information provided by personnel of the NASA's Electronics Research Center, Goddard Space Flight Center, and the Office of Data Tracking and Acquisition, NASA Headquarters.

Other personnel who contributed to this report include Norbert M. Katz, Joseph E. Orth, Frank C. Pethel, Jr., and Samuel S. Verner.

Respectfully Submitted  
IIT Research Institute

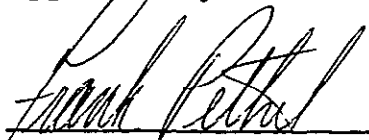


RICHARD J. OTERO



WILLIAM C. WANBAUGH

Approved by:



FRANK C. PETHEL  
Assistant Director of Research

IIT RESEARCH INSTITUTE

## TABLE OF CONTENTS

<u>SECTION</u>	<u>PAGE</u>
FOREWORD . . . . .	i
LIST OF FIGURES . . . . .	iv
LIST OF TABLES . . . . .	vii
1.0 SUMMARY . . . . .	1-1
1.1 Specific Recommendations by Experiment . . . . .	1-1
1.2 General Recommendations . . . . .	1-5
2.0 INTRODUCTION . . . . .	2-1
3.0 THE ANALYSIS APPROACH . . . . .	3.1-1
3.1 The Interference Analysis Procedure . . . . .	3.1-1
3.2 Sources of Satellite Experiment Data . . . . .	3.2-1
3.3 Environmental Data Sources . . . . .	3.3-1
3.4 Sensor Interference Threshold Evaluation Procedure . . . . .	3.4-1
3.5 Satellite Orbit Considerations . . . . .	3.5-1
4.0 THE INTERFERENCE ANALYSIS . . . . .	4.1-1
4.1 Microwave Spectrometer . . . . .	4.1-1
4.1.1 Purpose and Scientific Basis . . . . .	4.1-1
4.1.2 Environmental Signal Level Summary . . . . .	4.1-7
4.1.3 Interference Evaluation and Analysis . . . . .	4.1-7
4.2 Microwave Occultation Experiment . . . . .	4.2-1
4.2.1 Purpose and Scientific Basis . . . . .	4.2-1
4.2.2 Environmental Signal Level Summary . . . . .	4.2-2
4.2.3 Interference Evaluation and Analysis . . . . .	4.2-5
4.3 Electrically Scanning Microwave Radiometer for Mapping Earth Radiation and Cloud Structure . . . . .	4.3-1
4.3.1 Purpose and Scientific Basis . . . . .	4.3-1
4.3.2 Environmental Signal Level Summary . . . . .	4.3-2
4.3.3 Interference Evaluation and Analysis . . . . .	4.3-2

IIT RESEARCH INSTITUTE

## TABLE OF CONTENTS (Continued)

<u>SECTION</u>	<u>PAGE</u>
4.4 Satellite Microwave Radiometry to Sense the Surface Temperature of the World Oceans . . . . .	4.4-1
4.4.1 Purpose and Scientific Basis. . .	4.4-1
4.4.2 Environmental Signal Level Summary . . . . .	4.4-5
4.4.3 Interference Evaluation and Analysis. . . . .	4.4-5
4.5 Global Radar for Ocean Waves and Winds .	4.5-1
4.5.1 Purpose and Scientific Basis. . .	4.5-1
4.5.2 Environmental Signal Level Summary . . . . .	4.5-4
4.5.3 Interference Evaluation and Analysis. . . . .	4.5-4
4.6 Simplified Data Collection Experiment. .	4.6-1
4.6.1 Purpose and Scientific Basis. . .	4.6-1
4.6.2 Environmental Signal Level Summary . . . . .	4.6-1
4.6.3 Interference Evaluation and Analysis. . . . .	4.6-5
4.7 Nimbus-E Data Relay Link Through ATS-F. . . . .	4.7-1
4.7.1 Purpose and Scientific Basis. . .	4.7-1
4.7.2 Environmental Signal Level Summary . . . . .	4.7-9
4.7.3 Interference Evaluation and Analysis. . . . .	4.7-9
4.8 Wide-Band Real-Time Data Transmission. .	4.8-1
4.8.1 Purpose and Scientific Basis. . .	4.8-1
4.8.2 Environmental Signal Level Summary . . . . .	4.8-5
4.8.3 Interference Evaluation and Analysis. . . . .	4.8-5

## LIST OF FIGURES

<u>FIGURE</u>		<u>PAGE</u>
3.1-1	THE INTERFERENCE ANALYSIS PROCEDURE	3.1-3
3.4-1	RECEIVER SELECTIVITY FUNCTION MODELS	3.4-6
3.4-2	TRANSMITTER EMISSION SPECTRA MODEL	3.4-7
3.5-1	GEOMETRY OF SATELLITE ORBIT CONSIDERATIONS IN INTERFERENCE ANALYSIS	3.5-2
3.5-2	ORTHOGRAPHIC MERIDIONAL PROJECTION TECHNIQUE USED TO PRODUCE INTERFERENCE REGION PLOTS	3.5-4
3.5-3	SAMPLE PLOT OF INTERFERENCE REGION	3.5-5
3.5-4	SCATTER PATH GEOMETRY	3.5-8
3.5-5	THE FUNCTION $F(d\theta)$ FOR $N_s = 250$	3.5-9
4.1-1	WEIGHTING FUNCTIONS	4.1-3
4.1-2	MICROWAVE SPECTROMETER BLOCK DIAGRAM	4.1-5
4.1-3	TYPICAL RADIOMETER CHANNEL BLOCK DIAGRAM	4.1-6
4.1-4	FREQUENCY OVERLAP OF EXPERIMENT 7, 22.2 GHz RADIOMETER AND INDUSTRIAL-MEDICAL ALLOCATION	4.1-11
4.2-1	MICROWAVE OCCULTATION EXPERIMENT BLOCK DIAGRAM	4.2-4
4.2-2	EXPERIMENT NO. 10 PRE-CULL SPECTRUM OCCUPANCY AND EFFECTIVE RADIATED POWER SUMMARY	4.2-6
4.2-3	RECOMMENDED FREQUENCIES FOR THE OPERATION OF THE MICROWAVE OCCULTATION EXPERIMENT	4.2-10
4.3-1	BLOCK DIAGRAM OF ELECTRICALLY SCANNING RADIOMETER	4.3-3
4.4-1	BLOCK DIAGRAM OF SEA SURFACE TEMPERATURE RADIOMETER	4.4-3
4.4-2	EXPERIMENT NO. 13 PRE-CULL SPECTRUM OCCUPANCY AND EFFECTIVE RADIATED POWER SUMMARY	4.4-7

IIT RESEARCH INSTITUTE

LIST OF FIGURES (Continued)

<u>FIGURE</u>		<u>PAGE</u>
4.4-3	PLOT OF INTERFERENCE REGION FOR SATELLITE MICROWAVE RADIOMETRY TO SENSE THE SURFACE TEMPERATURE OF THE WORLD OCEANS (MICRAD) EXPERIMENT	4.4-8
4.5-1	GROW SYSTEM BLOCK DIAGRAM	4.5-3
4.5-2	EXPERIMENT NO. 14 PRE-CULL SPECTRUM OCCUPANCY AND EFFECTIVE RADIATED POWER SUMMARY	4.5-5
4.5-3	RADAR SEA RETURN VERSUS DISTANCE CALIBRATED AGAINST WIND SPEED IN KNOTS FOR FULLY DEVELOPED SEAS	4.5-8
4.5-4	STATISTICS OF PULSE TRAIN ENSEMBLE	4.5-9
4.5-5	PLOT OF POTENTIAL INTERFERENCE REGION FOR THE GROW EXPERIMENT	4.5-13
4.5-6	PLOT OF INTERFERENCE REGION WHERE A 5dB DEGRADATION IN RADAR CROSS-SECTION MEASUREMENT IS PREDICTED	4.5-16
4.6-1	SPACECRAFT DATA COLLECTION BLOCK DIAGRAM	4.6-2
4.6-2	EXPERIMENT NO. 26 PRE-CULL SPECTRUM OCCUPANCY AND EFFECTIVE RADIATED POWER SUMMARY	4.6-4
4.6-3	PLOT OF INTERFERENCE REGION FOR SIMPLIFIED DATA COLLECTION (DACOL) EXPERIMENT	4.6-7
4.7-1	NIMBUS DATA RELAY LINK THROUGH ATS	4.7-2
4.7-2	RELAY SATELLITE SYSTEM BLOCK DIAGRAM	4.7-3
4.7-3	SIGNAL SPECTRUM FOR NIMBUS-ATS LINK	4.7-4
4.7-4	EXPERIMENT NO. 28-1 and 28-3 PRE-CULL SPECTRUM OCCUPANCY AND EFFECTIVE RADIATED POWER SUMMARY	4.7-10
4.7-5	EXPERIMENT NO. 28-2 PRE-CULL SPECTRUM OCCUPANCY AND EFFECTIVE RADIATED POWER SUMMARY	4.7-11



LIST OF FIGURES (Continued)

<u>FIGURE</u>		<u>PAGE</u>
4.7-6	EXPERIMENT NO. 28-4 and 28-5 PRE-CULL SPECTRUM OCCUPANCY AND EFFECTIVE RADIATED POWER SUMMARY	4.7-12
4.7-7	EXPERIMENT 28-1 PLOT OF INTERFERENCE REGION FOR NIMBUS-E DATA RELAY LINK THROUGH ATS-F (DARELI)	4.7-13
4.7-8	EXPERIMENT 28-2 PLOT OF INTERFERENCE REGION FOR NIMBUS-E DATA RELAY LINK THROUGH ATS-F (DARELI)	4.7-15
4.8-1	SELF-FOCUSSING NIMBUS ANTENNA AND LOCAL GROUND STATION	4.8-3
4.8-2	EXPERIMENT NO. 26 PRE-CULL SPECTRUM OCCUPANCY AND EFFECTIVE RADIATED POWER SUMMARY	4.8-6

## LIST OF TABLES

<u>TABLE</u>		<u>PAGE</u>
1-1	SUMMARY OF EMC EVALUATION	1-7
3.2-1	SOURCES OF SATELLITE EXPERIMENT DATA USED FOR THE EMC EVALUATION	3.2-2
3.4-1	RECEIVER NOISE SENSITIVITIES	3.4-3
3.4-2	APPLICATION OF OFF-FREQUENCY REJECTION FUNCTION	3.4-4
4.1-1	EXPERIMENT 7, MICROWAVE SPECTROMETER SYSTEM CHARACTERISTICS	4.1-2
4.1-2	FREQUENCY ALLOCATIONS	4.1-8
4.2-1	EXPERIMENT 10, MICROWAVE OCCULTATION EXPERIMENT SYSTEM PARAMETERS	4.2-3
4.2-2	ENVIRONMENTAL SIGNAL LEVEL SUMMARY FOR MICROWAVE OCCULTATION EXPERIMENT	4.2-7
4.3-1	EXPERIMENT 12, ELECTRICALLY SCANNING MICROWAVE RADIOMETER FOR MAPPING EARTH RADIATION AND CLOUD STRUCTURE SYSTEM CHARACTERISTICS	4.3-4
4.4-1	EXPERIMENT 13, SATELLITE MICROWAVE RADIOMETRY TO SENSE THE SURFACE TEMP- ERATURE OF THE WORLD OCEANS CHARACTER- ISTICS	4.4-4
4.5-1	EXPERIMENT 14, GLOBAL RADAR FOR OCEAN WAVES AND WINDS SYSTEM PARAMETERS	4.5-2
4.5-2	ENVIRONMENTAL SIGNAL LEVEL SUMMARY FOR GROW EXPERIMENT	4.5-6
4.5-3	PULSE COUNT STATISTICS FOR VARIOUS ENVIRONMENTAL SIZES	4.5-12
4.5-4	ENVIRONMENTAL SIZE VERSUS RADAR CROSS- SECTION DEGRADATION	4.5-15
4.6-1	EXPERIMENT 26, SIMPLIFIED DATA COL- LECTION EXPERIMENT CHARACTERISTICS	4.6-3

LIST OF TABLES (Continued)

<u>TABLE</u>		<u>PAGE</u>
4.6-2	ENVIRONMENTAL SIGNAL LEVEL SUMMARY FOR DACOL EXPERIMENT	4.6-6
4.7-1	EXPERIMENT 28-1, DARELI, ATS TO NIMBUS LINK AT 1.8 GHz	4.7-5
4.7-2	EXPERIMENT 28-2, DARELI, ATS TO NIMBUS LINK AT 149 MHz	4.7-6
4.7-3	EXPERIMENT 28-3, DARELI, ATS TO EARTH AT 1.8 GHz	4.7-7
4.7-4	EXPERIMENT 28-4 and 28-5, DARELI, NIMBUS TO ATS AT 2253 MHz	4.7-8
4.8-1	EXPERIMENT 29, WIDE-BAND REAL-TIME DATA TRANSMISSION CHARACTERISTICS	4.8-4

## 1.0 SUMMARY

### 1.1 Specific Recommendations by Experiment

This section presents the findings and recommendations of a program to determine the electromagnetic compatibility of a number of experiments being considered by NASA in their Space Applications Program. The conclusions reported are based on the data, relating both to the electronic characteristics of the experiments studied, and the data base of environmental equipments available, as well as those assumptions necessitated by the inadequacy and unavailability of needed information. The analysis results are admittedly conservative, that is, when assumptions had to be made, they were weighted in the direction of predicting interference. In general, this study has demonstrated the feasibility of band-sharing between terrestrial systems and the satellite systems considered.

The following conclusions and recommendations are made regarding the experiments studied.

#### Experiment 7, Microwave Spectrometer (MICSPEC)

Findings: It is planned that this five channel radiometer will be designed to operate at 22.2, 31.46, 53.65, 60.82 and 64.47 GHz

The 22.1 to 22.3 GHz region is interference free at the present time, but Industrial, Scientific and Medical equipment could be type approved for use at 22.125 GHz  $\pm$ 125 MHz or reallocations could take place in the future (1971) to accommodate communication-satellite service between 17.7 and 23 GHz.

The 31.3 to 31.5 GHz radio astronomy band is used for fixed and mobile services by eight countries including the U.S.S.R. and the extent of potential interference is unknown.

The 53.65, 60.82 and 64.47 GHz frequencies are associated with near zero probability of encountering interference.

Recommendations: The three highest frequencies planned for use in this five channel radiometer are free of detrimental interference. The other two frequencies of 22.2 GHz and 31.46 GHz are most likely interference free at the present time even though some doubt is associated with 31.46 GHz due to unknown use by other countries. It is recommended that all five of the selected frequencies be used for Experiment 7.

IIT RESEARCH INSTITUTE

## Experiment 10, Microwave Occultation Experiment (MICOC)

Findings: The Microwave Occultation Experiment planned for operation in the 4.4-4.8 GHz band will experience interference at selected frequencies within the band. Interference within the band is capable of causing (1) false signal acquisition by the phase-lock loop receiver being used in the experiment, (2) loss of phase-lock of desired signal, and (3) excessive mean-square phase error. The interference threshold for each of these interference mechanisms is such that that level capable of causing an excessive mean-square error is less than that of either of the other two mechanisms. Thus, this mechanism was selected to evaluate the interference potential in this band. Since the experiment determines the distance between the Nimbus and sub-satellite by measuring the phase of a transmitted and received signal, and a requirement exists to measure this phase to 4° accuracy, environmental systems capable of producing interference levels that result in phase errors of this magnitude were culled. Due to the narrow sweep widths of the occultation phase-lock loop receiver and the wide dispersion of the 15 potential interference sources within the 4.4-4.8 GHz band, it was found that the experiment would be interfered with in almost all cases by only a single interference source. This interference was also found to occur only when the frequency of the interference source fell within the phase-lock loop sweep width, assumed to be in the order of 200 KHz.

Recommendations: It is recommended that the Microwave Occultation Experiment be operated in one of the 32 sub-bands identified in Section 4.2 of this report.

## Experiment 12, Electrically Scanning Microwave Radiometer for Mapping Earth Radiation and Cloud Structure (ESMR)

Findings: This single channel radiometer is planned for use at 19.35 GHz in the 19.3 to 19.4 GHz radio astronomy band. FCC Docket 18294 of August 1968 indicates the possible re-allocation of 17.7 to 23.0 GHz for use by down-links of the communication-satellite service in the 1970's.

Recommendations: The frequency selected is in an interference free radio astronomy band and is recommended for use. Review of the status of this band should be made after the World Administrative Radio Conference in 1970.

### Experiment 13, Satellite Microwave Radiometry to Sense the Surface Temperature of the World Oceans (MICRAD)

Findings: This microwave radiometer with a bandwidth of 140 MHz is planned for use at 2.69 to 2.83 GHz. The 669 emitters which can cause above noise threshold interference are all at 2.7 GHz and above, consisting primarily of weather and height finder radars. These emitters can produce signals above threshold level for a maximum of 45 minutes for a given Nimbus orbit or for a total of 33.6% of any 24 hour period, and for degradation 22 minutes and 9%.

Recommendations: The selected band for Experiment 13 should be moved down from 2.69-2.83 GHz, to 2.56-2.70 GHz to operate in an environment with a very low probability of interference.

### Experiment 14, Global Radar for Ocean Waves and Winds (GROW)

Findings: The Global Radar for Ocean Waves and Winds Experiment receiver will be interfered with if operated at the selected 3 GHz frequency. Interference will result from terrestrial radar systems operating in the western U.S. The interference from these radar systems will cause a biasing error in the GROW scatterometer radar cross-section measurements and hence an error in the wind speed predictions. A tolerable wind speed prediction error of approximately 5 knots was selected. An error of this magnitude will occur whenever the satellite flies over the western 7/8 of the U.S. and the eastern Pacific Ocean. Errors of this magnitude will persist for approximately 20 minutes during a single orbital pass. The maximum percent time over a 24 hour period that this wind speed error will persist is approximately 7 percent.

Recommendations: If it is determined that a 5 knot wind speed error is not acceptable for those time durations and geographical areas indicated, then it will be necessary to change the operating frequency of the GROW receiver. If some latitude in receiver tuning is available, it is recommended that the GROW system be operated at 3001 MHz. This frequency separation of 1 MHz from the interfering systems operating at 3 GHz, will result in a reduction of interference power sufficient to reduce the maximum wind speed error due to interference to less than 1 knot.

### Experiment 26, Simplified Data Collection Experiment (DACOL)

Findings: The 460 MHz receiver carried on Nimbus is designed for gathering data from a number of sensors located on

IIIT RESEARCH INSTITUTE

various rivers and streams. The analysis applied to the initial environment of 695 emitters, culled 30 emitters which could create levels above the receiver noise threshold. Based only on this criterion the receiver would be exposed a maximum of 32 minutes for one orbit or 26% of a 24 hour period. Using a desired signal to interference ratio of 3dB as an acceptable degradation criterion, only 12 emitters remained in the land mobile band environment. At this level the maximum time exposure for one orbit would be 11.6 minutes and for a 24 hour period the maximum exposure would occur for 2.85% of the time. However, it has been determined that the FSK modulation being used can provide a 1% bit error when operating at an S/I of -6dB for an interfering FM signal or an S/I of -12dB for an interfering AM signal. These levels provide a safety margin for the last 12 sources so that the received data will not be degraded beyond a 1% bit error.

Recommendations: It is recommended that 460 GHz be used for experiment 26 if FSK modulation is used, otherwise the potential degradation of data transmitted by a different modulation scheme should be reanalyzed against the environment.

#### Experiment 28, Nimbus Data Relay Link Through ATS (DARELI)

Findings: Experiment 28-1.

ATS to Nimbus link at 1.8 GHz. A total of 209 emitters were analyzed and only one transmitter in Colorado could produce a level above the noise threshold of the receiver. With a 100 KW output at 1800.00 MHz this transmitter can produce an interference level 2dB above the desired signal at the Nimbus receiver. The Colorado transmitter will produce a threshold signal or higher for a maximum of 19.8 minutes for one orbit and for a maximum percentage of time for a 24 hour period of 7.1%. Above the degradation threshold the results are 8 minutes and 1%.

#### Experiment 28-2

ATS to Nimbus link at 149 MHz. A total of 1484 emitters were identified and analyzed with the result that 7 were found to produce above noise threshold levels. The maximum time for exposure to these levels for one orbit of Nimbus is 47.5 minutes and the maximum percentage of time for a 24 hour period is 26.5%. However, 5 of the 7 emitters produce levels of 7dB or more below the desired signal level and the remaining 2 emitters produce levels equal to the desired signal. These emitters are located in Thailand and Mexico. The maximum time for a 1 orbit

IIIT RESEARCH INSTITUTE

exposure to interference above the degradation criterion of  $S/I = 7\text{dB}$  is 20 minutes and 8.0% of the time in a 24 hour period.

#### Experiment 28-3.

ATS to Earth at 1.8 GHz. The 209 emitter environment was analyzed for the earth to earth situation and only 37 could cause a noise threshold level signal at a distance of 6 miles or less. Beyond 6 miles only the 100 KW Colorado station could cause this level and then only out to a distance of 52 miles.

#### Experiment 28-4 and 28-5.

Nimbus to ATS at 2253 MHz. The total environment of 133 emitters were eliminated by analysis as potential sources of interference to this critical link of the data relay experiment.

Recommendations: It is recommended that the chosen frequencies be used for the various links of the data relay experiment for a minimum of degradation.

#### Experiment 29, Wide-Band Real-Time Data Transmission (DATRAN)

Findings: The 2.2 GHz receiver on Nimbus is used to receive a beacon signal from earth to allow a phased array antenna to be properly oriented towards a data station. A total of 953 emitters were located in the vicinity of 2.2 GHz to form the environment which was analysed against the Nimbus 2.2 GHz receiver. A total of 67 were left after the power cull and on-tune rejection function application and this quantity was reduced to 0 by use of the receiver selectivity model.

Recommendations: The frequency of 2200 MHz is recommended for use for interference free operation of Experiment 29 with a high probability of success.

Table 1-1 summarizes the findings and recommendations of this study.

### 1.2 General Recommendations

The objective of this study was to provide responsive EMC guidance to NASA program managers. The lessons learned and problems encountered in this analysis have pointed to methods for improving the form of this guidance, and to increase the speed with which it must be provided in order to be incorporated, together with other considerations, in the selection of experiments for a particular satellite



program, or to allow system design changes while these changes may still be practicable. In the course of the EMC analysis, two problems arose, making it difficult to provide, in all cases, the frequency utilization guidance desired.

The first, and probably most serious, of the problems was the unavailability of the DOD/ECAC data base. Since this data bank contains large amounts of environmental electronic information not available elsewhere, it was not possible to determine whether all military equipments operating within the frequency bands of interest were contained in the data available representing U.S. government allocations, namely the IRAC Frequency Files. During the course of the study, several formal written requests for this data were generated. Replies to these requests were either ignored or answered stating that the data could not be released to NASA because of need-to-know security problems. Direct discussions between IITRI personnel and the ECAC relating to the release of this data were also without success. The need for a face-to-face meeting between interested high level NASA personnel and representatives of the U.S. Joint Chiefs of Staff responsible for the administration of the ECAC is obvious and recommended.

The second major problem was generated by the inability to establish at an early point in the analysis, a direct communication channel between the IITRI staff and the principal investigators. Without this contact, the analysis team often had to rely on a general, sketchy and incomplete description of the systems to be analyzed. While it is recognized that many of the experiments are in the proposal stage and thus, much of the technical data is of a preliminary nature, it is also felt that a direct contact with the principal investigators would have made available to the analysis staff an additional level of detail that is often required and missing from the available documentation, as well as the benefit of latest thinking regarding the experiment. This type of direct contact is certainly recommended for any future studies of this type.

TABLE 1-1  
SUMMARY OF EMC EVALUATION

EXPERIMENT NO	EXPERIMENT	REPORT REFERENCE SECTION	FREQUENCY GHz	BAND ALLOCATIONS GHz	NUMBER OF ENVIRONMENTAL EMITTERS ANALYZED	SINGLE ORBIT MAXIMUM EXPOSURE TIME, MINUTES		MAXIMUM PERCENT EXPOSURE TIME FOR 24 HOUR PERIOD		SUMMARY
						ABOVE NOISE THRESHOLD	ABOVE DEGRADATION THRESHOLD	ABOVE NOISE THRESHOLD	ABOVE DEGRADATION THRESHOLD	
7	Microwave Spectrometer (MICSPEC)	4.1	22.2 31.46 53.65 60.87 64.47	Fixed Mobile Radio Astronomy Not Allocated	0	0	0	0	0	All five frequencies are predicted to be interference free even though 31.46 GHz is used by 8 countries for fixed and mobile services.
10	Microwave Occultation Experiment (MLOCC)	4.2	4.4 to 4.8	Fixed, Mobile, Communication-Satellite (earth to satellite) 4.4-4.7 Fixed, Mobile 4.70-4.99	2886	20	20	7	7	It is recommended that Experiment 10 be operated in one of the 32 sub-bands identified in Section 4.2 to minimize the phase error producing effects of interference signals.
12	Electrically Scanning Microwave Radiometer for Mapping Earth Radiation and Cloud Structure (ESMR)	4.3	19.35	Radio Astronomy 19.30-19.40	0	0	0	0	0	This experiment is predicted to be free of interference at the present time. (Review for possible re-allocation to communication-satellite use after World Administrative Radio Conference (1970).
13	Satellite Microwave Radiometry to Sense the Surface Temperature of the World Oceans (MICRAD)	4.4	2.69 to 2.83	Radio Astronomy 2.690-2.700 Aeronautical Radionavigation, Radiolocation 2.7-2.9 Fixed Mobile 2.550-2.690	705	45	22	33.6%	9%	Interference is possible within frequency range proposed for experiment. Recommend that frequency range be moved away from weather and height finder radars by using 2.55 to 2.70 GHz to achieve very low probability of interference.
14	Global Radar for Ocean Waves and Winds (GROW)	4.5	3.0	Radionavigation, Radiolocation 2.9-3.1	25	30	20	30	7	If a 5 knot wind speed error is not acceptable, frequency should be changed from 3.000 GHz to 3.001. The 1 MHz change will reduce incremental wind speed error caused by emitters at 3.0 GHz to less than 1 knot.
26	Simplified Data Collection Experiment (DACOL)	4.6	0.460	Land Mobile .450-.470	695	32	11.6	26%	2.8%	It is recommended that 460 MHz be used for Experiment 26 only if the plan to use FSK modulation is adhered to. Sources of AM and FM in the land mobile band could cause degradation in excess of 1% bit error for other modulation types.
28	Nimbus Data Relay Link Through ATS (DARELL)	4.7	1.8	Fixed Mobile 1.790-2.290	209	19.8	8.0	7.1%	1.1%	It is recommended that the chosen frequencies for all links be used for successful operation of Experiment 28.
28-1	ATS to Nimbus Link		0.149	Fixed Mobile .1480-.1499		47.5	20.0	26.3%	8.0%	
28-2	ATS to Nimbus Link		1.8	Fixed Mobile 1.790-2.290		Not Applicable	-	-	-	
28-3	ATS to Earth Link		2.253	Fixed Mobile 1.790-2.290		0	0	0	0	
28-4 & 5	Nimbus to ATS Link (Data and Sidebands)				133					
29	Wide-Band Real-Time Data Transmission (DATRAN)	4.8	2.2	Fixed Mobile 1.790-2.290	953	0	0	0	0	The frequency of 2200 MHz is recommended for interference free operation of Experiment 29.

FOLDOUT FRAME -

FOLDOUT FRAME - 2 B

## 2.0 INTRODUCTION

In April 1968, the Space Applications Program Directorate of the National Aeronautics and Space Administration contracted with the IIT Research Institute to perform a study to investigate potential electromagnetic compatibility problems that might exist between the satellite sensor systems of NASA's Space Applications Program and terrestrial equipments. The results of this evaluation are presented in this report. The objective of this study was to identify those satellite experiments which by virtue of their selected frequency of operation are likely to be interfered with by terrestrial electronic systems sharing a common frequency or band of frequencies with the satellite system, and to recommend solutions to any problems encountered. The study concentrated primarily on the EMC/frequency utilization of those experiments that, at the outset of this study, were being considered for the Nimbus-E program. The list of experiments to be analyzed varied from month to month during the early stages of the study. Several experiments on which analysis effort had been expended were removed by NASA from the list of those to be analyzed. Among these were the Ryan Scatterometer and UHF Sferics experiments. Effort was also expended in providing data in support of the Data Relay Satellite Program to Mr. John W. Bryan of the Goddard Space Flight Center. The experiments to which this report directs itself are as follows:

1. Experiment 7, Microwave Spectrometer.
2. Experiment 10, Microwave Occultation Experiment.
3. Experiment 12, Electrically Scanning Microwave Radiometer for Mapping Earth Radiation and Cloud Structure.
4. Experiment 13, Satellite Microwave Radiometry to Sense the Surface Temperature of the World Oceans.
5. Experiment 14, Global Radar for Ocean Waves and Winds.
6. Experiment 26, Simplified Data Collection Experiment.
7. Experiment 28, Nimbus-E Data Relay Link Through ATS-F.
8. Experiment 29, Wide-Band Real-Time Data Transmission.

The report is structured into two major sections. The first major section, titled, "The Analysis Approach", discusses the general EMC analysis methodology applied to each experiment to analyze its potential to interference. The sources of satellite experiment information and environmental data are identified in this section. A procedure for determining the threshold to interference of each experiment studied is formulated in this portion of the report together with a justification for the assumptions necessitated by shortcomings in both the experiment electronic data and environmental information sources. Also included within this section is a technique developed to display the geographical influence of interference sources along the satellite ground tracks. A method for predicting the single orbit maximum exposure time to an interference environment is also discussed.

The second major section, titled, "The Interference Analysis", contains a detailed evaluation of the interference potential of each experiment. The purpose and scientific basis for each experiment is discussed to a level necessary to outline the operating characteristics used in the interference evaluation. The present allocation and assignment occupancy for each of the frequencies selected for use by the experiments is identified in this section. An environmental signal summary, depicting the interference sources exceeding both the receiver noise threshold and developed degradation levels is also presented. Finally, within each sub-section is presented the rationale for the interference predictions and recommendations for band-sharing of these satellite systems with terrestrial emitters. The geographical influence of the interference environment on the operation of each experiment is portrayed on a world map, from which the maximum exposure time during a single orbit and percent time over a 24 hour period was predicted.

### 3.0 THE ANALYSIS APPROACH

#### 3.1 The Interference Analysis Procedure

Figure 3.1-1 summarizes the five major procedural steps followed in the EMC evaluation of aerospace sensors.

The first step, "Environmental Data Collection", consisted of extracting those records from available frequency files of environmental emitters operating on or about the given planned frequencies of operation of the satellite sensor receivers. A search was also made of each of the five sub-harmonic bands relating to each sensor frequency. The spectral occupancy in the desired band of operation was evaluated to determine the relative difficulty of band-sharing as well as to identify as quickly as possible whether enough unoccupied channels existed in the band to make the frequency assignment routine simply a process of selecting one of these clear channels.

The second step, "System Modelling and Power Cull" consisted of (1) determining the sensor selectivity and sensitivity characteristics, (2) structuring power spectral density representations for the environmental emitters, (3) developing a level to represent the mutual antenna gain of satellite and terrestrial systems, and (4) selecting a propagation path loss model to represent system coupling beyond radio line-of-sight conditions. A cull was executed in this phase of the analysis and those environmental systems whose received power exceeded the receiver noise sensitivities were extracted for further processing.

The third step, "Degradation Analysis", consisted of modelling the sensor receiver demodulation and post processing elements to whatever degree made possible by the available data. The waveform and time characterization of interference signals was also established during this phase. A receiver degradation level, associated with a performance requirement of the sensor, was established and a determination was made of whether the interference signals would exceed this degradation level. The result of this process was a revised summary of potential interferers.

The fourth step, "Satellite Exposure Analysis", consisted of determining the influence of those emitters still remaining on a geographical basis to the satellite in orbit. Interference regions representing satellite ground track locations where signals exceeding the established degradation levels might be encountered were plotted on world maps. From these maps, exposure to interference parameters, such as the single orbit maximum exposure time to interference and maximum percent time exposure over a 24 hour period were predicted.

IIT RESEARCH INSTITUTE

The fifth and final step, "Band Sharing Analysis", consisted of determining the accommodations necessary in the sensor tuned frequencies that would have to be made to reduce the remaining unacceptable interference levels below the developed degradation and tolerable exposure time limits. The result of this process was a band-sharing recommendation in the form of a new frequency assignment for those experiments experiencing unacceptable interference at the selected frequencies.

The assumptions, techniques and rationale for these analysis procedures are described in greater detail in the sections that follow.

### 3.2 Sources of Satellite Experiment Data

The documentation made available to the EMC analysis team is presented in Table 3.2-1. Most of the information was contained in proposals to NASA from the principal investigators. Thus, the information in these documents was of a preliminary nature, often sketchy, and did not, in most cases, contain the level of detail necessary to perform an in-depth interference analysis. Realizing that waiting for the necessary design details to become firm would delay providing the necessary frequency utilization guidance, it was decided to model the missing but necessary system parameters on a most likely basis. The specific values assumed for these parameters is discussed in the "Interference Analysis" section under each appropriate experiment.

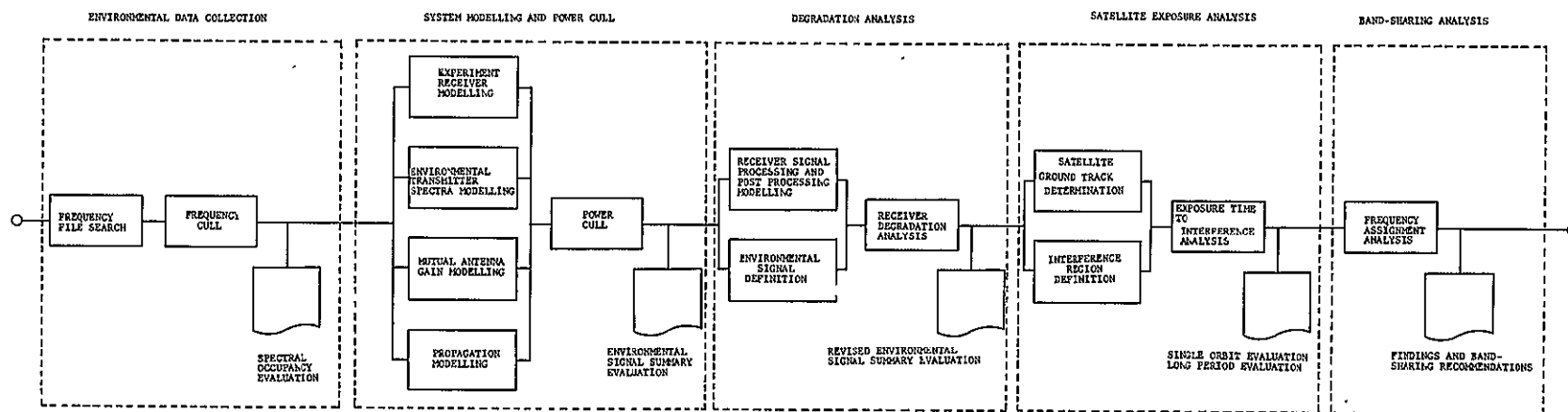


FIGURE 3 1-1  
THE INTERFERENCE ANALYSIS PROCEDURE



TABLE 3.2-1  
SOURCES OF SATELLITE EXPERIMENT DATA USED FOR THE EMC EVALUATION

EXPERIMENT NO.	EXPERIMENT NAME	EXPERIMENT DATA SOURCES
7	Microwave Spectrometer (MICSPEC)	"Experiment Proposal for Nimbus E Microwave Spectrometer", by D. H. Staelin, February 1968.
10	Microwave Occultation Experiment (MICOG)	"Proposal for a Microwave Occultation Experiment on the Nimbus E Meteorological Satellite", by the Stanford Electronics Laboratories, February 1968.  "A Preliminary Study of Atmospheric Density Measurements by Means of Satellites", B. B. Lusignan, Final Report SU-SEL-68-038, NASA Contract NAS9-7020 to Stanford Electronics Laboratories, March, 1968.
12	Electrically Scanning Microwave Radiometer for Mapping Earth Radiation and Cloud Structure (ESMR)	"Proposal for Mapping Earth Radiation and Cloud Structure with an Electrically Scanning Microwave Radiometer (ESMR) on Nimbus E", W. Nordberg, 1968.
13	Satellite Microwave Radiometry to Sense the Surface Temperature of the World Oceans (MICRAD)	"Scientific Experiment for Satellite Microwave Radiometry to Sense the Surface Temperatures of the World Oceans", G.C.Ewing, The Woods Hole Oceanographic Institution, 1968.
14	Global Radar for Ocean Waves and Winds (GROW)	"Global Radar for Ocean Waves and Winds", an experiment submitted to NASA, W. J. Pierson, Jr., R. K. Moore and M. I. Schneebaum, June 1968.
26	Simplified Data Collection Experiment (DACOL)	"Proposal for Nimbus E Simplified Data Collection Experiment", by RCA Astro-Electronics Division, February 1968.
28	Nimbus Data Relay Link Through ATS (DARELI)	"A Proposal for a Technological Experiment Nimbus E Data Relay Link Through ATS-F", C. Cote, P. Hefferman, G. Hogan, and C. Laughlin, GSFC, March 1968.
29	Wide-Band Real-Time Data Transmission (DATRAN)	"Proposal for Nimbus E Wide-Band Real-Time Data Transmission", by RCA Astro-Electronics Division, February 1968.

### 3.3 Environmental Data Sources

The operating frequencies, locations, and electronic characteristics of the environmental interference sources were extracted from three major data banks. Worldwide frequency allocation data were derived from the Radio Regulations of the International Telecommunication Union (ITU). U.S. frequency allocation data were extracted from Rules and Regulations of the Office of the Director of Telecommunication Management (ODTM) and the Federal Communications Commission (FCC). Worldwide frequency assignment data were extracted from the International Frequency Lists of the ITU. U.S. frequency assignment data were extracted from the frequency files of the Interdepartment Radio Advisory Committee (IRAC).

It is important to realize that none of these data bases were designed to be used for making interference predictions. The IRAC file is basically an administrative file used in the main to keep records of users and their operating frequencies. The file is almost void of information relating to receiver characteristics making it almost impossible to evaluate interference effects in these systems. Antenna, modulation and even nomenclature data are missing in the great majority of circumstances. The ITU frequency lists are even less suitable for EMC evaluation purposes. This file is largely an assignment list rather than a usage list. That is, there is no guarantee that those users appearing in the list are making use of the associated frequencies, merely that these frequencies, often blocks of frequencies, have been assigned to the user. This list is still of some value, since it represents a readily available compilation of frequency use outside of the U.S. more comprehensive than any other with the possible exception of that data collected by the U.S. National Security Agency (NSA).

### 3.4 Sensor Interference Threshold Evaluation Procedure

A sensor or receiver power threshold was established for each experiment. The threshold level was used to cull or identify those terrestrial emitters which would be further analyzed to establish their interference potential. The threshold is an interference signal power level above which interference is likely. The threshold does not reflect when, where or how long the interference will occur nor does it necessarily infer, when compared to the level of received interference signal, a degree of severity of the amount of degradation to the sensor receiving system. It does provide for the quick elimination from consideration of those terrestrial emitters that will have an extremely low probability of causing degraded sensor operation. The evaluation of the effect of undesired signals in excess of this threshold is not made in this section, but rather in Section 4.0 where each experiment is analyzed separately.

The expression used to evaluate this threshold is given by

$$T_I = kTB_R + F + 10 \log \frac{B_T}{B_R} + \Phi(\Delta F) \quad \text{for } B_T > 10 B_R$$

$$T_I = kTB_R + F + \Phi(\Delta F) \quad \text{for } B_R > 10 B_T \quad (3.4-1)$$

$$T_I = kTB_R + F + \Phi(\Delta F) + \Phi_0 \quad \text{for } .1 B_T \leq B_R \leq 10 B_T$$

where  $T_I$  = the interference power threshold in dB

$k$  = Boltzmann's constant =  $1.38 \times 10^{-23}$  joule/deg.

$T$  = temperature in degrees Kelvin

$B_R$  = receiver bandwidth in MHz

$F$  = receiver noise figure in dB

$B_T$  = transmitter emission bandwidth in MHz

$\Phi(\Delta F)$  = a receiver off-frequency rejection function depicting the amount, in dB, of receiver attenuation of a received signal as the signal is detuned from the receiver frequency

III RESEARCH INSTITUTE

$\Phi_0$  = the amount of receiver rejection to an on-tune undesired signal having a bandwidth within an order of magnitude of the receiver bandwidth

The threshold expression is thus not only a function of the receiver noise sensitivity  $kTB_R + F$ , but also varies with the emission bandwidth, shape of the undesired signal emission spectra and frequency separation between desired and undesired signals. Table 3.4-1 is a summary of the receiver noise sensitivities for each experiment. The application and form of the off-frequency rejection function was dependent on (1) the magnitude of the frequency separation between transmitter and receiver frequencies, (2) the relative magnitudes of transmitter emission and receiver selectivity bandwidths, (3) the functions assumed to represent the transmission emission spectra and receiver selectivity functions and (4) the tuning capability of both transmitter and receiver. Table 3.4-2 summarizes the use of the off-frequency rejection function for all interference situations. The expression used to compute the off-frequency rejection function in those cases when it did apply is given by

$$\Phi(\Delta F) = \int_{-\infty}^{\infty} W_T(f) (f - f_R - \Delta F) \left| H(f - f_R) \right|^2 df \quad (3.4-2)$$

where  $W_T(f)$  = the normalized power spectral density of the interfering transmitter

$\Delta F$  = the frequency separation between victim receiver and interference source

$\left| H(f) \right|^2$  = the normalized satellite receiver selectivity function

Setting  $\Delta F=0$  in this expression, which is equivalent to assuming the on-tune case, yields the expressions used to arrive at values of  $\Phi_0$ . For values of receiver bandwidth much greater than transmitter bandwidth and transmitter bandwidths, much greater than receiver bandwidths, the off-frequency rejection function takes the form of the receiver selectivity function or transmitter emission function respectively. This fact can be shown intuitively by assuming the limiting case when either function can be represented by a Dirac delta function,  $\delta(f)$ , in Equation 3.4-2. Thus, for example, letting

$$W_T(f - f_R - \Delta F) = \delta(f - f_R - \Delta F) \quad (3.4-3)$$

TABLE 3.4-1

RECEIVER NOISE SENSITIVITIES

EXPERIMENT NUMBER	EXPERIMENT	FREQUENCY GHz	BANDWIDTH MHz	NOISE FIGURE, dB OR EFFECTIVE TEMPERATURE T, DEGREES KELVIN	NOISE SENSITIVITY ( $kTB_R + F$ ) dBm
7	Microwave Spectrometer (MICSPEC)	60.82 64.47 22.2 31.46 53.65	200	T=1000	-86
10	Microwave Occultation Experiment (MICOC)	4.4 - 4.8	.001	12	-132
12	Electrically Scanning Microwave Radiometer for Mapping Earth Radiation and Cloud Structure (ESMR)	19.35	600	T=1000	-81
13	Satellite Microwave Radiometry to Sense the Surface Temperature of the World Oceans (MICRAD)	2.7	140	T=1000	-87
14	Global Radar for Ocean Waves and Winds (GROW)	3.0	.037	4	-124
26	Simplified Data Collection Experiment (DACOL)	.460	.100	4	-120
28-1 28-2 28-3 28-4 28-5	Nimbus-E Data Relay Link Through ATS-F (DARELI)	1800 149 1799.2 1800.0 1803.0 2253 2253	.100 .0005 .050 .050 .050 2.0 .800	6.8 8.5 8 8 8 8 8	-117 -138 -119 -119 -119 -103 -107
29	Wide-Band Real-Time Data Transmission (DATRAN)	2.2	1.0	10	-104

TABLE 3.4-2

## APPLICATION OF OFF-FREQUENCY REJECTION FUNCTION

FREQUENCY OPERATION MODE	TRANSMITTER FREQUENCY, $f_T$ and RECEIVER FREQUENCY, $f_R$ RELATIONSHIP	BANDWIDTH RELATIONSHIPS	OFF-FREQUENCY REJECTION FUNCTION $\bar{\Phi}(\Delta F)$	ON-TUNE REJECTION FUNCTION $\bar{\Phi}_O$
Single Frequency	$f_T = f_R$	$B_T > 10 B_R$ $B_R > 10 B_T$ .1 $B_T \leq B_R \leq 10 B_T$	$\bar{\Phi}(\Delta F) = 0$ $\bar{\Phi}(\Delta F) = 0$ $\bar{\Phi}(\Delta F) = 0$	$\bar{\Phi}_O = 10 \log B_T/B_R$ $\bar{\Phi}_O = 0$ $\bar{\Phi}_O = \int_{-\infty}^{\infty} W_T(f-f_R)  H(f-f_R) ^2 df$
Single Frequency	$f_T \neq f_R$	$B_T > 10 B_R$ $B_R > 10 B_T$ .1 $B_T \leq B_R \leq 10 B_T$	$\bar{\Phi}(\Delta F) = W_T(f=f_R)$ $\bar{\Phi}(\Delta F) =  H(f=f_T) ^2$ $\bar{\Phi}(\Delta F) = \int_{-\infty}^{\infty} W_T(f-f_R-\Delta F)  H(f-f_R) ^2 df$	Same as above
Multiple Frequencies	$f_T$ selected such that $ f_T - f_R $ is a minimum	Same as above	Same as above	Same as above
Range Tuned Frequencies	$f_T = f_R$ if tuning range overlaps $f_R$ otherwise $f_T$ selected such that $ f_T - f_R $ is a minimum	Same as above	Same as above	Same as above

and recalling that, in general

$$F(f)\delta(f-k) = F(k)\delta(f-k) \quad (3.4-4)$$

the expression for  $\Phi(\Delta F)$  becomes

$$\begin{aligned} \Phi(\Delta F) &= \int_{-\infty}^{\infty} \delta(f-f_R-\Delta F) |H(f-f_R)|^2 df \\ &= \int_{-\infty}^{\infty} \delta(f-f_R-\Delta F) |H(f_R+\Delta F)|^2 df \quad (3.4-5) \\ &= |H(f_R+\Delta F)|^2 \end{aligned}$$

Thus, in this limiting case, the off-frequency rejection function is exactly the receiver selectivity function evaluated at  $f=f_R+\Delta F$ . Of course, for actual emission or selectivity functions, the solution of  $\Phi(\Delta F)$  is not exact but is still an adequate approximation for those bandwidth relationships indicated in Table 3.4-2.

The models used to represent the normalized satellite receiver selectivity functions are shown in Figure 3.4-1. They are characterized by 0 dB attenuation within the nominal bandwidth of the receiver and a 40 db per decade of frequency roll-off from that point on. The experiment numbers are indicated within the circles on the figure. The 40 dB per decade roll-off was assumed in the absence of any receiver filter selectivity characteristics and is considered a conservative estimate. That is, it is very likely that the actual roll-offs, determined after these equipments are designed, will exceed this value, resulting in steeper receiver skirts and more receiver attenuation to adjacent channel signals than was predicted.

The model used to represent the normalized power spectral density function for environmental emitters is shown in Figure 3.4-2. It is characterized by 0 dB power spectral density level within the nominal emission bandwidth and a 20 dB/decade of frequency roll-off from that point on. The model chosen to represent the transmitter emission functions is a conservative one. Although techniques are available to more precisely represent these emission function, these routines are strongly dependent on a knowledge of more fine grain emission data than was contained in those data files available to NASA for this analysis. Thus, for example, while

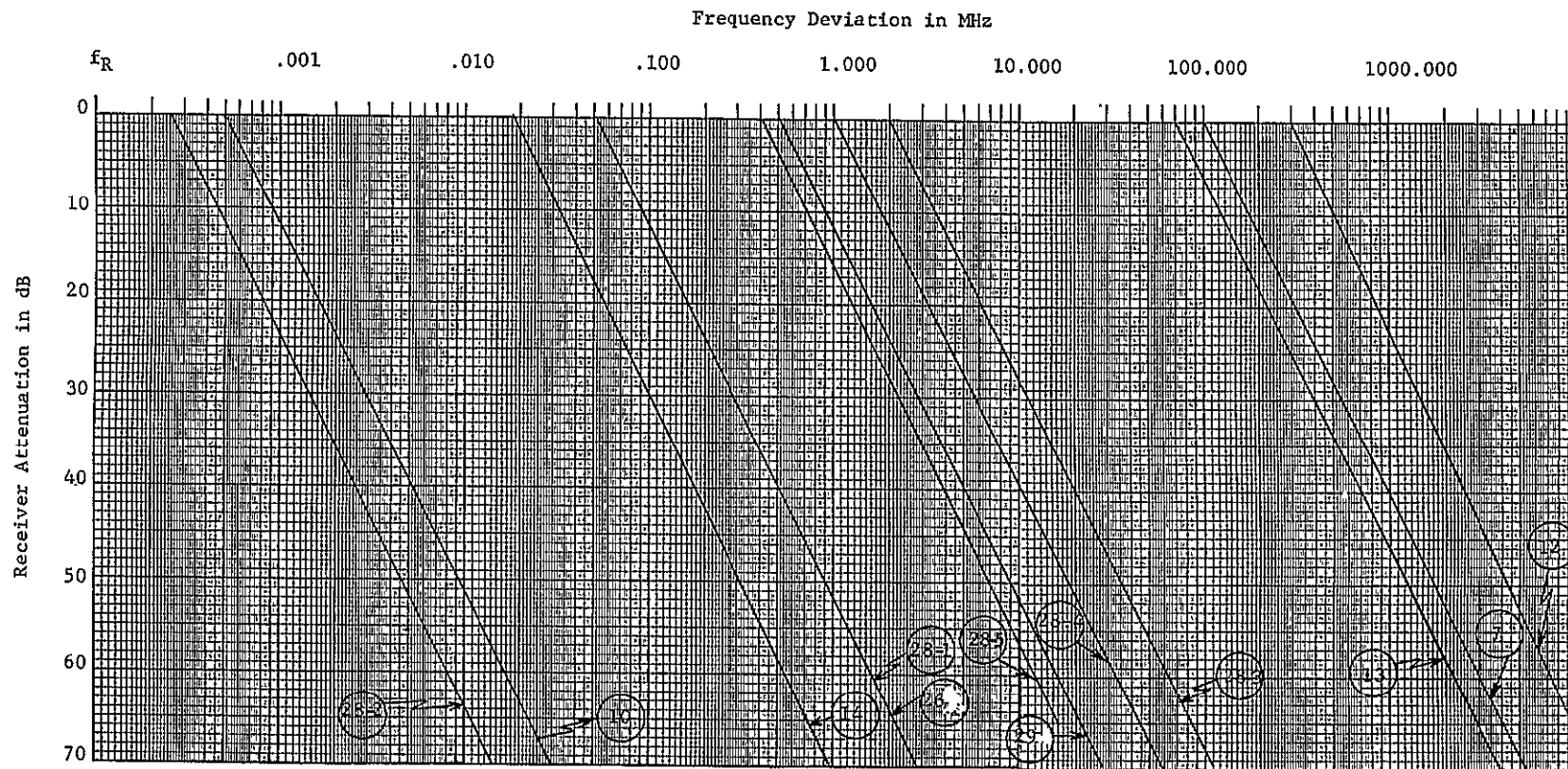


FIGURE 3.4-1  
RECEIVER SELECTIVITY FUNCTION MODELS



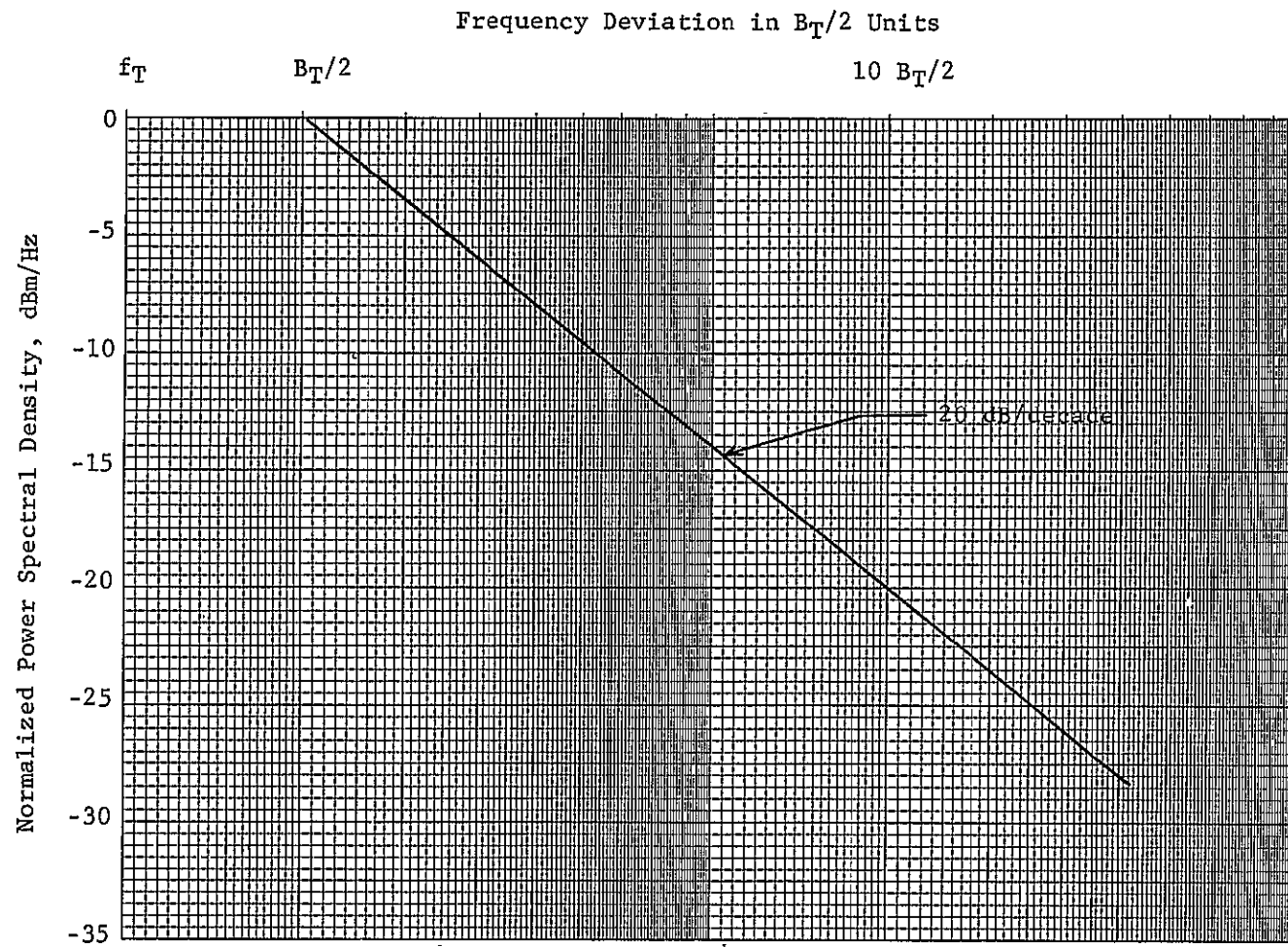


FIGURE 3.4-2

TRANSMITTER EMISSION SPECTRA MODEL

a pulsed CW emitter spectrum can be adequately approximated from a knowledge of the peak envelope power, pulse width, pulse repetition rate and rise and fall times of the pulse, the only data contained in the available files to allow a spectral density approximation was the power and emission bandwidth figures.

### 3.5 Satellite Orbit Considerations

A very simple technique was used to determine the geometrical aspects of the interference, that is, locating where along the satellite orbit undesired signals above those described in Section 3.4 would occur. Also determined was the maximum exposure time to interference during a single orbital pass, as well as the maximum percent time the satellite receiver would experience interference above threshold for a twenty-four hour period.

The evaluation technique consisted of the following steps:

1. Utilizing a  $4/3$  effective radius earth model (Figure 3.5-1), the maximum distance,  $R_{\max}$ , at which the interference power at the satellite receiver is equal to the receiver interference threshold was computed using Equation 3.5-1.

$$I/T_I - \Delta L = 0 \quad (3.5-1)$$

where  $I/T_I$  = the interference to threshold ratio, in dB, computed at the minimum separation distance between interference source and satellite receiver

$\Delta L$  = the additional propagation path loss required to attenuate the interference signal to a level equal to the receiver interference threshold

The expression for  $\Delta L$  is given by:

$$\Delta L = 20 \log \frac{R_{\max}}{R_{\min}} + L \quad (3.5-2)$$

where  $R_{\min}$  = the minimum separation distance between interference source and satellite receiver  
 $R_{\min}$  was set equal to the satellite orbit altitude of 690 statute miles

$L$  = the additional propagation path loss beyond that attributable to the basic wave spreading loss

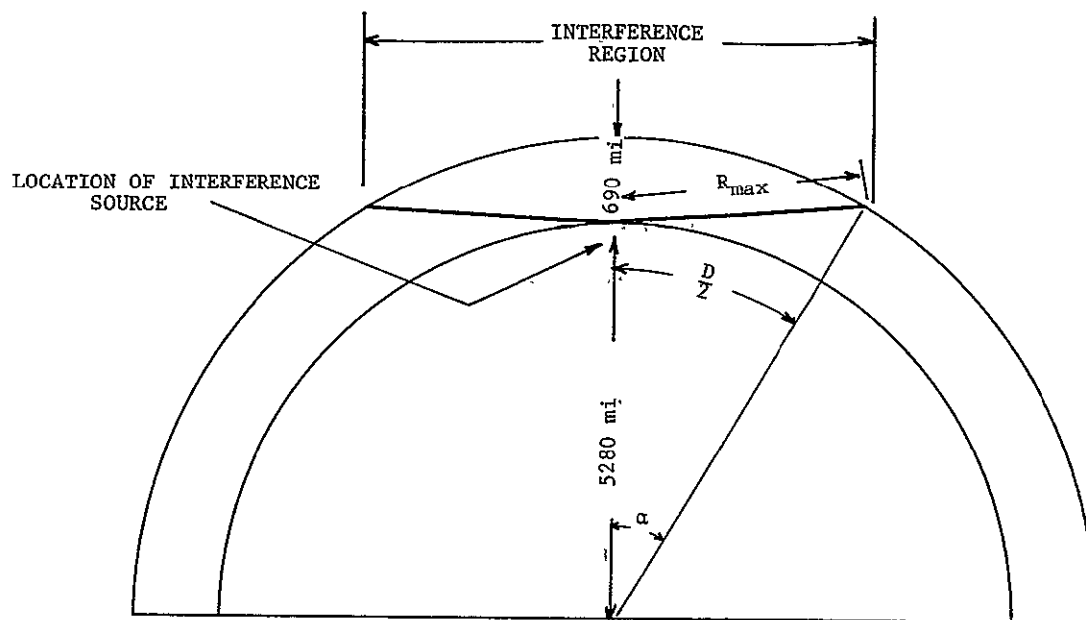


FIGURE 3.5-1

GEOMETRY OF SATELLITE ORBIT CONSIDERATIONS IN  
INTERFERENCE ANALYSIS

Combining Equations 3.5-1 and 3.5-2 and solving for  $R_{\max}$  yields

$$R_{\max} = \text{antilog} \left( \frac{I/TI}{20} + 2.839 - \frac{I}{20} \right) \quad (3.5-3)$$

Given a solution for  $R_{\max}$ , the ground track extent of the interference region,  $D$ , is found to be

$$D = 184.4 \text{ arc cosine} \left\{ 1.008 - \frac{1}{63 \times 10^6} \left[ \text{antilog} \left( \frac{I/TI}{20} + 2.839 - \frac{I}{20} \right) \right]^2 \right\} \quad (3.5-4)$$

The latitude or longitude extent,  $\beta$ , in degrees, on an actual versus  $4/3$  effective radius earth is given by

$$\beta = \frac{D}{69} \quad (3.5-5)$$

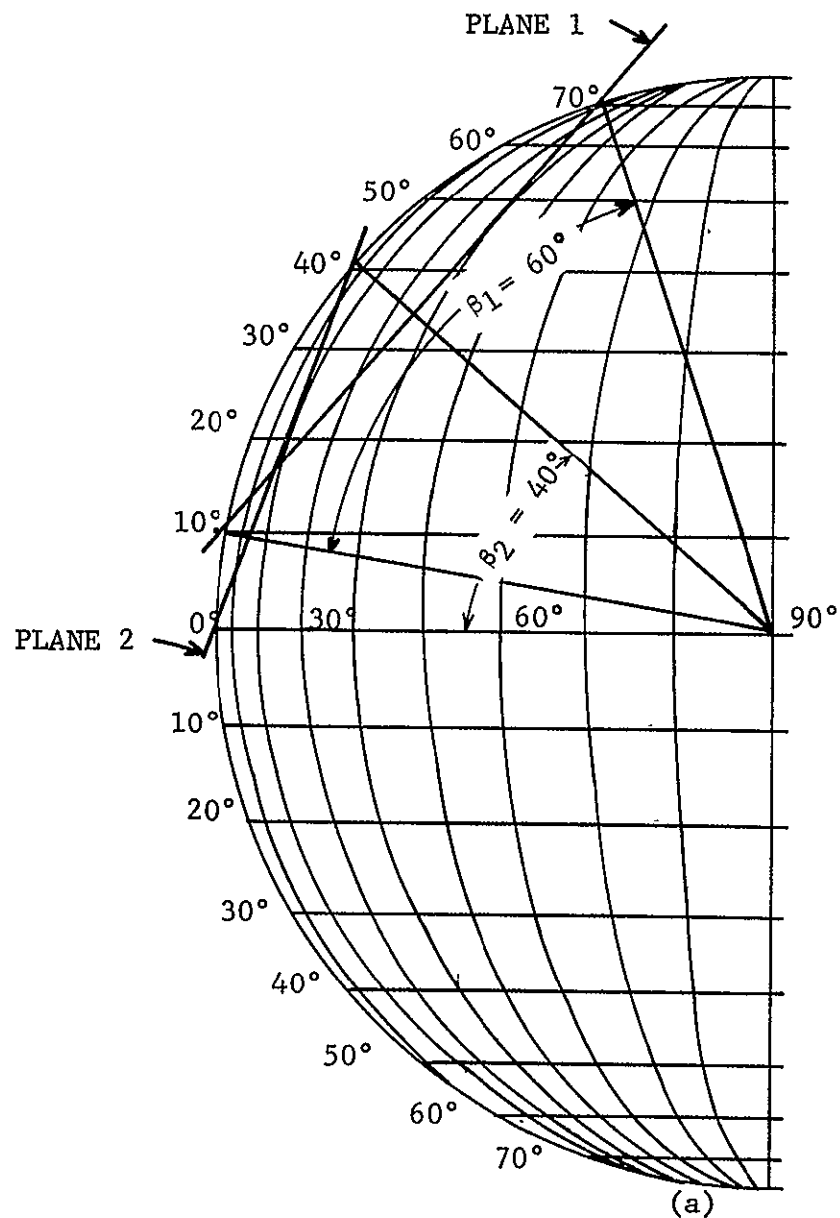
2. The interference region, that is the projection onto the earth of the contour representing those orbital positions where interference from a combination of sources is predicted was computed and plotted using an approximate method. Figure 3.5-2a shows an orthographic meridional projection of the earth used to produce these interference region plots. The latitude and longitude points on the plot were derived by passing, through the earth, a number of planes oriented such that their intersection with the earth was everywhere  $\beta/2$  degrees in latitude and longitude from the site of each interference source. For example, consider two interference sources, located at  $40^\circ\text{N}$  Latitude,  $120^\circ\text{W}$  Longitude and  $20^\circ\text{N}$  Latitude,  $90^\circ\text{W}$  Longitude for which  $\beta$  values of  $60^\circ$  and  $40^\circ$  respectively have been predicted. From Figure 3.5-2a, the intersection of planes 1 and 2 with the earth yield a series of latitude and longitude points, shown in Figure 3.5-2b, from which an interference region can be plotted. The resultant plot is shown in Figure 3.5-3.

3. The maximum exposure time to interference during a single orbital pass was computed next. The orbital period,  $P$ , of the satellite, assuming a perfectly circular orbit, was approximated by using the following equation.

$$P = \frac{2\pi a^{3/2}}{\mu^{1/2}} \quad (3.5-6)$$

where  $a$  = the orbital altitude in kilometers, measured from the earth's center

$$\mu = Gm_p = 5.164 \times 10^{12} \text{ km}^3/\text{hr}^2 \text{ for earth}$$



SITE 1		$\beta_1 = 60^\circ$	
Latitude $40^\circ$ N		Longitude $120^\circ$ W	
Interference Region			
Latitude		Longitude	
$70^\circ$ N		$120^\circ$ W	
$69^\circ$ N		$100^\circ$ W, $140^\circ$ W	
$62^\circ$ N		$90^\circ$ W, $150^\circ$ W	
$50^\circ$ N		$82^\circ$ W, $158^\circ$ W	
$40^\circ$ N		$83^\circ$ W, $157^\circ$ W	
$30^\circ$ N		$86^\circ$ W, $154^\circ$ W	
$26^\circ$ N		$90^\circ$ W, $150^\circ$ W	
$17^\circ$ N		$100^\circ$ W, $140^\circ$ W	
$13^\circ$ N		$110^\circ$ W, $130^\circ$ W	
$10^\circ$ N		$130^\circ$ W	

SITE 2		$\beta_2 = 40^\circ$	
Latitude $20^\circ$ N		Longitude $90^\circ$ W	
Interference Region			
Latitude		Longitude	
$40^\circ$ N		$90^\circ$ W	
$39^\circ$ N		$80^\circ$ W, $100^\circ$ W	
$30^\circ$ N		$72^\circ$ W, $108^\circ$ W	
$28^\circ$ N		$70^\circ$ W, $110^\circ$ W	
$20^\circ$ N		$69^\circ$ W, $111^\circ$ W	
$16^\circ$ N		$70^\circ$ W, $110^\circ$ W	
$10^\circ$ N		$74^\circ$ W, $106^\circ$ W	
$4^\circ$ N		$80^\circ$ W, $100^\circ$ W	
$0^\circ$ N		$90^\circ$ W	

(b)

FIGURE 3.5-2  
ORTHOGRAPHIC MERIDIONAL PROJECTION TECHNIQUE USED TO PRODUCE INTERFERENCE REGION PLOTS

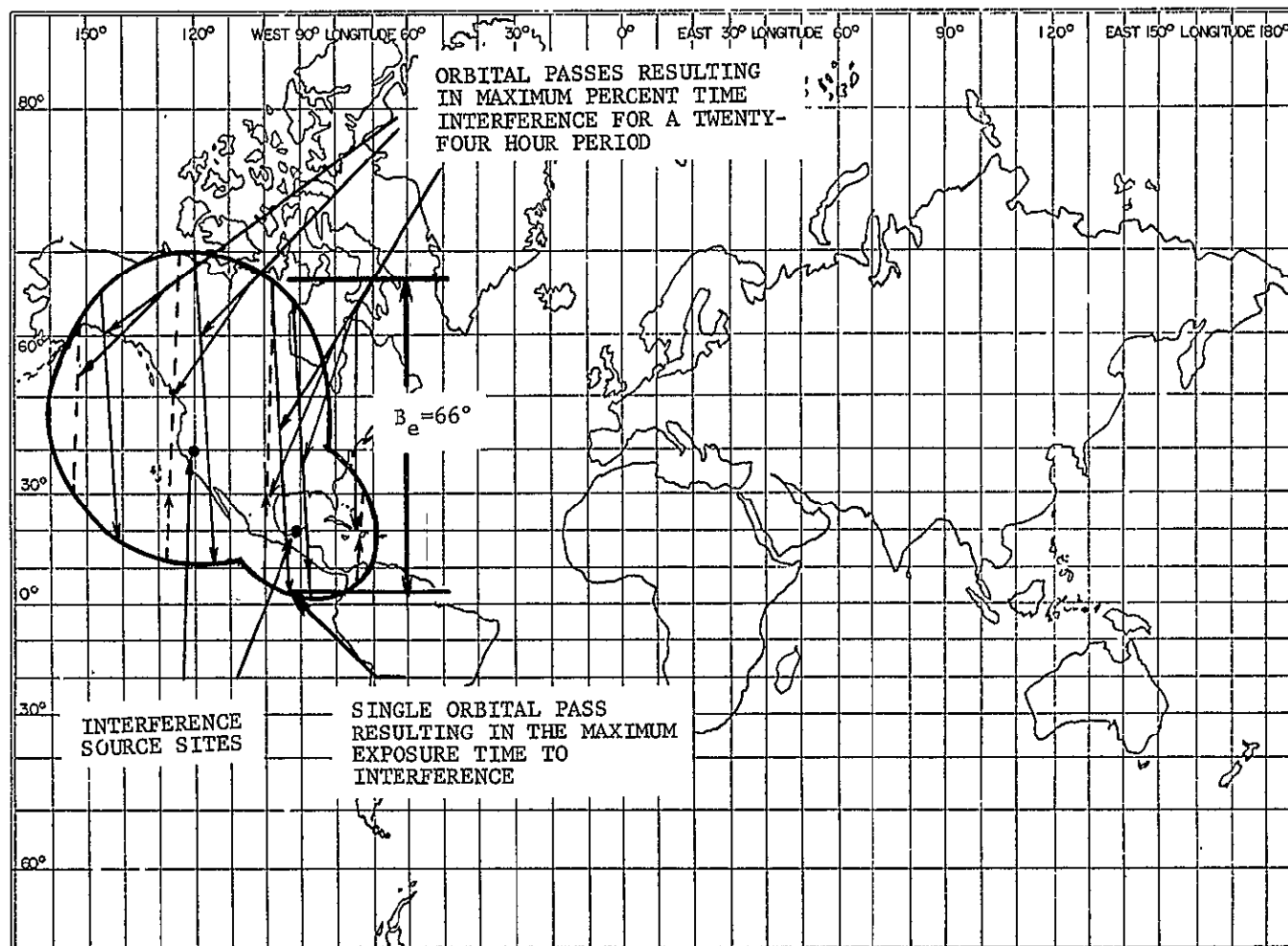


FIGURE 3.5-3

SAMPLE PLOT OF INTERFERENCE REGION

$G$  = the gravitation constant =  
 $8.64 \times 10^{-13} (\text{km})^3/\text{kg}(\text{hr})^2$

$m_p$  = the planetary mass

For a value of  $a = 4650$  statute miles,  $P = 1.77$  hours. The orbital velocity,  $v$ , of the satellite, again assuming a 690 statute mile circular orbit, was computed to be  $v = 16,500 \text{ mi/hr.} = 7.34 \text{ km/sec.}$  The maximum exposure time to interference during a single orbital pass,  $t_m$ , was computed assuming the orbital track to either (1) bisect the interference region for the single interference source case, or (2) be located such that the track length within a composite of single source interference regions is a maximum. The expression used to compute the various values of  $t_m$  is given by

$$t_m = \frac{C}{v} \quad (3.5-7)$$

where  $C$  = that fraction of the orbital circumference that leads to a maximum exposure time to interference

Since  $C$  is merely the product of the orbital radius, 4650 statute miles and the maximum exposure angle, the expression for  $t_m$  can be written as

$$t_m = 0.295 \beta_e \text{ minutes} \quad (3.5-8)$$

where  $\beta_e$  = the maximum effective exposure angle to interference resulting from a combination of interference sources. For the single interference source case,  $\beta_e = \beta$ .

For example, the maximum effective exposure angle for the sample interference case shown in Figure 3.5-3 is found to be,  $\beta_e = 66^\circ$ , from which  $t_m \approx 20$  minutes.

4. The maximum percent time that the satellite receiver would experience interference above threshold for a twenty-four hour period was computed next. The approximate number of degrees of longitude between ascending or descending orbits, given an orbital period of 1.77 hours, was estimated to be 26.5 degrees. A near polar orbit was assumed for the Nimbus satellite. The maximum percent time figure was computed by selecting that positioning of the satellite ground tracks such that the total exposure angle,  $\beta_e$  was a maximum. Figure 3.5-3, shows an orbital spacing from which  $\beta_e \approx 351^\circ$  and consequently the maximum percent time is approximately 7 percent.



5. An equivalent parameter to  $R_{\max}$ , denoted by  $d$ , for those propagation paths beyond the radio line-of-sight was computed assuming that the path losses could be approximated using tropospheric scatter loss theory. This approach was necessitated by the lack of data for beyond radio line-of-sight paths involving terrestrial to satellite coupling. The scatter path geometry is shown in Figure 3.5-4. The expression used to evaluate the long-term hourly median transmission loss due to tropospheric scatter,  $L_b$ , is given below

$$L_b = 30 \log f - 40 \log d + 20 \log r_o + F(d\theta) \quad (3.5-9)$$

where  $f$  = the transmission frequency in MHz

$d$  = the sea level path length in km

$r_o$  = the straight line distance between the transmitter and receiver in km

$F(d\theta)$  = the path attenuation function which is given graphically in Figure 3.5-5

The curves of Figure 3.5-5 are plotted for a value of refractivity  $N_s = 250$  and several values of the path asymmetry parameter  $S$ . The parameter  $S$  is given by

$$S = \frac{\alpha_{oo}}{\beta_{oo}} \quad (3.5-10)$$

where  $\alpha_{oo}$  and  $\beta_{oo}$  are defined as shown in Figure 3.5-5. If  $S > 1$ , the reciprocal of  $S$  is used to determine  $F(d\theta)$ . The argument of  $F$  is the product of the sea level path length  $d$ , in kilometers and the angular distance  $\theta$ , in radians. The angular distance is defined by

$$\theta = \alpha_{oo} + \beta_{oo} \quad (3.5-11)$$

The specific procedure used to arrive at  $d$  was an iterative one and consisted of the following steps:

a. The propagation path loss (free-space) at  $R_{\min} = 690$  miles was added to each  $I/T_I$  prediction. The resultant quantity is now the value of propagation path loss necessary to reduce the interference signal to the satellite receiver threshold level. For example, for a value of  $I/T_I = 25$  and a value of free-space path loss at 690 miles,  $L_{fs} = 162$  dB, the required path loss  $L_b = 187$  dB.

IIT RESEARCH INSTITUTE

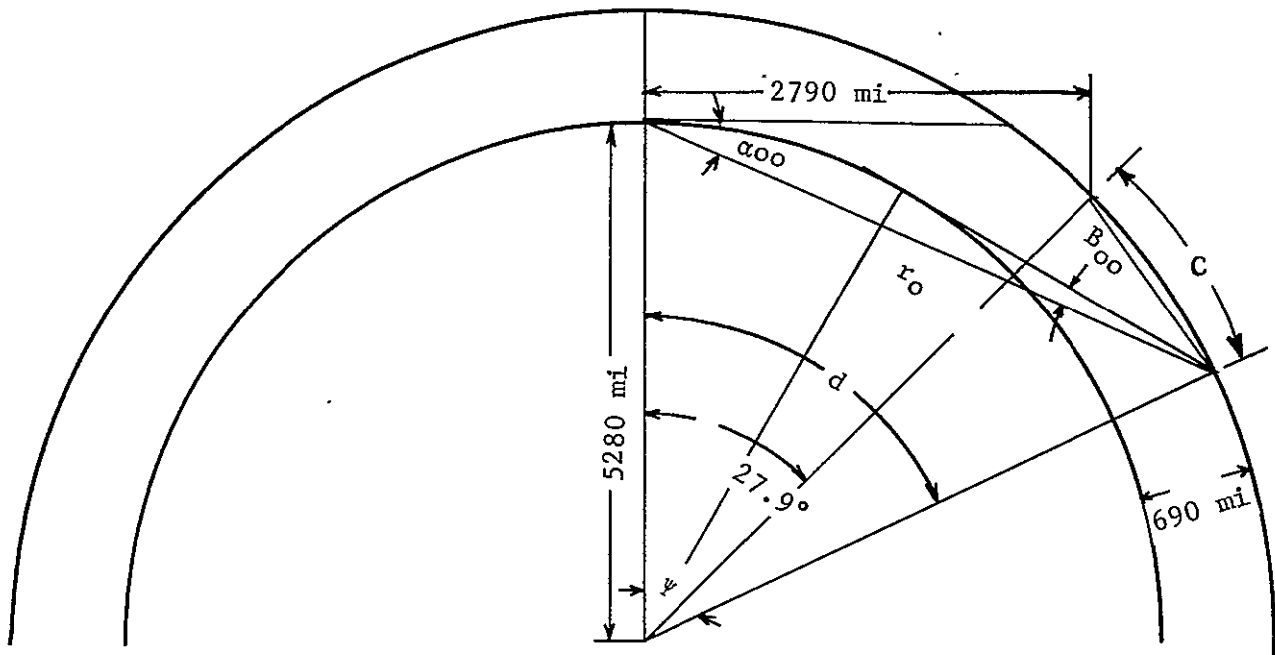


FIGURE 3.5-4

SCATTER PATH GEOMETRY

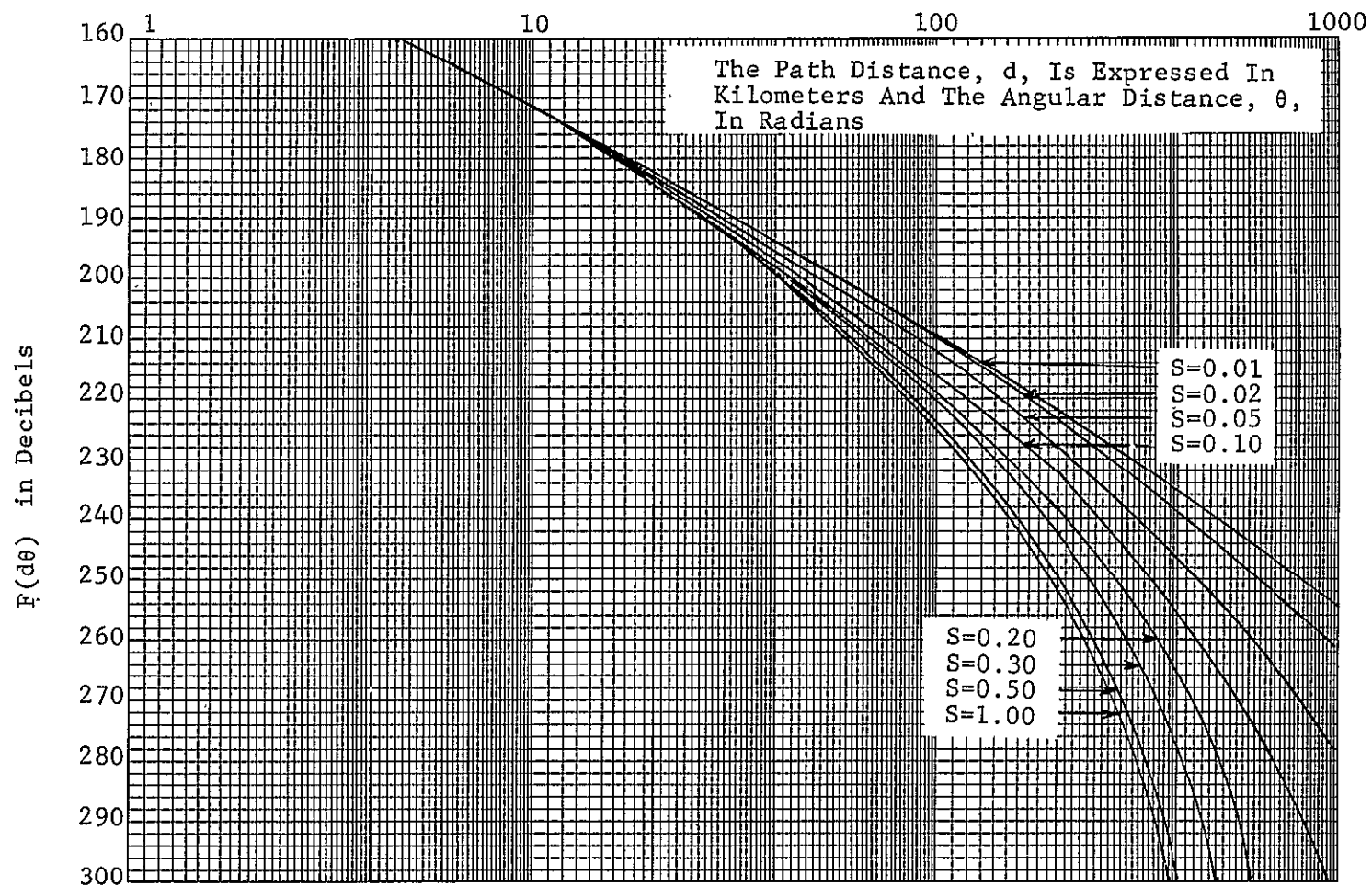


FIGURE 3.5-5

THE FUNCTION  $F(d\theta)$  FOR  $N_s = 250$

b. A value of the distance  $d$  was then arbitrarily selected. From this value of  $d$ , the angle  $\Psi$  was computed from

$$\Psi = .01085 d \quad (3.5-12)$$

The parameter  $r_0$  was computed from the assumed value of  $d$  and the computed value of  $\Psi$  using the expression

$$r_0 = (63.5 \times 10^6 - 63.2 \times 10^6 \cos .01085d)^{1/2} \quad (3.5-13)$$

The angle  $\theta$ , in radians, is also computed using the assumed value of  $d$  according to

$$\begin{aligned} \theta &= \alpha_{00} + \beta_{00} \\ &= \Psi - \eta \\ &= \frac{.01085 d - 27.9}{57.3} \end{aligned} \quad (3.5-14)$$

The parameter  $C$ , is shown in Figure 3.5-4 and is given by

$$C = 11,940 \sin \frac{.01085d - 27.9}{2} \quad (3.5-15)$$

Given the computed values of  $r_0$  and  $C$ , the angle  $\alpha_{00}$  is calculated from

$$\alpha_{00} = \arccos \frac{r_0^2 - C^2 + 7.79 \times 10^6}{5580 r_0} \quad (3.5-16)$$

The angle  $\beta_{00}$  is then computed from

$$\beta_{00} = \theta - \alpha_{00} \quad (3.5-17)$$

Using these values of  $\alpha_{00}$  and  $\beta_{00}$ , the path asymmetry parameter  $S$  is computed from Equation 3.5-10. Given this value of  $S$ , and computing  $d\theta$  allows a value of  $F(d\theta)$  to be read from Figure 3.5-5.

c. The required value of  $L_b$  is then compared against that obtained by assuming a value for  $d$  and solving Equation 3.5-9. The process is repeated, that is subsequent values of  $d$  are chosen until the equality in Equation 3.5-9 holds.

## 4.0 THE INTERFERENCE ANALYSIS

### 4.1 Microwave Spectrometer (MICSPEC)

#### 4.1.1 Purpose and Scientific Basis

This experiment will demonstrate the capabilities and limitations of microwave sensors for measuring tropospheric temperature profiles, water vapor abundance and cloud water content, even in the presence of many cloud types which block infrared sensors. The instrument will measure thermal radiation at three wavelengths near 5 mm corresponding to atmospheric temperatures at 0-18 km altitude, and two wavelengths near 1 cm corresponding to water vapor and liquid water in the troposphere.

The principal atmospheric constituents which interact with microwaves are oxygen, water vapor, and liquid water. Ozone and ice crystals interact weakly and can be observed only with difficulty.

The frequencies of observation suggested for this experiment are listed in Table 4.1-1. Each frequency is affected to a different degree by the terrestrial surface, clouds, precipitation, water vapor, and temperature profile, and therefore by appropriately interpreting a set of simultaneous equations most of these meteorological parameters can be separately estimated.

The experiment can be considered as composed of two parts: 1) three channels near 5 mm wavelength which probe primarily the temperature profile, and 2) two channels near 1 cm wavelength which over oceans are sensitive to water vapor and liquid water, and which over land can indicate surface temperature. Although these two parts could operate separately, the performance is superior when they are interpreted simultaneously. That is, the water vapor and liquid water estimates will improve the temperature profile measurements, and vice-versa.

The experiment functions approximately as follows. The three channels near 5 mm wavelengths are situated on the wing and between peaks of the 5 mm complex of strong  $O_2$  resonances, and each channel corresponds to a different weighting function similar to those at infrared wavelengths. That is, the observed brightness temperature  $T$  is approximately  $\int_0^{\infty} T(h) W(v, h) dh$  where  $W(v, h)$  is the weighting function. The weighting functions have half-widths  $\Delta h$  of 8-11 km and will peak at altitudes near 4, 12 and 18 km. The weighting functions are shown in Figure 4.1-1.

TABLE 4.1-1

EXPERIMENT 7, MICROWAVE SPECTROMETER SYSTEM CHARACTERISTICS

RECEIVER		ANTENNA	
FREQUENCY	22.2 GHz 31.46 GHz 53.65 GHz 60.82 GHz 64.47 GHz	TYPE	3 Horns
		GAIN	20 dB at each frequency
		BEAMWIDTH	10°
BANDWIDTH	RF 200 MHz IF 200 MHz		
SENSITIVITY	-86 dBm		
TYPE	RADIOMETER		

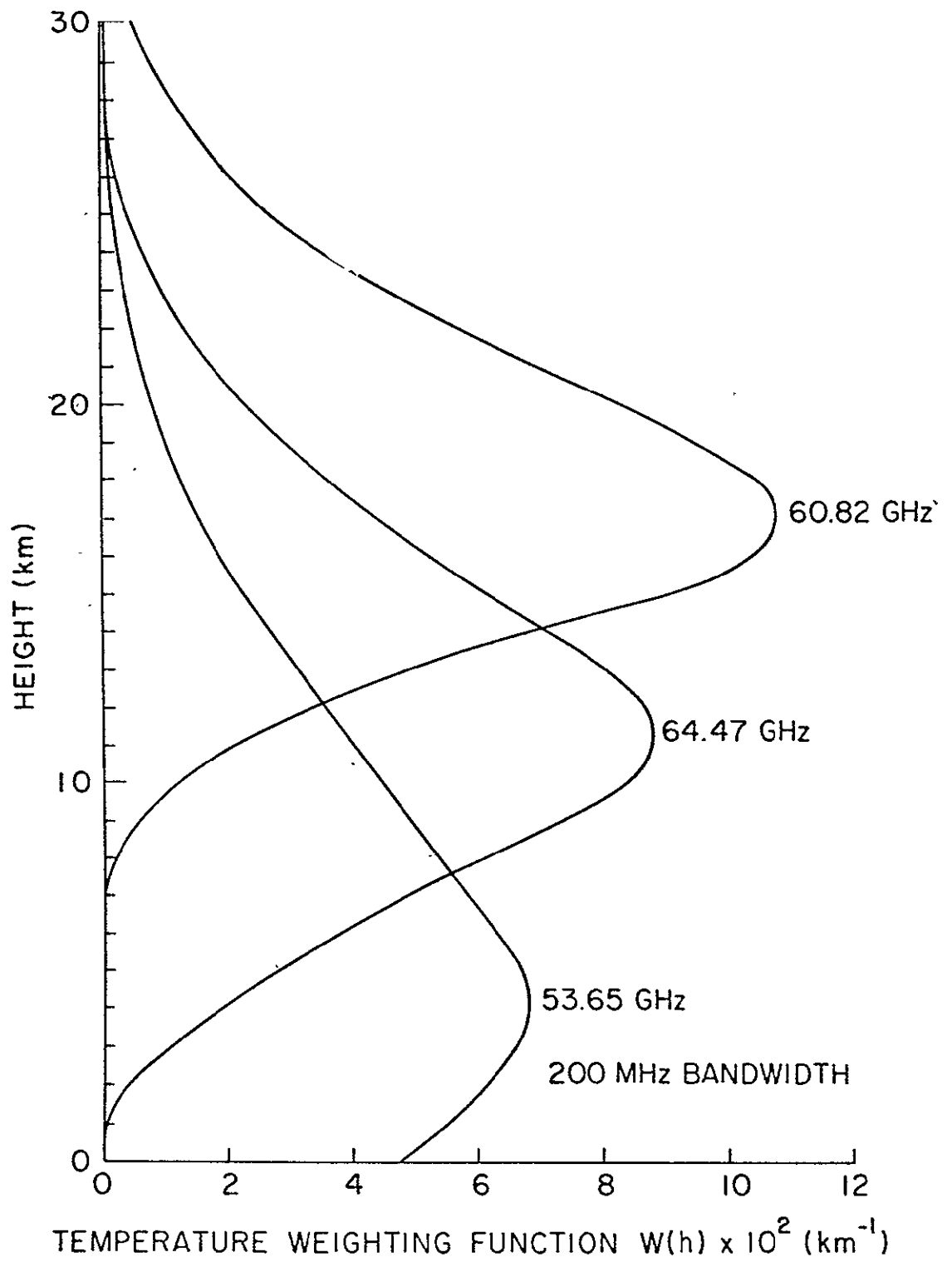


FIGURE 4.1-1  
WEIGHTING FUNCTIONS

The instrument is a five channel microwave radiometer system. The individual radiometers are of the Dicke-superheterodyne type utilizing all solid-state components. The instrument is designed to be rigidly mounted to the lower surface of the Nimbus ring, with a clear view of the nadir. In addition, calibration horn antennas on the side of the package will be oriented to view cold sky at all times.

The sensitivity of the individual channels is expected to be better than 1 degree Kelvin RMS for a four-second integration time. The absolute accuracy will be better than  $2^{\circ}$  K RMS and the dynamic range shall be 0-400°K with  $\pm 0.1\%$  linearity. Engineering and data outputs of the system shall be 12-bit digital words at a rate of approximately 60 bits per second. Internal commutation of the data and engineering outputs will be processed in the standard Nimbus format.

Figure 4.1-2 is a block diagram of the instrument configuration. The three O<sub>2</sub> radiometers (53.6, 60.82 and 64.47 GHz) share common signal and reference antennas. The H<sub>2</sub>O radiometers (22.2 and 31.4 GHz) each have their own antennas. In this manner, three signal antennas and three small reference antennas are used. Internal switching is used to automatically calibrate the radiometers by sequential observations of signal antenna, reference antenna, and black-body load. Figure 4.1-3 is a block diagram of a typical radiometer channel. The system characteristics are given in Table 4.1-1.



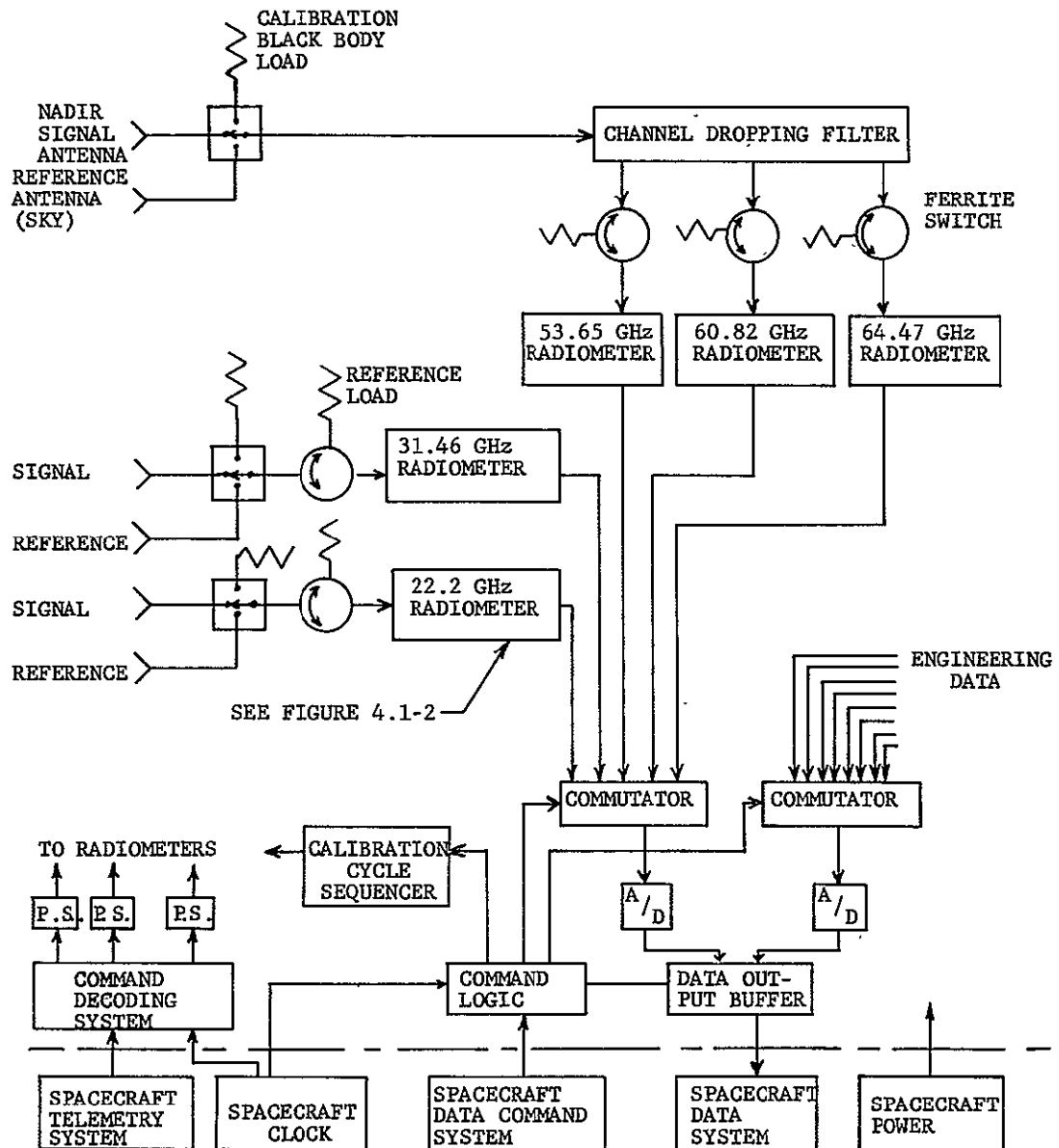


FIGURE 4.1-2

MICROWAVE SPECTROMETER BLOCK DIAGRAM

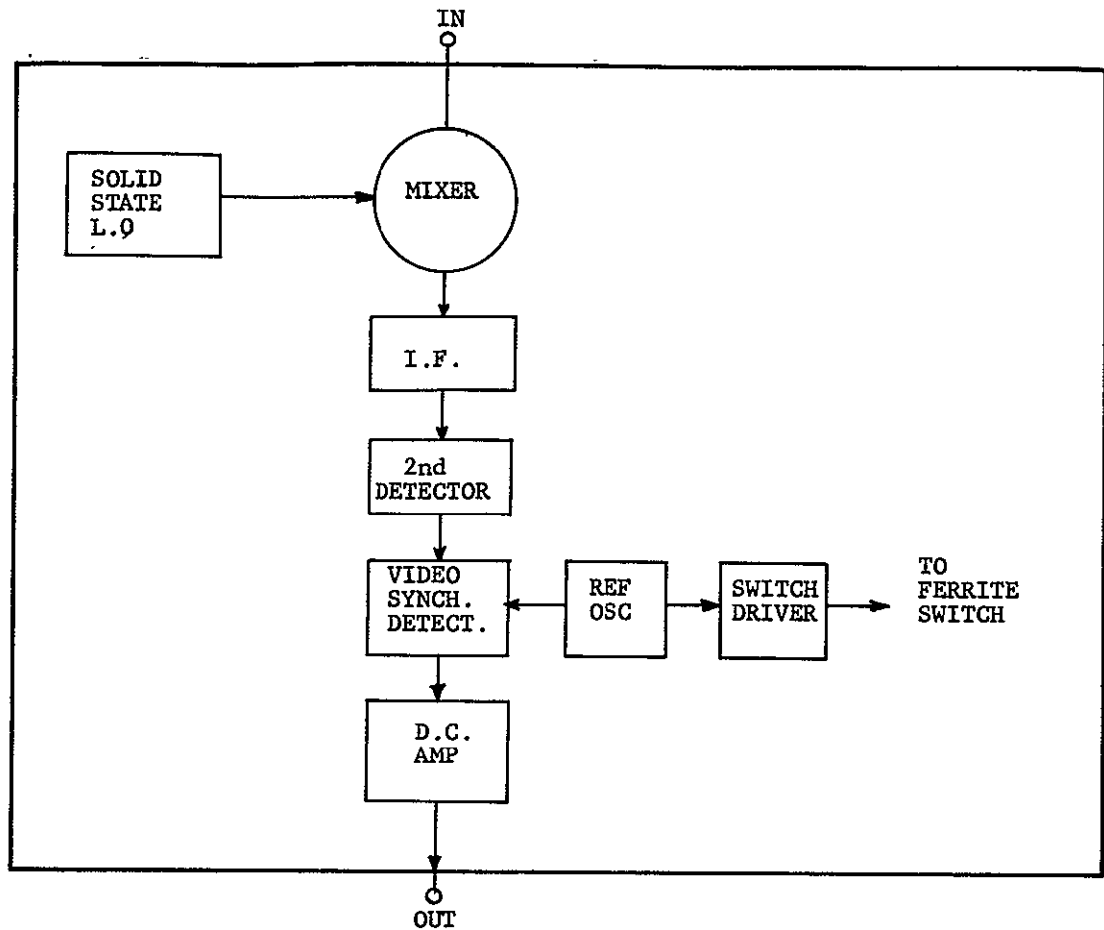


FIGURE 4.1-3  
TYPICAL RADIOMETER CHANNEL BLOCK DIAGRAM

#### 4.1.2 Environmental Signal Level Summary

No specific potential sources of interference were found in the IRAC or ITU lists for the five frequencies planned for the microwave spectrometer. Table 4.1-2 shows the allocated uses of the bands containing these frequencies. The notes used in Table 4.1-2 follow.

##### NOTES:

- 410 - The frequency 22.125 GHz is designated for industrial, scientific and medical purposes. Emissions must be confined within the limits of  $\pm 125$  MHz of that frequency. Radio-communication services operating within those limits must accept any harmful interference that may be experienced from the operation of industrial, scientific and medical equipment.
- 412A - In Bulgaria, Cuba, Hungary, Poland, the United Arab Republic, Roumania, Czechoslovakia and the U.S.S.R., the band 31.3-31.5 GHz is also allocated to the fixed and mobile services.
- US74 - The radio astronomy service shall be protected from extra-band radiation only to the extent such radiation exceeds the level which would be present if the offending station were operating in compliance with the technical standards or criteria applicable to the service in which it operates.
- US1000 - In the Additional Protocol to the Final Acts of the Space EARC, Geneva, 1963, a declaration on behalf of the USA states that the USA cannot accept any obligation to observe the exception claimed by Cuba in those footnotes to the Table of Frequency Allocations which were adopted by the EARC and which specifically name Cuba.

#### 4.1.3 Interference Evaluation and Analysis

Although no specific sources of interference were found in the lists consulted, international footnote 401 from the Radio Regulations, Geneva, 1959, included in 4.1.2 explains that 22.125 GHz  $\pm 125$  MHz is designated for industrial, scientific and medical purposes. Since the

IIT RESEARCH INSTITUTE

TABLE 4.1-2

FREQUENCY ALLOCATIONS

FREQUENCY GHz	BAND GHz	INTERNATIONAL ALLOCATION	UNITED STATES ALLOCATION	NOTES
22.2	22.0-23.0	Fixed. Mobile.	Gov't., Fixed. Mobile.	410
31.46	31.3-31.5	Radio Astronomy	Gov't., Non-Gov't.	412A, US74 & 100
53.65	above 40	Not Allocated	Gov't., Non-Gov't.	Experimental and Amateur
60.82	above 40	Not Allocated	Gov't., Non-Gov't.	Experimental and Amateur
64.47	above 40	Not Allocated	Gov't., Non-Gov't.	Experimental and Amateur

receiver bandwidth of Experiment 7 is 200 MHz, the 22.2 GHz radiometer could record emissions in the 22.1 to 22.3 GHz frequency range. The emissions from the industrial and medical equipments are allowed to occupy 22.0 to 22.25 GHz resulting in the overlap shown in Figure 4.1-4. International note 410 is essentially a warning to other users that they must accept any harmful interference experienced in the region 22.125 to 22.250 GHz.

The Federal Communications Commission records indicate that no equipment has been type approved for use at 22.125 GHz. FCC Docket No. 18294, August 1968, discusses the possible shift of the Industrial Scientific and Medical allocation to the band 22-24.25 GHz is one of a set of proposed re-allocations to accommodate communication-satellite service between 17.7 and 23 GHz for a satellite-to-earth path. Based on the above information the frequency range of 22.1 to 22.3 GHz should be free of interference at the present time but the possibility of either industrial or satellite use of this frequency range exists for the future.

International note 412A indicates that several countries have allocated 31.3 to 31.5 GHz to fixed and mobile services although this band is regarded as a radio astronomy band by the U.S. The extent of potential interference arising from fixed and mobile users in Bulgaria, Cuba, Hungary, Poland, United Arab Republic, Roumania, Czechoslovakia and the U.S.S.R. is unknown.

Although no specific emitters are known to exist at any of the frequencies selected for this experiment, the effective radiated power (ERP) for an earth based transmitter to produce a threshold signal in the radiometer at Nimbus altitude is calculated below.

$$P_T = L - G_R + R_S$$

where  $P_T$  = ERP in dBw for earth emitter for threshold signal

$$L = \text{propagation loss} = 20 \log f(\text{MHz}) + 20 \log d(\text{miles}) + 37$$

$$G_R = \text{radiometer antenna gain} = 20\text{dB}$$

$$R_S = \text{radiometer sensitivity} = -86\text{dBm} = -116\text{dBw}$$

For  $f = 22.2$  GHz and  $d = 690$  statute miles,

IIT RESEARCH INSTITUTE

$$P_T = 180.6 -20 -116$$

$$P_T = 44.6 \text{ dBw} = 28.8 \text{ KW}$$

For  $f = 64.47 \text{ GHz}$  and  $d = 690 \text{ statute miles}$ ,

$$P_T = 189.8 -20 -116$$

$$P_T = 53.8 \text{ dBw} = 240 \text{ KW}$$

Due to the large propagation losses for the frequencies involved it has been shown that large ERP's would be required to achieve threshold levels at the radiometer. Consideration of a possible emitter on a satellite at a synchronous altitude of 22,000 miles requires an additional 30dB of ERP to achieve threshold. Additional protection is afforded the radiometer due to the orientation of its signal horns towards the earth. The reference horns pointed at cold sky possibly could be oriented towards a synchronous altitude satellite for brief periods of time but even at 22.2 GHz the ERP from an emitter on the satellite would have to be 58.8 KW to exceed the threshold level.

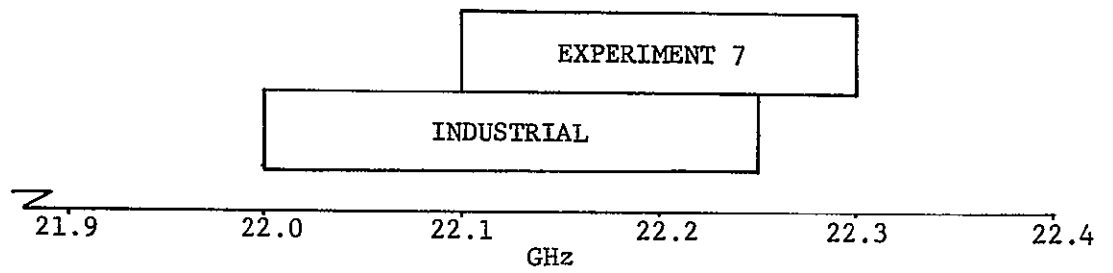


FIGURE 4.1-4

FREQUENCY OVERLAP OF EXPERIMENT 7, 22.2 GHz RADIOMETER AND  
INDUSTRIAL-MEDICAL ALLOCATION

## 4.2 Microwave Occultation Experiment (MICOC)

### 4.2.1 Purpose and Scientific Basis

This experiment is designed to flight test a coherent microwave satellite occultation system to demonstrate the ability of this system to provide the high-precision global pressure measurements essential to advanced weather prediction. The results of an earlier study indicated that a combination of passive microwave temperature sounding and the active occultation measurements showed the most promise of being able to acquire all of the needed atmospheric parameters remotely by satellite.

Two satellites will be placed in the same orbit but spaced so that radio waves from one to the other pass through the atmosphere. While in the atmosphere the radio waves propagate not with the speed of light,  $c$ , but with a reduced velocity,  $v$ , given by

$$v = cn$$

where,  $n$ , is the refractive index given by,

$$n = 1 - N \times 10^{-6}$$

and  $c$  is the speed of light. The modulus of refraction,  $N$ , is proportional to the air density and in the lower part of the atmosphere, to the air density and the water vapor.

The changes in refractive index have two effects on the radio waves. First, since the waves travel slower, the path appears to be longer; i.e., the waves take a longer time to traverse the path and there are more wavelengths along the path. The size of this effect is proportional to the integral of  $N$  along the ray path. Second, since the atmospheric density, and therefore  $N$ , decreases with altitude there is a gradient in refractive index perpendicular to the path. This causes a bending of the ray path by a small angle,  $\epsilon$  which is proportional to the integral of the normal derivative of  $N$  along the ray path. In getting from satellite to satellite the rays thus pass along a bent path that is longer than the path in a vacuum. These two effects combine to give a path length between satellites that is longer than the free space path length. The size of this total effect for a standard atmosphere has been calculated.



The radio system in the satellite is designed to measure the path length to very high precision. A continuous radio wave is transmitted from the master satellite to the repeater where it is retransmitted phase coherently back to the master. At the master it is received and compared with the transmitted frequency. Any difference in transmitted and received frequency is recorded on a counter in the master. One count is recorded for each wavelength change in the two-way path between satellites. At a frequency of 5 kHz each wavelength is 6 cm long giving the system a precision of 3 cm along the one-way path. Since the total effect of the atmosphere density is about 530 meters, the ultimate precision resolves the atmosphere to one part in 18,000.

In addition to the continuous signal, the master satellite also transmits a 3 MHz modulation signal to be repeated by the subsatellite. Measurement of the phase of the returned signal to  $4^\circ$  accuracy gives absolute range accuracy to about  $1/2$  meter on the one-way path.

In the proposed experiment a subsatellite carrying a radio repeater would be separated from the Nimbus satellite. The distance between satellites would be allowed to change slowly so that in many rotations around the earth,  $h$ , the minimum altitude of the ray between satellites would vary from hundreds of kilometers to zero altitude i.e., complete occultation. The Nimbus would record about once every 10 seconds the phase path length (a binary counter), the modulation phase, the signal amplitude, and the rms variation of phase and amplitude. These observations would be used in conjunction with weather data from the United States and Europe and with data from other Nimbus sensors.

The Microwave Occultation Experiment system parameters used in the interference evaluation are shown in Table 4.2-1. A block diagram of the system is shown in Figure 4.2-1.

#### 4.2.2 Environmental Signal Level Summary

A survey of the international and national frequency allocations regulations indicate that the band chosen for the Microwave Occultation Experiment is not allocated for the class of service for which it is to be used. The band of frequencies from 4400-4700 MHz is presently a government band for use by the Fixed, Mobile, and Communication-Satellite (Earth-to-satellite) services. The band from 4700-4990 MHz, also a government band, is

IIT RESEARCH INSTITUTE

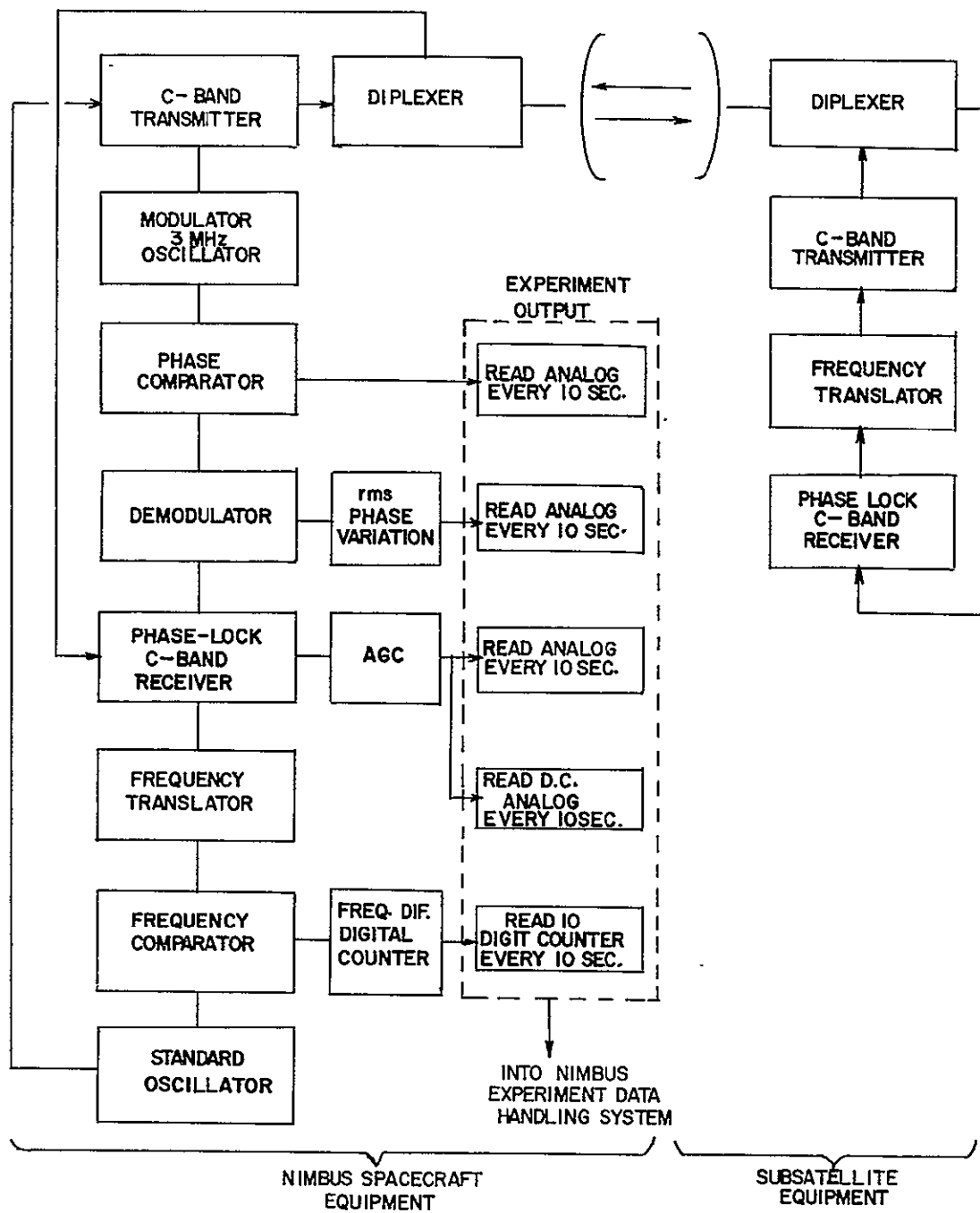


FIGURE 4.2-1

MICROWAVE OCCULTATION EXPERIMENT BLOCK DIAGRAM

TABLE 4.2-1  
EXPERIMENT 10, MICROWAVE OCCULTATION EXPERIMENT SYSTEM PARAMETERS

TRANSMITTER		RECEIVER		ANTENNA	
FREQUENCY	4.4-4.8 GHz	S/N	9.5dB	<u>NIMBUS</u>	
MODULATION	3 MHz Phase Modulation	NOISE FIGURE	12dB	TYPE	Parabolic Dish
POWER	500mw	SENSITIVITY	-132dBm	GAIN	29dB
		BANDWIDTH	1 KHz	<u>SUBSATELLITE</u>	
				TYPE	Parabolic Dish
				GAIN	8dB

allocated to the Fixed, and Mobile classes of service. Therefore, the experiment will have to share the band with existing equipments. A search of the IRAC and ITU files uncovered 2886 systems worldwide that operate in the band from 4400-4800 MHz. Figure 4.2-2 illustrates the spectrum occupancy and effective radiated powers in this band. Table 4.2-2 is an environmental signal summary listing the 15 systems exceeding the established noise threshold. A discussion of the impact of these 15 systems on the operation of the Microwave Occultation system is discussed next.

#### 4.2.3 Interference Evaluation and Analysis

The effects of the 15 potential interference sources shown in Table 4.2-2 on the Nimbus and subsatellite receivers of the Microwave Occultation experiment were evaluated assuming that this interference would cause one of the following degradation mechanisms in these receivers.

1. False signal acquisition.
2. Loss of phase lock of desired signal attributable to interference.
3. Excessive mean-square phase error when interference is present.

The first of these mechanisms might occur when a signal carrier or its modulation overlap in frequency, the sweep bandwidth of the phase-lock loop at a sufficiently high interference-to-noise ratio to be acquired by the loop. Since the loop will lose lock in the general operation of the experiment, and both Nimbus and subsatellite receivers are being equipped with an automatic sweep acquisition capability, it is well within reason that false lock-on is a potential problem. In general, a signal-to-noise ratio of 6dB or more is needed for acquisition, thus, this level will serve as the minimum interference-to-noise ratio below which, interference will not be considered capable of causing this interference mechanism. Using this threshold, 7 of the potential 15 interference sources of Table 4.2-2 are eliminated from further consideration. It should be emphasized that in addition to an interference-to-noise ratio of 6dB or more, the interference signal must be at a frequency within the sweep bandwidth of the receiver. It was necessary to estimate the magnitude of the sweep width parameter, since it was not made available to the

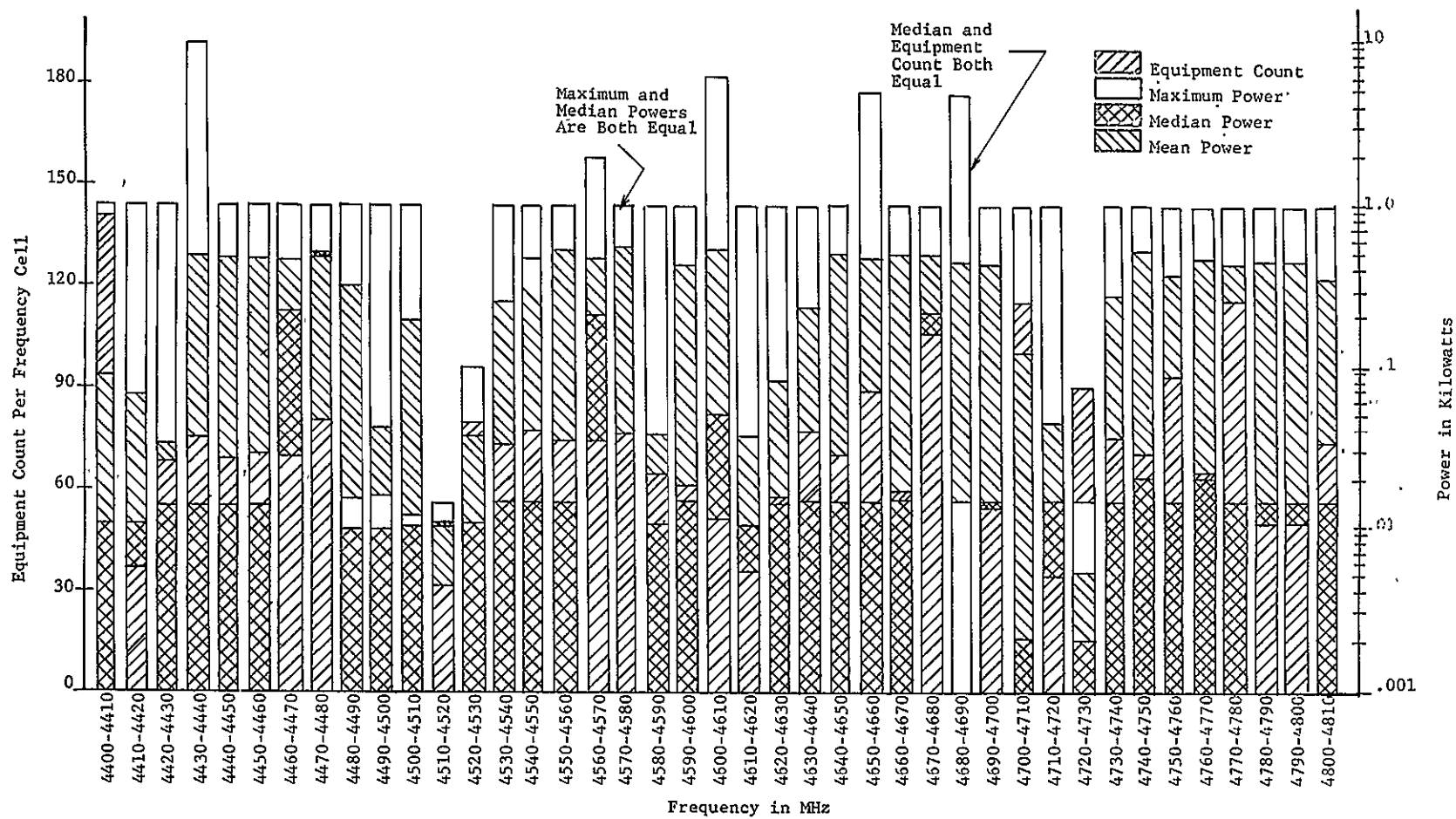


FIGURE 4.2-2

EXPERIMENT NO. 10 PRE-CULL SPECTRUM OCCUPANCY AND EFFECTIVE RADIATED POWER SUMMARY

TABLE 4.2-2

## ENVIRONMENTAL SIGNAL LEVEL SUMMARY FOR MICROWAVE OCCULTATION EXPERIMENT

ASSIGNED FREQUENCY MHz	STATE/ COUNTRY	STATION CLASS	CLASS OF EMISSION	EFFECTIVE RADIATED POWER, KW	dB ABOVE NOISE THRESHOLD
4478.0	Ala., USA	Mobile Station Exclusive Use Station Con- cerned	40F3	.5	5
4478.0	Ark., USA	"	40F3	.5	5
4478.0	Ky., USA	"	40F3	.5	5
4478.0	N.J., USA	"	40F3	.5	5
4400.0	Texas, USA	Experimental Research Station	.OP	1.0	24
4439.5	Md., USA	Coast Station	3.A7J	10	34
4460.2	Okla., USA	Fixed Station	100F3	1.0	4
4469.2	"	"	"	"	"
4478.2					
4496.2					
4521.4					
4526.8					
4539.4					
4566.4					
4511.8					
4589.8					
4607.0					
4631.8					
4637.2					
4674.4					
4679.8					
4697.0					
4715.0					
4730.2					
4735.6					
4748.2					
4764.4					
4769.8					
4787.8					
4805.8					
4500.0	N.Y., USA	Experimental Testing Station	.OAO	.01	4
4500.0	Ohio, USA	"	.OAO	.02	7
4700.0	"	"	"	"	"
4595.0	Colo., USA	Experimental Research Station	.OAO	1.0	24
4595.0	Colo., USA	"	"	.01	4
4600.0	Va., USA	Experimental Testing Station	.OAO	.04	10
4600.0	"	"	"	"	"
4685.0	Wash., USA	"	.OOP	.1	14
4750.0	Calif., USA	"	.OOAO	.15	16

IIT RESEARCH INSTITUTE

analysis team. This width, W was estimated from

$$W = R t_o \quad (4.2-1)$$

where  $R$  = the modulation rate transmitted between Nimbus and the subsatellite.  $R$  was taken at 3 MHz/sec.

$t_o$  = the round trip propagation time between the Nimbus and subsatellite, taken at a distance relating to occultation. The distance between the two satellites at occultation was assumed to be 5580 statute miles.

For the assumed and extracted values, W was computed to be 180 KHz. A value of 200 KHz was henceforth assumed for the sweep width.

Based on the assumed sweep-width and a look at the operating frequencies of those emitters in Table 4.2-2 whose interference-to-noise ratio is in excess of 6dB, we are lead to believe that even if one were to choose one of these frequencies to operate on, only a single emitter would be the cause of interference. In this unusual instance, the maximum exposure time to interference during a single orbital pass would be approximately 20 minutes. The maximum percent time that the satellite would experience interference above threshold for a twenty four hour period is approximately 7 percent.

The second of these interference mechanisms might occur as the result of an interference signal decreasing the equivalent loop signal-to-interference ratio to such a point as to result in the loss of desired signal lock. It is known that in general, a CW or narrowband signal may cause a degradation in loop signal-to-noise ratio of roughly 3dB for every 6dB of interference power above the noise power level. If we assume that the loop will lose lock when the signal-to-noise ratio drops to 0dB, then, when the loop is operated at approximately 9dB, then interference signals somewhere in the neighborhood of 18dB above the noise will cause the loop to unlock. A look at Table 4.2-2 indicates that there are 3 emitters capable of causing this type of interference mechanism. Again, since these emitters will not affect the occultation receivers simultaneously, the maximum exposure time and percent times are as calculated before.

The third of these interference mechanisms might occur as a result of the interference signal causing a mean-square phase error in the loop in excess of the tolerable phase measurement accuracy needed in the experiment. The needed phase accuracy was taken to be 4 degrees. The mean-square phase error caused by CW or narrowband interference such as those systems shown in Table 4.2-2 may be estimated by assuming a small frequency difference to exist between the interfering signal and desired signal, so that the phase term  $\gamma$  is tracked by the loop. The mean-square value of  $\gamma$ ,  $\overline{\gamma^2}$  is approximately

$$\overline{\gamma^2} \approx \frac{1}{2} \frac{I}{S} \quad (4.2-2)$$

where  $\frac{I}{S}$  = the interference-to-signal power ratio

For a mean-square phase error of 4 degrees, the interference-to-signal ratio becomes -9.5dB. Thus, for an operating signal-to-noise ratio of 9.5dB, the level of interference-to-noise ratio that will result in phase errors of this magnitude is approximately 0dB. Thus, each system shown in Table 4.2-2 is capable of producing errors of this magnitude.

A frequency chart indicating those frequencies within the 4.4-4.8 GHz band where the Microwave Occultation Experiment may operate without being interfered with is shown as Figure 4.2-3. The recommended frequencies were based on a tolerable interference-to-noise ratio of 0dB and a frequency separation between desired and undesired signals of 200 KHz.



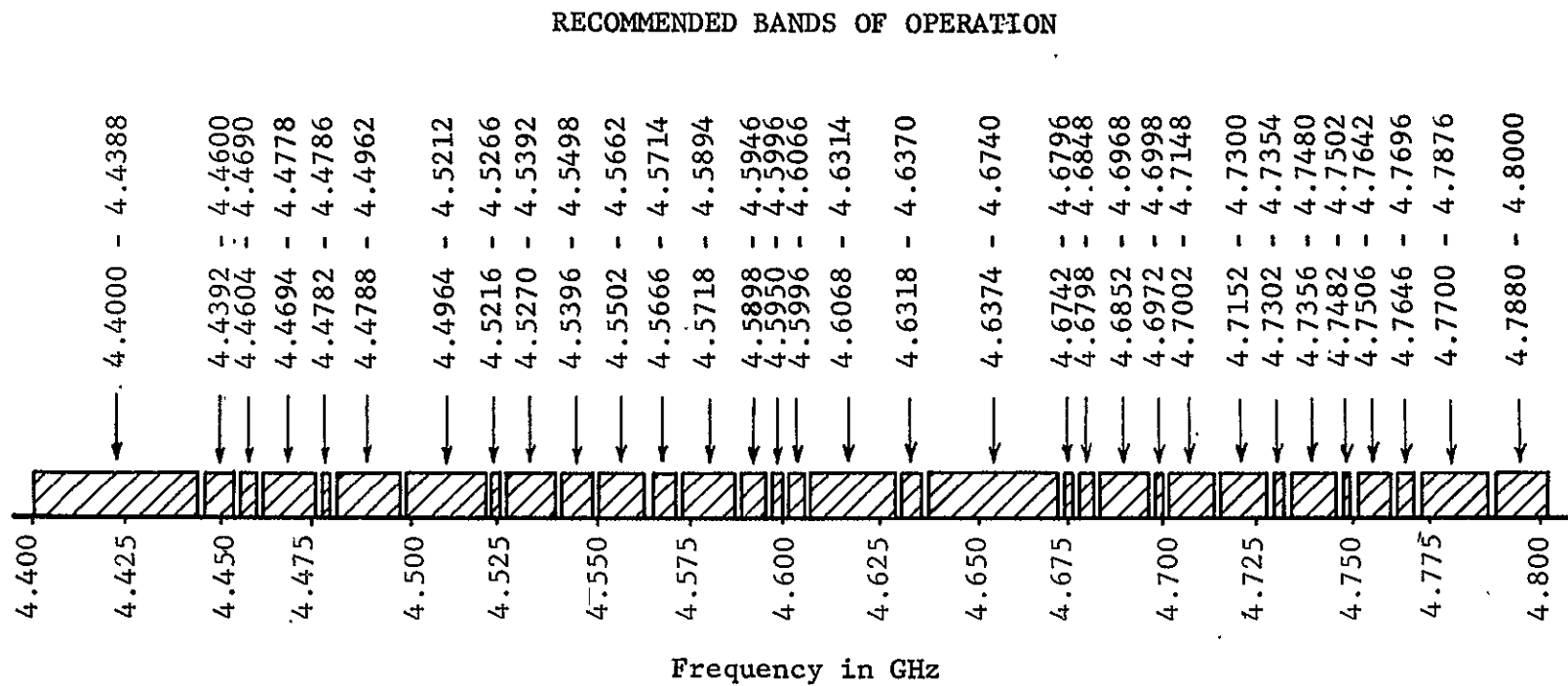


FIGURE 4.2-3

RECOMMENDED FREQUENCIES FOR THE OPERATION OF THE MICROWAVE OCCULTATION EXPERIMENT

### 4.3 Electrically Scanning Microwave Radiometer for Mapping Earth Radiation and Cloud Structure (ESMR)

#### 4.3.1 Purpose and Scientific Basis

The objective of this experiment is to map globally and contiguously the thermal radiation emitted by the earth's surface and by the atmosphere at a wavelength of approximately 1.55 cm. The measured absolute intensity of this radiation and, in particular, the mapped radiation patterns reflect a number of important physical properties of the surface and meteorological conditions in the atmosphere. Over water, brightness temperatures measured by the satellite in the nadir direction will vary between 120 and 240°K depending primarily on the thickness and liquid water content of the overlying clouds. Heavy rain clouds which, for example, may be indistinguishable in the visible or infrared from cirrus or stratus clouds containing little liquid water will be easily identified and tracked at this wavelength.

For the purpose of this experiment, a microwave radiometer was designed to make precise measurements of the intensity of thermal radiation at a wavelength of 1.55 cm (a frequency of 19.35 GHz). The narrow beam of the phased-array antenna is scanned electrically in one dimension through an angle of  $\pm 50^\circ$  with respect to the normal to the array and perpendicular to the direction of motion of the satellite, so that the radiometer builds up an image of the earth as the satellite advances. Spatial resolution is a major consideration for this experiment. It is determined strictly by the antenna. The present antenna covers an area of 46 x 46 cm. This permits an angular beam width of  $2.85^\circ$ . From a height of 1000 km, an area element of 50 x 50 km will thus be resolved.

Since the objectives of the experiment are to make the observations of thermal radiation from the earth's surface, and from heavy clouds, it is desirable to choose the wavelength at which the radiometer will operate such that emission from atmospheric gases is minimized. The strongest gaseous emitters of microwave radiation in the earth's atmosphere are  $O_2$  and  $H_2O$  at 0.5 cm and 1.35 cm, respectively. Also, the longer the wavelength (in the range from about 0.8 to 8 cm), the more pronounced will be the distinction between heavy cumulus clouds consisting of large water droplets and fog or stratus clouds, containing smaller droplets.

Another consideration which led to the particular choice of 1.55 cm (19.35 GHz) was that interference with

IIT RESEARCH INSTITUTE

ground-based radar systems becomes an important consideration at wavelengths longer than 2 cm (frequencies below 15 GHz). The Geneva Conference of 1963 (Smith-Rose 1964) allocated in this region two channels for radio-astronomy, one from 15.35 to 15.40 GHz, and the other from 19.30 to 19.40 GHz. The first channel overlaps the 9th harmonic of the Nimbus S-band telemetry system. Since ground-based interference is likely to become an ever more serious problem during the years ahead, it was decided to center the experiment at 19.35 GHz, even if the bandwidth of the instrument spilled over the reserved channel, since noisy radar sets are not likely to be located close to the reserved channel's edge. Figure 4.3-1 is a block diagram of the electrically scanning radiometer. The system characteristics are given in Table 4.3-1.

#### 4.3.2 Environmental Signal Level Summary

No sources of potential interference were found in the ITU or IRAC frequency assignment lists.

#### 4.3.3 Interference Evaluation and Analysis

Although no potential sources of interference were identified as would be expected in the 19.3 to 19.4 GHz band now allocated to radio astronomy, the following pertinent comments were extracted from FCC Docket No. 18294.

"The commission and the Director of Telecommunications Management (DTM), anticipating an early Space WARC and being of the view that accommodation above 10 GHz must be found for the communication-satellite service for use in the decade ahead, examined the current usage of the radio spectrum between 10 and 40 GHz, as well as its projected usage for the foreseeable future. This examination resulted in the conclusion that the existing and projected loading between 10 and 17.7 GHz is such as to generally preclude accommodation of the wide-band requirements of the communication-satellite service on an exclusive basis. However, it appeared that that service could be accommodated between 17.7 and 23 GHz for the satellite-to-earth path and in either of the bands 27.525 - 31.3 GHz or 38.6 - 40 GHz (and up) for the earth-to-satellite path. This conclusion assumed some adjustment in band limits for Government and non-Government allocations and assumed also that suitable alternative accommodation could be found for the radio astronomy service now allocated 19.3 - 19.4 GHz; the amateur service now allocated 21-22 GHz and the

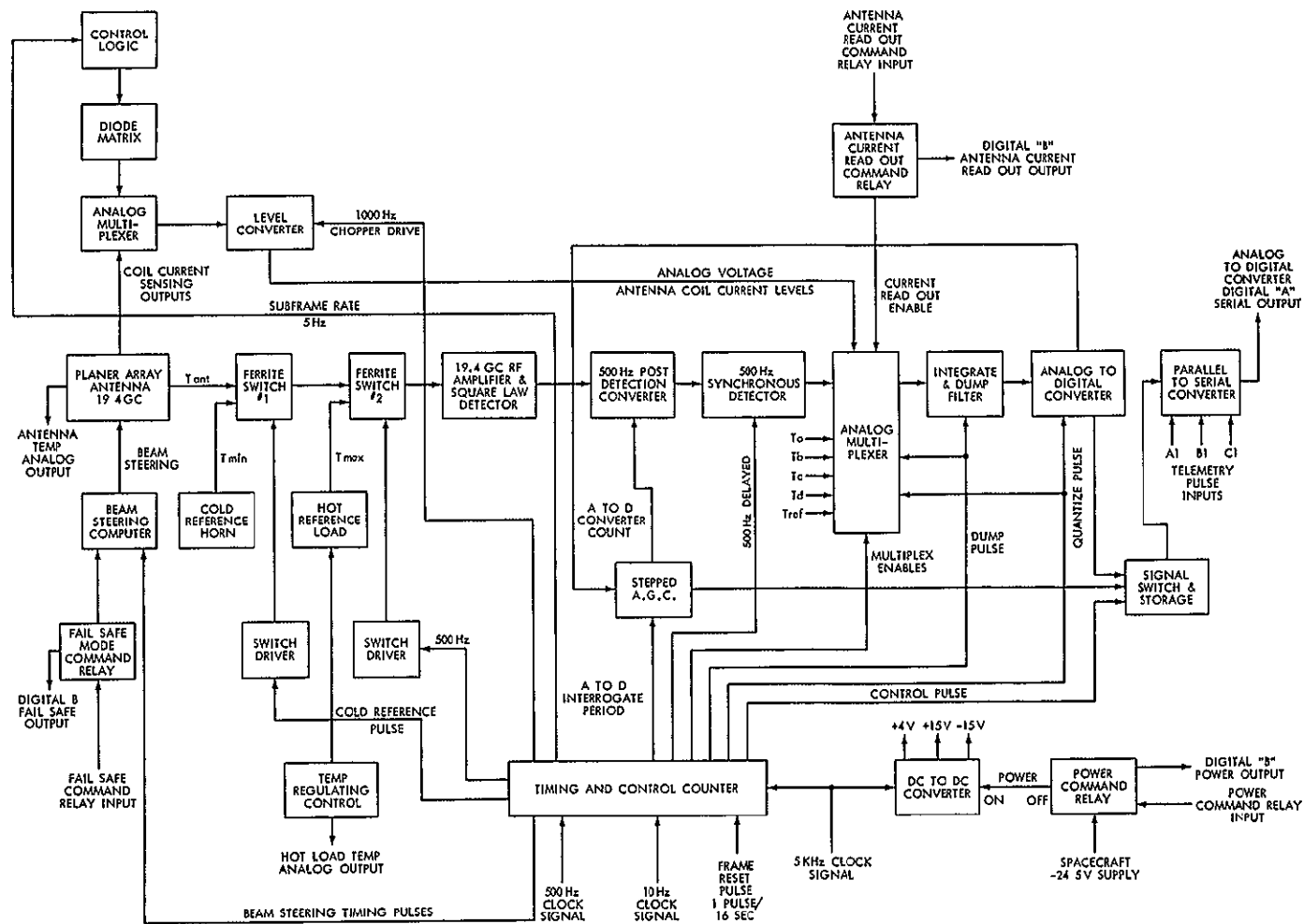


FIGURE 4.3-1

BLOCK DIAGRAM OF ELECTRICALLY SCANNING RADIOMETER

TABLE 4.3-1

EXPERIMENT 12, ELECTRICALLY SCANNING MICROWAVE RADIOMETER  
FOR MAPPING EARTH RADIATION AND CLOUD STRUCTURE SYSTEM CHARACTERISTICS

RECEIVER		ANTENNA	
FREQUENCY	19.35 GHz	TYPE	Electrically scanning phased array
BANDWIDTH	RF 600 MHz IF N.A.	GAIN	36 dB
SENSITIVITY	-81 dBm	BEAMWIDTH	2.85°
INTEGRATION TIME	25 millisec.	SCANS	±50° in 2 secs.
TYPE	Radiometer		
T =	1000°		

Industrial, Scientific and Medical (ISM) designation at  $22.125 \pm .125$  GHz, all of which now enjoy world-wide allocation status. Our records indicate that throughout the world there is but one radio astronomy observatory making use of the band 19.3 - 19.4 GHz and that one is an installation operated by the U.S. Government. Since the band is used for continuum rather than spectral line observations, its ultimate reallocation should pose no problem."

Obviously, the proposed changes to accomodate the communication-satellite service in the next decade could affect the 19.3 to 19.4 GHz radio astronomy band but for the next few years it should remain interference free.

The effective radiated power  $P_T$  of an earth emitter necessary to create an above threshold signal at the radiometer is

$$P_T = L - G_R + R_S$$

where  $P_T$  = ERP in dBw for earth emitter

$$\begin{aligned} L &= \text{propagation loss} \\ &= 20 \log f(\text{MHz}) + 20 \log d \text{ miles} + 37 \end{aligned}$$

$$G_R = \text{radiometer antenna gain} = 36\text{dB}$$

$$R_S = \text{radiometer sensitivity} = -81\text{dBm} = -111\text{dBw}$$

For  $f = 19.35$  GHz and  $d = 690$  miles,

$$P_T = 179.5 - 36 - 111$$

$$P_T = 32.5\text{dBw} = 1.78 \text{ KW}$$

If the emitter is located on a satellite at synchronous altitude an additional 30dB of ERP is required to create a threshold level signal at the Nimbus radiometer.

#### 4.4 Satellite Microwave Radiometry to Sense the Surface Temperature of the World Oceans (MICRAD)

##### 4.4.1 Purpose and Scientific Basis

The objective of the proposed experiment is to measure sea surface temperature over the entire world ocean on a semi-diurnal all-weather schedule with a thermal resolution better than  $1^{\circ}\text{K}$  absolute and  $0.1^{\circ}$  relative and a spatial resolution of 270 nautical miles. This will be accomplished by means of a passive microwave radiometer at 2.7 GHz.

Currently, our knowledge of the sea surface temperature is based on historic data updated by reports from weather ships, research vessels and on reports gathered from naval and commercial ships of opportunity. In well traveled areas this produces a reasonably detailed estimate of recent thermal conditions, and the daily and seasonal departures from normal. On the other hand, there are vast areas of the ocean from which virtually no current temperature data is available so that heavy reliance must be placed on historic information. Although conditions in such uninhabited areas do not affect maritime activities directly, they are breeding grounds of storms, biological activity and many other events important to man.

Presently these remote oceanic areas can be monitored by Tiros and Nimbus satellites by means of infrared sensors. Since infrared radiation is strongly absorbed by water vapor, only such data as can be obtained from cloud-free areas is available. Consequently, in regions that are commonly obscured by clouds, the sampling frequency is very low. In addition, some of the infrared radiometers employed only gather data during the dark hours. For a retrograde polar orbit these hours represent considerably less than half the day and the data is heavily biased toward nighttime conditions.

A microwave radiometer of suitable design operating in the S-band region will yield a "brightness temperature" record from which the true molecular temperature can be calculated, without interruption by ordinary stratus clouds that overlie much of the ocean. Clouds associated with heavy rainfall will still interfere but these are not generally of long persistence in a single location. Such a (nearly) allweather system would provide data not presently available by economically feasible means.

The chief limitation on a microwave radiometer system installed in a Nimbus satellite is that the spatial resolution obtainable is low. Because of size and weight constraints imposed by the small dimension of the Nimbus vehicle, the

IIT RESEARCH INSTITUTE

antenna that can be used gives a  $25^\circ$  cone angle at the required wavelength. From an orbit altitude of 600 miles this gives a "footprint" of 270 miles diameter. The radiometer system consists basically of a Dicke radiometer modified for gain stabilization and continuous calibration. To obtain the required temperature resolution the RF bandwidth is determined to be approximately 140 MHz, which is easily accomplished with tunnel diode amplifiers. The noise must be amplified to give a level 20 dB above the tangential sensitivity of the square law detector which is about -60dBm. With an expected input to the RF amplifiers of -87 dBm, an RF amplifier gain of 47 dB is required. This can be accomplished with 3 tunnel diode stages. A block diagram of the proposed system is shown in Figure 4.4-1.

The frequency chosen for this experiment includes the portion of the S-band allotted for radio astronomy, 2.69 to 2.70 GHz.

The use of astronomical bands is advantageous, since by international agreement, they have been set aside for scientific use and will be free from radar and other sources of radio frequency interference.

Since the bandwidth required for the specified accuracy is greater than the bandwidth of the radio astronomy channel, portions of adjacent channels must be included in the radiometer, thus the radiometer bandwidth will be arbitrarily set at 2.69-2.83 GHz.

The above choice of operating frequency is dictated by the following two requirements. First, the system must operate in all weather conditions. Propagation through the atmosphere in the S-band region is relatively unaffected by the presence of water vapor, clouds and rain.

Second, calculations have been made, which show that the apparent sea temperature is very nearly directly proportional to its molecular temperature. However, at frequencies above S-band, it turns out that the emissivity becomes temperature dependent in such a way as to tend to reduce the apparent temperature variation. In fact, at about 19 GHz the apparent temperature becomes almost independent of molecular temperature in the interesting range from 0-30°C. Thus, frequencies near 19 GHz would be unsuited for the measurement of molecular temperatures. The system characteristics are given in Table 4.4-1.



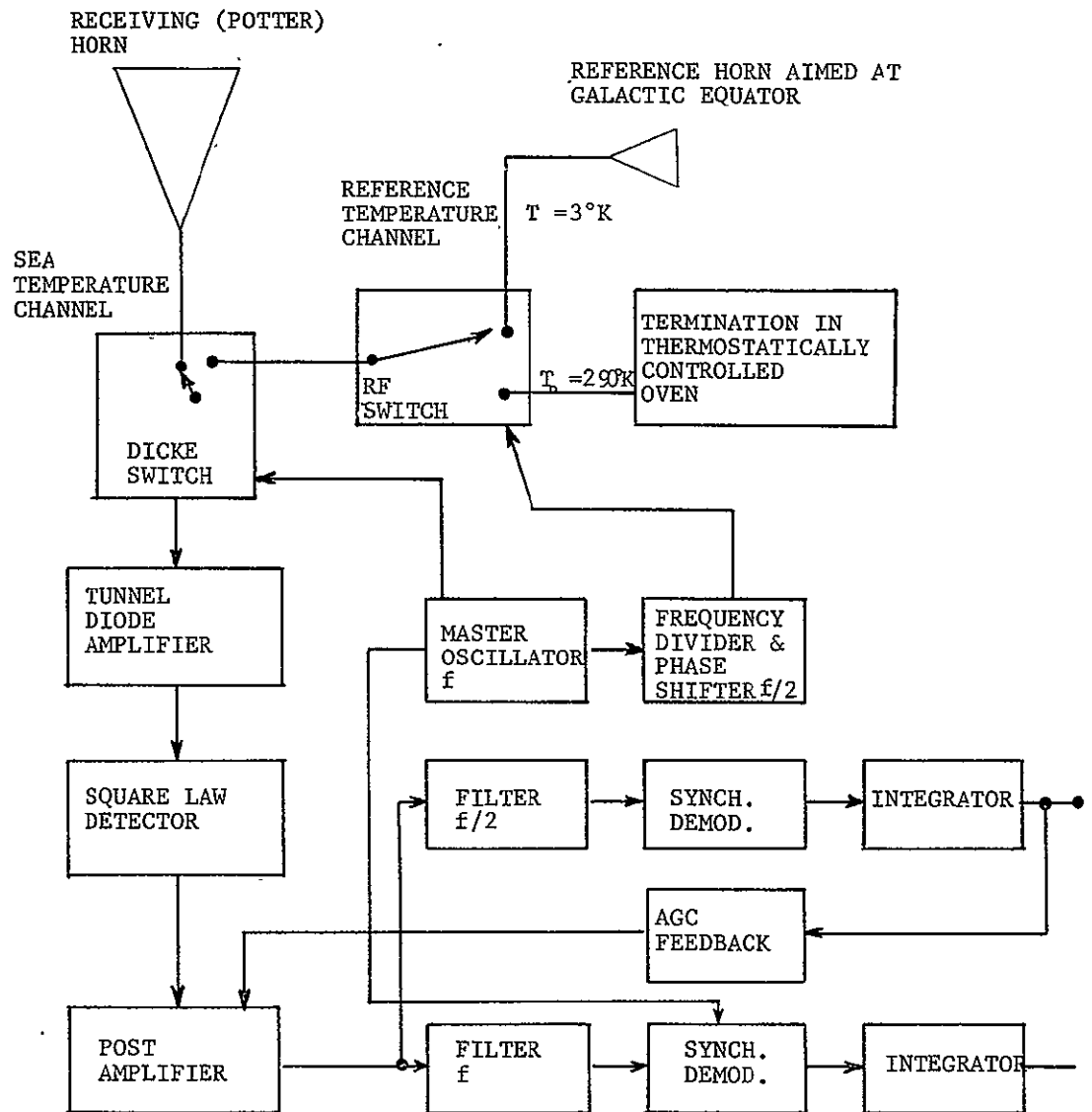


FIGURE 4.4-1

BLOCK DIAGRAM OF SEA SURFACE TEMPERATURE RADIOMETER

TABLE 4.4-1

EXPERIMENT 13 SATELLITE MICROWAVE RADIOMETRY TO SENSE THE SURFACE  
TEMPERATURE OF THE WORLD OCEANS CHARACTERISTICS

RECEIVER		ANTENNA	
FREQUENCY	2.7 GHz	TYPE	Potter Horn (Sig) Diagonal " (Ref)
BANDWIDTH	RF 140 MHz IF N.A.	GAIN	15 dB
SENSITIVITY	-87 dBm	BEAMWIDTH	25°
INTEGRATION TIME	1.5 Sec.		

#### 4.4.2 Environmental Signal Level Summary

Although the band 2.69 to 2.70 GHz is reserved for radio astronomy, the radiometer of Experiment 13 has a bandwidth set at 2.69 to 2.83 GHz. Examination of the frequency lists disclosed 705 potential interference sources at 2.70 GHz as shown in Figure 4.4-2. The emitters are weather radars, height finders such as AN/FPS-6's and other pulse modulated equipments located throughout the United States.

#### 4.4.3 Interference Evaluation and Analysis

Application of the analysis procedure of Section 3.4 resulted in the culling out of only 36 emitters, leaving 669 emitters as potential sources of interference. Further, applying the analysis procedure of Section 3.5 resulted in the interference region plotted in Figure 4.4-3.

The objective of the experiment to measure the sea surface temperature over the entire world ocean could be slightly impaired by the pulsed emission levels above the radiometer threshold over a substantial portion of the world as shown on the map, Figure 4.4-3.

It is recommended that the radiometer bandwidth be moved down in frequency so that the upper end does not extend above 2700 MHz. Examination of Figure 4.4-2 shows that according to the IRAC and ITU lists, the interference problem will be solved by placing the 140 MHz required bandwidth of the radiometer between 2.56 GHz and 2.70 GHz. Most of the equipments listed at 2.7 GHz are actually spread out above 2.7 GHz depending upon the frequency of the magnetron in use. The applicable international frequency allocations are 2550-2690 MHz, Fixed and Mobile; 2690-2700 MHz, Radio Astronomy; and 2700-2690 MHz, Aeronautical Radionavigation and Radio-location. High power pulse type equipments would not be found in the 2550-2690 MHz band. Therefore the radiometer could be operated in the 140 MHz band from 2.56 GHz to 2.70 GHz and it is recommended that the change be made to ensure the successful acquisition of the required data.

If the frequency is not moved as recommended, the above noise threshold regions plotted on the map of Figure 4.4-3 will yield 45 minutes as the maximum orbit intercept time during one orbit and a maximum percent of time in a 24 hour period of 33.6%.

IIIT RESEARCH INSTITUTE

Based on peak pulse power, the above threshold values for the 669 emitters ranged between 2 and 25dB with a median of 13dB. All of the 669 emitters are pulse equipments and for typical pulse widths and pulse repetition frequencies encountered with height finders and weather radars the duty cycles will range between .001 and .01. Based on these duty cycles the average power will be in the range of 30 to 20dB less than the peak power and because the radiometer has a 1.5 second integration time any average power above threshold will cause degradation of the radiometer measurements. A total of 129 emitters were found with peak powers between 21 to 25dB above noise threshold which would result in an average power range of 1 to 5dB above threshold if the duty cycles of the emitters are all .01. The actual duty cycles are not known and the worst case was assumed. For the .001 duty cycle the average power would fall below the radiometer threshold for all known emitters. Based on a duty cycle of .01, (worst case) average power above threshold (degradation criteria) can occur for a maximum of 22 minutes for a single orbit and for 9% of a 24 hour period if the frequency is not changed from 2.69 - 2.83 GHz to 2.56 - 2.70 GHz as recommended.

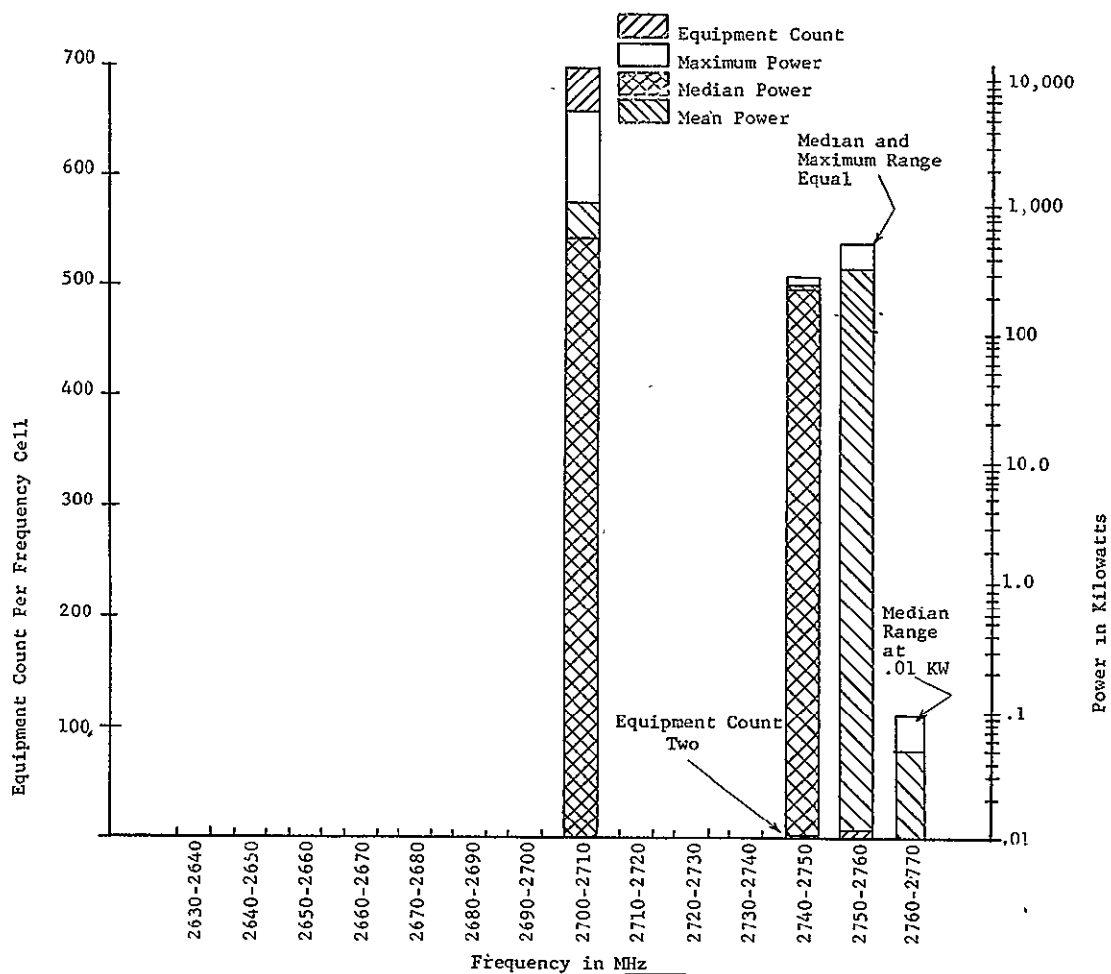


FIGURE 4.4-2

EXPERIMENT NO. 13 PRE-CULL SPECTRUM OCCUPANCY AND EFFECTIVE.  
RADIATED POWER SUMMARY

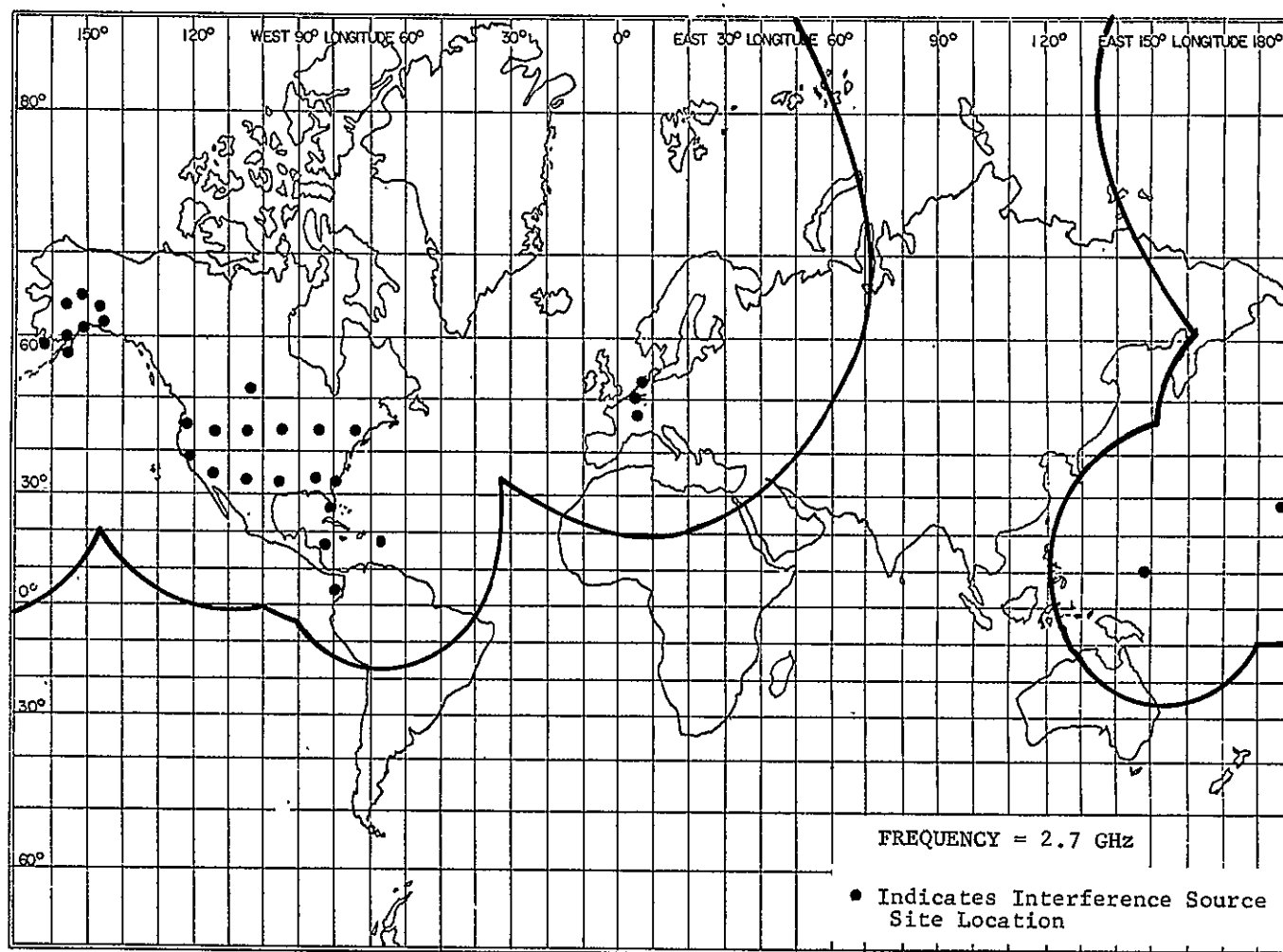


FIGURE 4.4-3  
PLOT OF INTERFERENCE REGION FOR SATELLITE MICROWAVE RADIOMETRY TO SENSE THE  
SURFACE TEMPERATURE OF THE WORLD OCEANS (MICRAD) EXPERIMENT

## 4.5 Global Radar for Ocean Waves and Winds (GROW)

### 4.5.1 Purpose and Scientific Basis

A side looking radar scatterometer will be used to collect data from which the wind speed at the surface of the world's oceans will be predicted, using the Nimbus-E spacecraft. These measurements serve as input to a computer program, together with surface observations, wind and wave histories for the preceding period, and data from satellite cloud photographs, and will be used to determine the wind field and the waves over the entire ocean on a synoptic basis.

The scatterometer will also be operated at times over land and over the polar ice. Because of its gross resolution (somewhat comparable to a microwave radiometer) the overland measurements will be restricted to such uses as determining melt zones in the Arctic, establishing major rain patterns in previously dry regions, and keeping track of major features of the polar ice.

The scatterometer operates by measuring the radar cross-section of a patch of ocean. The cross-section is governed, at the radar frequency chosen, primarily by the portion of the wave spectrum due to the local wind field. Hence, the observed value can be used to establish the wind speed.

The GROW system parameters used in the interference evaluation are shown in Table 4.5-1.

The scatterometer proposed for the GROW application uses a frequency modulated intermittent continuous wave modulation to provide the required range resolution. A block diagram of the system is shown in Figure 4.5-1. The transmitted signal is a linearly frequency modulated 7 millisecond pulse. The frequency within the pulse has a 3 MHz linear deviation from the 3 GHz carrier. The ocean swath illuminated by the scatterometer therefore returns a signal whose time-frequency coordinates determine a range resolution cell. The receiver has a listening period of approximately 14 milliseconds. The return signal is heterodyned down to a frequency band of 2 to 6 MHz in mixer number 2 by a signal determined by the signal generator and the offset oscillator. The signal generator continues to provide a signal

III RESEARCH INSTITUTE

TABLE 4.5-1

EXPERIMENT 14, GLOBAL RADAR FOR OCEAN WAVES AND WINDS SYSTEM PARAMETERS

TRANSMITTER		RECEIVER		ANTENNA	
Frequency	3000 MHz	Output S/N	16 dB	Type	Parabolic Cylinder Dipole Feed
Modulation	FM ICW	Dynamic Range	50 dB	Size	7' x 1'
Peak Power	200 watts	Noise Figure	4 dB	Gain	27.5 dB
Average Power	50 watts	Sensitivity	-123 dBm	Pattern	Cosecant Squared
Pulse Width	7 ms	Range Resolu- tion	20 km	Beamwidth	20° x 2.4°
Frequency Deviation	3.0 MHz	Integration Time	1 sec.		



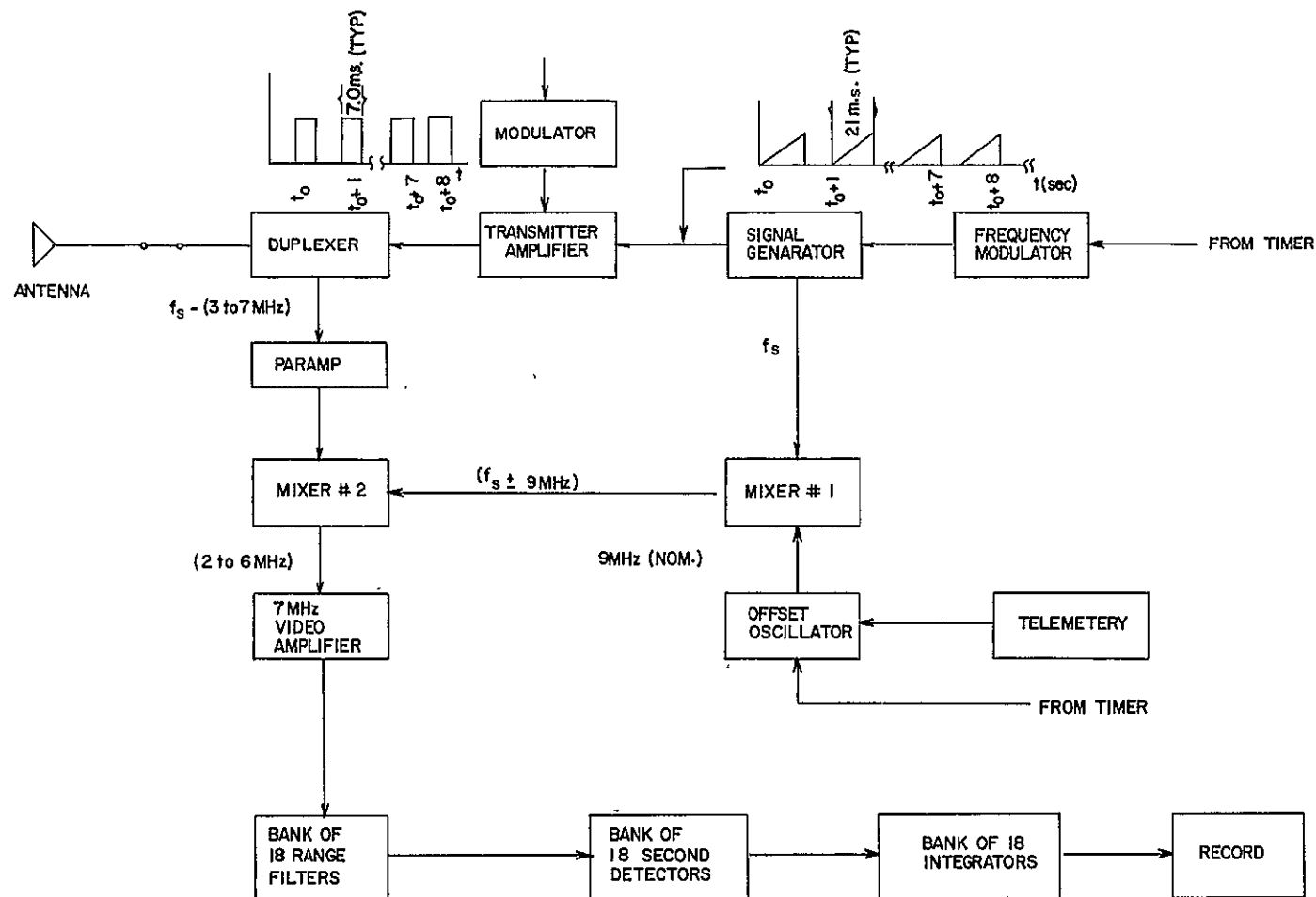


FIGURE 4.5-1

GROW SYSTEM BLOCK DIAGRAM

to mixer number 1 even after the pulse transmission is completed, for the entire pulse repetition period of approximately 21 milliseconds. The signal output from mixer number 2 is then amplified in a 7 MHz bandwidth video amplifier and sent through a range filter bank of 18 filters. These filters correspond to the 18 resolution cells per swath per sweep. The bandwidth of each of these filters is determined by the difference in slant range to the closest and farthest bounds of each resolution cell and range from approximately 19 KHz to 38 KHz in bandwidth. The signal output from each of these filters is detected, integrated over a 1 second period and then recorded.

#### 4.5.2 Environmental Signal Level Summary

A survey of the international and national frequency allocations regulations indicate that the 3 GHz frequency chosen for the GROW experiment is not allocated for the class of service for which it is to be used. The band of frequencies from 2900-3100 MHz is presently allocated to the Radionavigation and Radiolocation services on a worldwide basis and to the Maritime Radionavigation and Radiolocation services on a U.S. basis. Thus, the scatterometer if it is to be used in this band at all, will have to share the band with existing equipments. A search of the IRAC and ITU files uncovered 25 systems worldwide that operate nominally in the band from 2995-3005 MHz. Figure 4.5-2 illustrates the spectrum occupancy and effective radiated powers in this band. As shown in the figure, 23 out of the total of 25 equipments uncovered were reported as operating at 3 GHz. Table 4.5-2 is an environmental signal summary listing the 18 systems exceeding the established noise threshold. A discussion of the impact of these 18 systems on the operation of the GROW system is discussed next.

#### 4.5.3 Interference Evaluation and Analysis

The susceptibility of the GROW receiver to interference was based on the assumption that the interference would cause one or both of the following mechanisms to occur.

1. Range filter output amplitude biasing causing an error in radar cross-section prediction.

III RESEARCH INSTITUTE

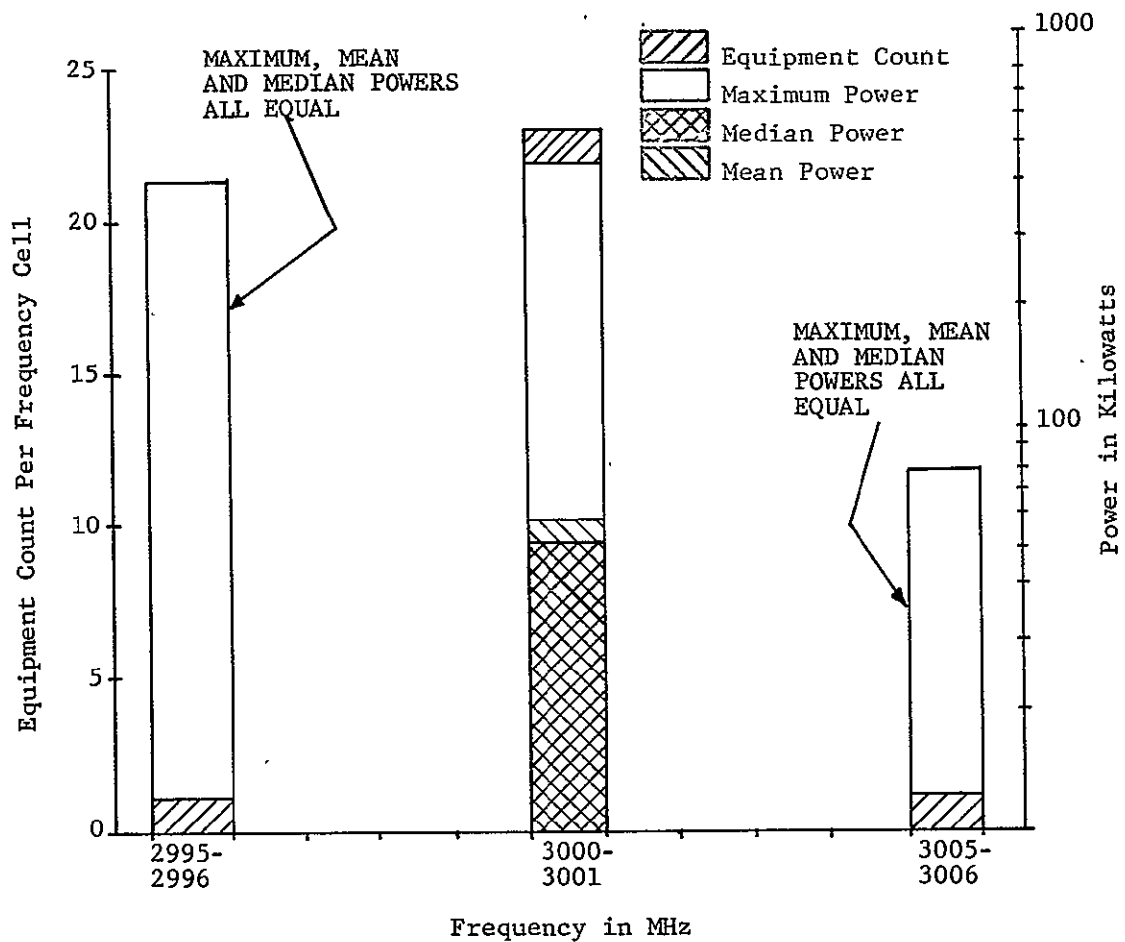


FIGURE 4.5-2

EXPERIMENT NO. 14 PRE-CULL SPECTRUM OCCUPANCY AND EFFECTIVE  
RADIATED POWER SUMMARY

TABLE 4.5-2

ENVIRONMENTAL SIGNAL LEVEL SUMMARY FOR GROW EXPERIMENT

ASSIGNED FREQUENCY MHz	STATE/ COUNTRY	STATION CLASS	CLASS OF EMISSION	EFFECTIVE RADIATED POWER, KW	dB ABOVE NOISE THRESHOLD
3000.0	New Zealand	Radiolocation Mobile Station	24000 PO	70	10
3000.0	Australia	Aeronautical Radionavigation Land Station/ Non-Directional Radiobeacon	PO	.5	7
3000.0	Luxembourg	Radiolocation Mobile Station	7000 PO	450.0	18
3000.0	Calif./USA	Radiolocation Mobile Station	PO	50.0	27
3000.0	Calif./USA	Radiolocation Mobile Station	PO	60.0	28
3000.0	Calif./USA	Radiolocation Mobile Station	PO	50.0	27
3000.0	Calif./USA	Radiolocation Mobile Station	PO	60.0	28
3000.0	Calif./USA	Radiolocation Mobile Station	PO	50.0	27
3000.0	Calif./USA	Radiolocation Mobile Station	PO	60.0	28
3000.0	Calif./USA	Radiolocation Mobile Station	PO	50.0	27
3000.0	Calif./USA	Radiolocation Mobile Station	PO	60.0	28
3000.0	N.J./USA	Radiolocation Mobile Station	PO	50.0	27
3000.0	N.Y./USA	Radiolocation Mobile Station	PO	50.0	27
3000.0	Wash./USA	Radiolocation Mobile Station	PO	50.0	27
3000.0	Guam	Radiolocation Mobile Station	PO	60.0	28
3000.0	Calif./USA	Experimental Testing Station	AO	.015	2
3000.0	Calif./USA	Experimental Testing Station	AO	.015	2
3000.0	Wash./USA	Experimental Testing Station	PO	.1	1

## 2. Erroneous range filter output due to natural signal heterodyning.

The first of these mechanisms occurs when a desired and undesired signal are present simultaneously in one of the 18 range filters resulting in an output whose amplitude is incorrectly biased by the interference. Since the range filter output is directly proportional to the radar cross-section estimate and this estimate will be used to predict the wind speed, the interference will have a biasing influence on these predictions as well. Figure 4.5-3 illustrates the relationship between radar cross-section and wind speed. The interference threshold was established for this mechanism by assuming that a 5 knot or less error could be tolerated in the recorded data. It was further assumed that this error could be brought about in the worst case by a 5dB error in radar cross-section measurements, an estimate based on the data in Figure 4.5-3. Assuming the scatterometer operates at a minimum signal-to-noise ratio of 16dB, then the maximum interference-to-noise ratio allowable to assure no more than a 5dB cross-section error is 5dB. This assumes that the peak envelope power of the desired signal and the average power of the interference signal add directly. The establishment of this threshold eliminates from consideration the last 3 systems presented in Table 4.5-2, reducing the total number of systems capable of causing the data biasing interference mechanism to 15.

It was noted at this time that all of the potential interference sources remaining were pulse modulated. Thus, an estimate had to be made of the effects of this intermittent versus continuous time signal on the GROW receiver and a determination of whether or not the effects of multiple potential interference sources were cumulative. It was decided to compute the number of radar pulses falling within any single range filter. Since each range filter is effectively gated on for a period proportional to its bandwidth, the largest bandwidth range filter, having a bandwidth of 38 KHz was used for these computations. The scatterometer signal generator sweeps at a rate of 400 MHz/sec, thus, the 38 KHz of bandwidth is sampled in .095 milliseconds. The problem was then to predict, in general, the number of pulses from a given number of radars falling within a .095 millisecond period. In this prediction, it was assumed that the pulse trains formed an ensemble as shown in Figure 4.5-4a and that the pulse start times were statistically independent random variables uniformly distributed in the interval  $(0, R_i)$ . The pulse recurrence times for each radar are

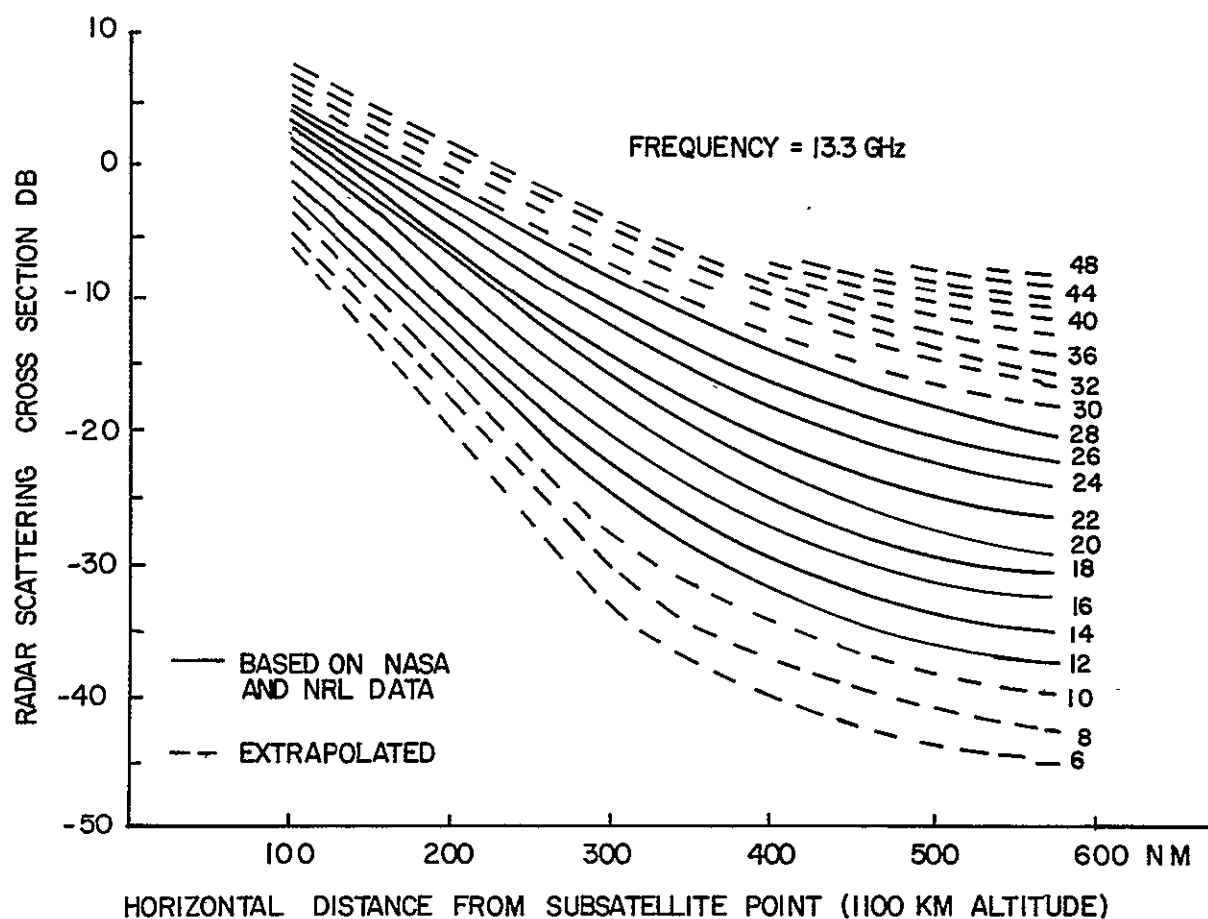


FIGURE 4.5-3  
RADAR SEA RETURN VERSUS DISTANCE CALIBRATED AGAINST WIND SPEED  
IN KNOTS FOR FULLY DEVELOPED SEAS

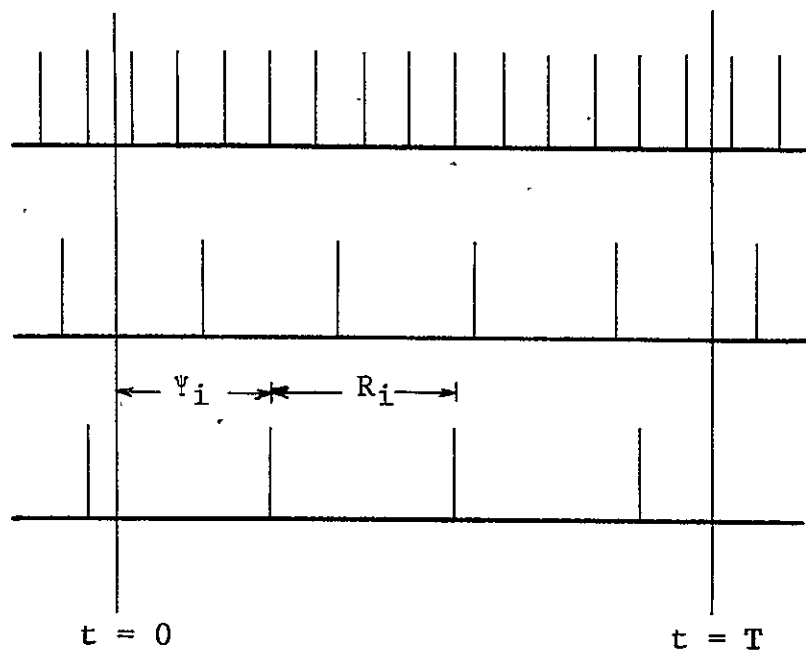


FIGURE 4.5-4a  
ENSEMBLE OF PERIODIC PULSE TRAINS

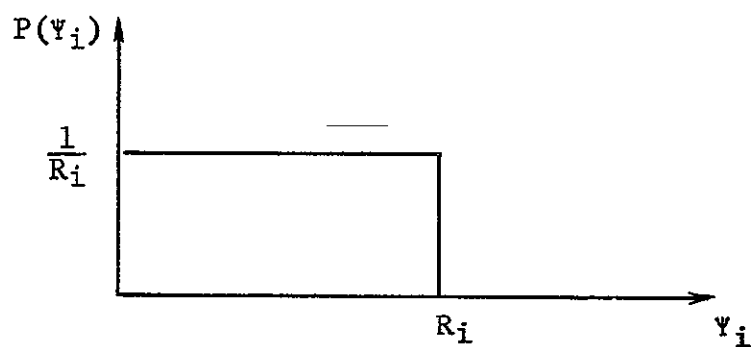


FIGURE 4.5-4b  
ASSUMED PULSE START TIME DISTRIBUTION

FIGURE 4.5-4  
STATISTICS OF PULSE TRAIN ENSEMBLE

designated by  $R_i$  and the width of each pulse has been assumed to have a negligible effect in these computations. The number of pulses,  $N(t)$  due to  $m$  pulse trains falling in any  $T$  interval of time, assuming that all radars are tuned to the same frequency is given by

$$N(t) = n_1(t) + n_2(t) + \dots + n_m(t) \quad (4.5-1)$$

where  $n_i(t)$  = the number of pulses due to the  $i$ th pulse train, falling any any  $T$  interval of time.

The probability distribution for the random variable  $n_i(t)$  is given by

$$P \left[ n_i(t) = k \right] = k + 1 - \frac{T}{R_i} \quad (4.5-2)$$

It also follows that

$$\begin{aligned} P \left[ n_i(t) = k + 1 \right] &= 1 - P \left[ n_i(t) = k \right] \\ &= \frac{T}{R_i} - k \end{aligned} \quad (4.5-3)$$

The expected or average number of pulses from a single radar in the  $T$  interval is given by

$$\begin{aligned} E \left[ n_i(t) \right] &= E \left[ n_i(t) = k \right] + E \left[ n_i(t) = k + 1 \right] \\ &= \sum_{k=0}^{\lambda-1} (k+1) P \left[ n_i(t) = k+1 \right] \\ &= \frac{T}{R_i} \end{aligned} \quad (4.5-4)$$

Since each of the random variables  $n_i(t)$  are statistically independent, their sum,  $N(t)$  has an expected value given simply by

$$E \left[ N(t) \right] = T \sum_{i=1}^m \frac{1}{R_i} \quad (4.5-5)$$

IIT RESEARCH INSTITUTE



This expected value not only assumes all of the radars to be tuned to the same frequency, but that the receiver is listening 100 percent of the time. To correct for the fact that the listening time duty cycle is only .667, the expected value estimate must be weighted by this factor. Thus,  $E[N(t)]$  becomes

$$E[N(t)] = .667T \sum_{i=1}^m \frac{1}{R_i} \quad (4.5-6)$$

Table 4.5-3 lists the expected values for several environmental sizes. A pulse recurrence rate of 250 pulses per second was assumed for each of the environmental emitters. Also shown in the table are the expected number of interference pulses after 50 integrations over a one second period.

Figure 4.5-5 shows a plot of the potential interference region for the GROW experiment based on the interference values shown in Table 4.5-2. Also shown in this figure (within the circles) are the numbers of emitters having a level above the GROW noise threshold and their respective geographical areas of influence. As noted, the maximum number of emitters having a simultaneous influence is ten. It was decided to carry on the analysis assuming this size environment to see whether the cumulative effects of interference after receiver integration could cause actual receiver degradation.

If ideal integration is assumed and an integration improvement factor of 400 is used, then the per pulse desired signal-to-noise ratio is computed as

$$\frac{S_1}{N_1} = \frac{S_{50}}{N_{50}} \frac{1}{nE_i(n)} \quad (4.5-7)$$

where  $\frac{S_1}{N_1}$  = the per pulse signal-to-noise ratio

$\frac{S_{50}}{N_{50}}$  = the signal-to-noise ratio after 50 pulse integrations

$nE_i(n)$  = the integration improvement factor

For a value of  $\frac{S_{50}}{N_{50}} = 16\text{dB}$ , the value of  $\frac{S_1}{N_1} = -10\text{dB}$ .

TABLE 4.5-3

PULSE COUNT STATISTICS FOR VARIOUS ENVIRONMENTAL SIZES

	Number of Environmental Emitters						
	1	2	3	4	8	9	10
Expected Number of Pulses (No Integration)	.0159	.0318	.0477	.0636	.1272	.1431	.1590
Expected Number of Pulses (50 Pulses Integrated)	.7950	1.5900	2.3850	3.1800	6.3600	7.1550	7.9500

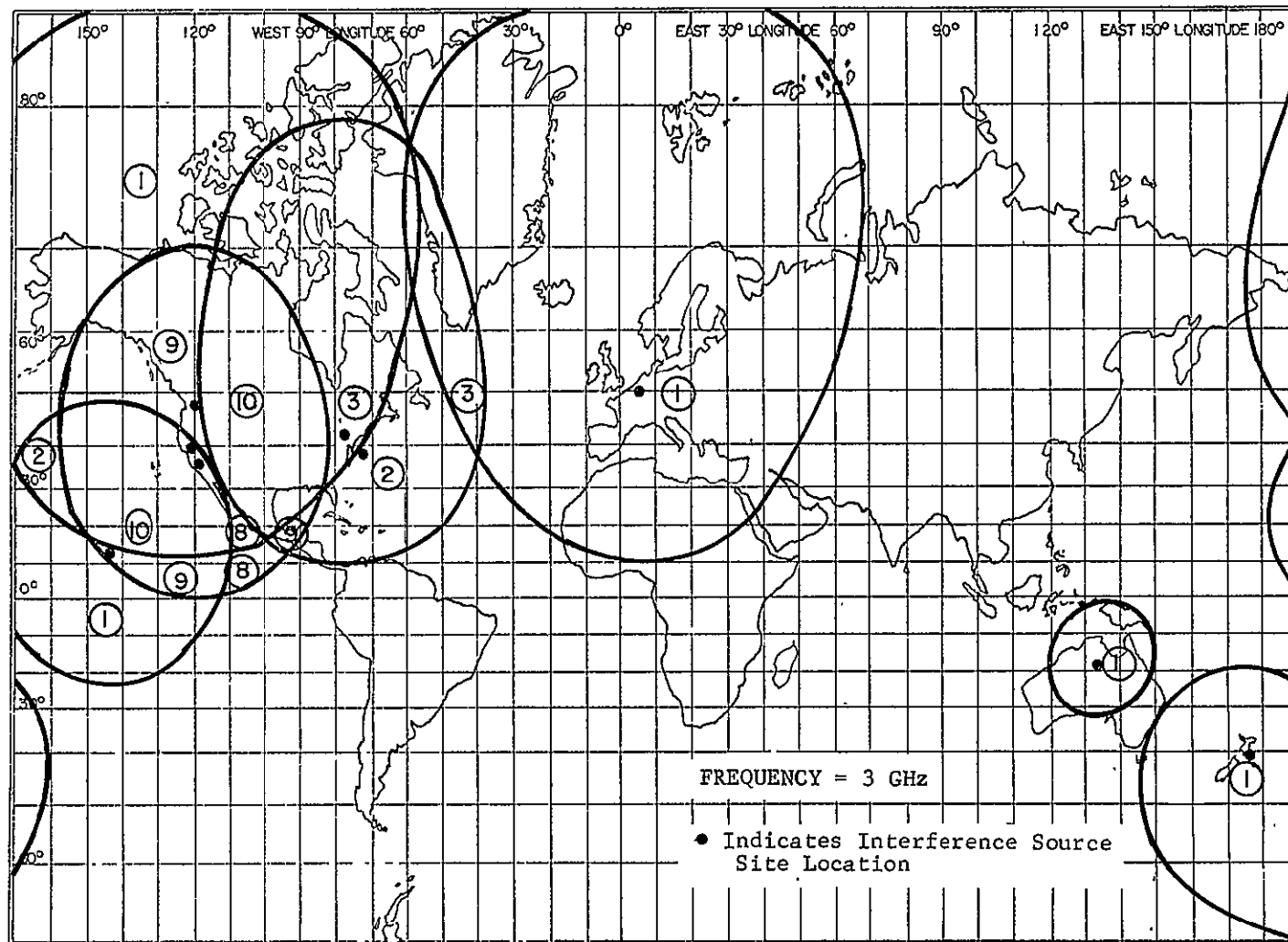


FIGURE 4.5-5  
PLOT OF POTENTIAL INTERFERENCE REGION FOR THE GROW EXPERIMENT

Since the highest interference-to-noise threshold ratio in Table 4.5-2 is 28dB, the maximum interference-to-signal ratio on a per pulse basis is  $I/S = 38\text{dB}$  or on a voltage basis  $I/S = 79.5$ . It was decided to use this relative voltage ratio to compute the signal error after degradation in the presence of interference pulses. Assuming that the ideal integrator voltage output was directly proportional to the area of its input voltage waveforms, the dB error after integration in the presence of interference pulses was computed using

$$\text{dB Error} = 20 \log \frac{\frac{I}{S} \times \epsilon \tau_I E[N(t)]_{\max} + 50\tau_D}{50\tau_D} \quad (4.5-7)$$

where  $\epsilon \tau_I$  = the effective pulse width of the interference signal.  $\tau_I$  was assumed to be 5μsec and  $\epsilon = 2$ .

$E[N(t)]_{\max}$  = the maximum number of expected pulses per T interval after 50 integrations.

$\tau_D$  = the effective desired signal pulse width, .095 ms

Substituting for the variables in Equation 4.5-7 yields

$$\begin{aligned} \text{dB Error} &= 20 \log \frac{(79.5)(10^{-5})(8) + 4.75 \times 10^{-3}}{4.75 \times 10^{-3}} \quad (4.5-8) \\ &= 7.4\text{dB} \end{aligned}$$

This amount of error in integration output, which as previously assumed is proportional to the error in radar cross-section and hence, wind speed, is considered too large to be negligible. This computation was carried out for the worst or largest environmental size. A similar estimate for each of the other environmental sizes is shown in Table 4.5-4. As shown in the table, an environmental size of 4 or less will result in less than a 5dB error, the assumed acceptable degradation level. A plot of the resultant interference region, that is, the satellite ground track locations where degradation above this level is predicted is shown in Figure 4.5-6. From this plot, the maximum exposure time to interference causing the stated amount of degradation during a single orbital pass was computed to be approximately 20 minutes.

TABLE 4.5-4

ENVIRONMENTAL SIZE VERSUS RADAR CROSS-SECTION DEGRADATION

	Number of Environmental Emitters						
	1	2	3	4	8	9	10
Radar Cross-Section Degradation (dB)	1.1	2.0	2.9	3.7	6.3	6.7	7.4

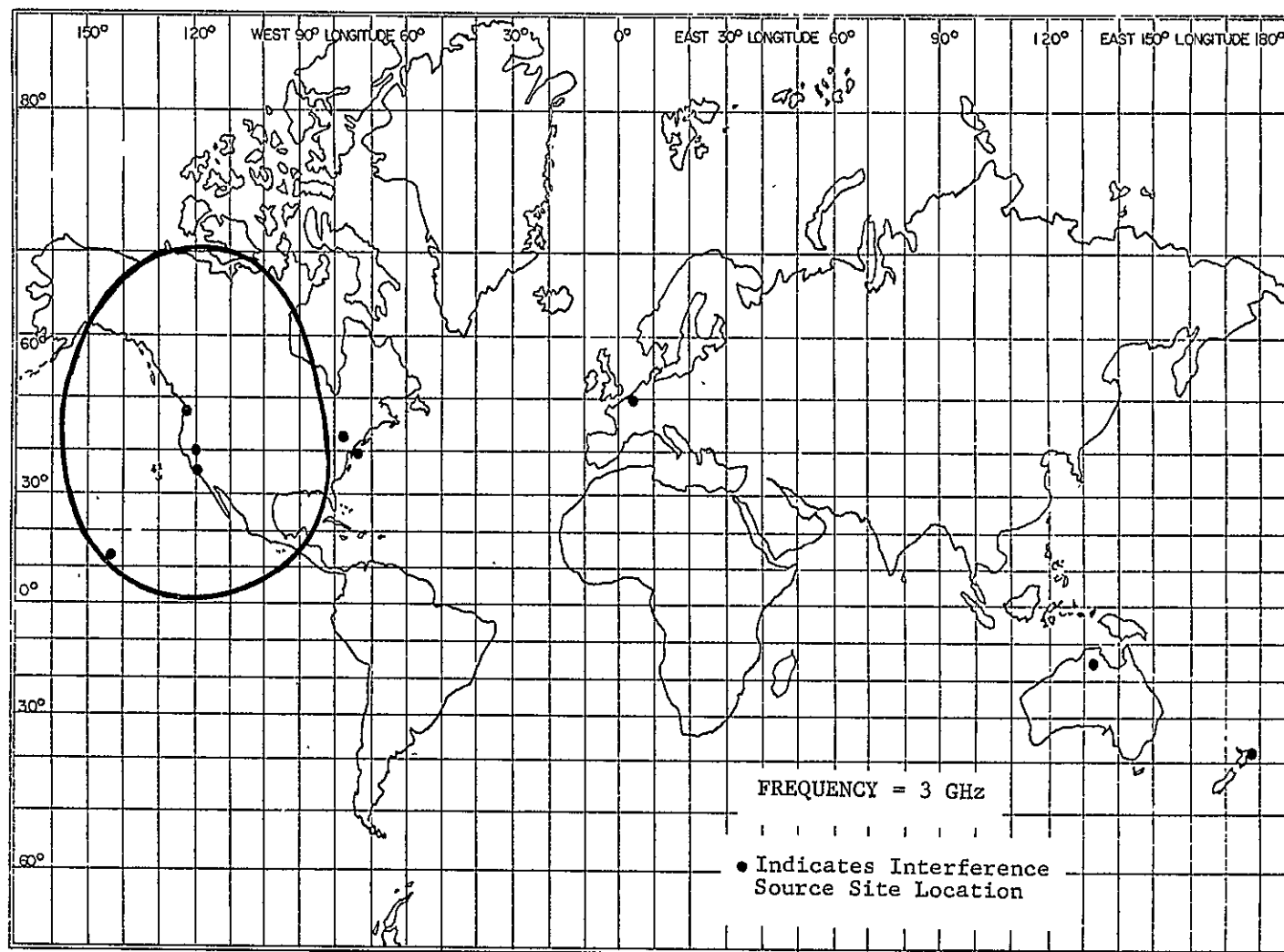


FIGURE 4.5-6  
PLOT OF INTERFERENCE REGION WHERE A 5dB DEGRADATION IN RADAR CROSS-SECTION MEASUREMENT IS PREDICTED

The maximum percent time that the scatterometer will experience interference above this threshold for a twenty four hour period was calculated to be approximately 7 percent. Based on this same result, the erroneous range filter output due to natural signal heterodyning interference mechanism is predicted to have no more serious effect on the GROW receiver as that caused by an error in radar cross-section measurement.

If some latitude in the tuned frequency of the GROW system is available it is possible, from Equation 4.5-7 and an available off-frequency rejection function, to recommend a new frequency, close to the 3 GHz frequency, that will result in negligible interference. This frequency was computed by first noting the worst dB error in the measured data, selecting a tolerable level of error, computing the level of interference-to-signal ratio necessary to yield this level, and then, from the applicable off-frequency rejection function determining the frequency offset from the on-tune case to yield the difference between those two I/S levels. From Table 4.5-3, the worst dB error predicted is approximately 8dB, resulting from an environment with a maximum interference-to-signal ratio of 38dB. If a 1dB tolerable error is selected, the interference-to-signal ratio computed from Equation 4.5-7 is approximately 18dB. Thus, a 20dB reduction in the interference level must be achieved by detuning the GROW receiver from 3 GHz. Based on the techniques discussed in Section 3, the frequency separation required to ensure this additional loss in interference power is approximately 1 MHz. It is recommended that the GROW receiver be tuned to 3001 MHz such that only negligible interference will occur.

## 4.6 Simplified Data Collection Experiment (DACOL)

### 4.6.1 Purpose and Scientific Basis

The Office of Hydrology of the United States Weather Bureau currently operates 8,000 river stations in the continental United States. These stations monitor river height and rainfall in remote locations; the data from these stations is collected either by leased land lines or, in some cases, by a manned inspection of the site. The proposed satellite data collection system would operationally provide twice a day contact with each of these river stations. The development of the system includes an initial feasibility demonstration using ten (10) remote platforms working with the Nimbus-E satellite. This can be expanded to handle up to 250 sensor stations per orbit. Operationally, the system could accommodate ten thousand sensor platforms in the United States plus many thousands throughout the world.

The experiment proposed for Nimbus moves a step closer to complete system feasibility by operating from ten, low cost sensor platforms with the design constraints to be imposed on a fully operational system accommodating 10,000 sensor platforms. This is an important consideration since the critical problems in such a system are sensor access time, and data handling time at the central ground station. In particular, to service 10,000 sensor platforms in the United States (3300 platforms per pass) from an orbiting satellite, with an overhead time of six minutes, each platform is allocated an average of 0.1 seconds total contact time. In this time the platform is interrogated, and transmits its identifier and previously collected data from its sensors. Figure 4.6-1 is a block diagram of the spacecraft Data collection system. The system characteristics are given in Table 4.6-1.

### 4.6.2 Environmental Signal Level Summary

A total of 695 emitters make up the environment of potential interference sources to the receiver for the simplified data collection experiment. The nature of the environment is shown in Figure 4.6-2. The frequency range of 450 to 470 MHz is internationally designated as fixed mobile and in the U.S., the FCC has allocated blocks of this frequency range to various land mobile users such as public safety, industrial and land transportation.



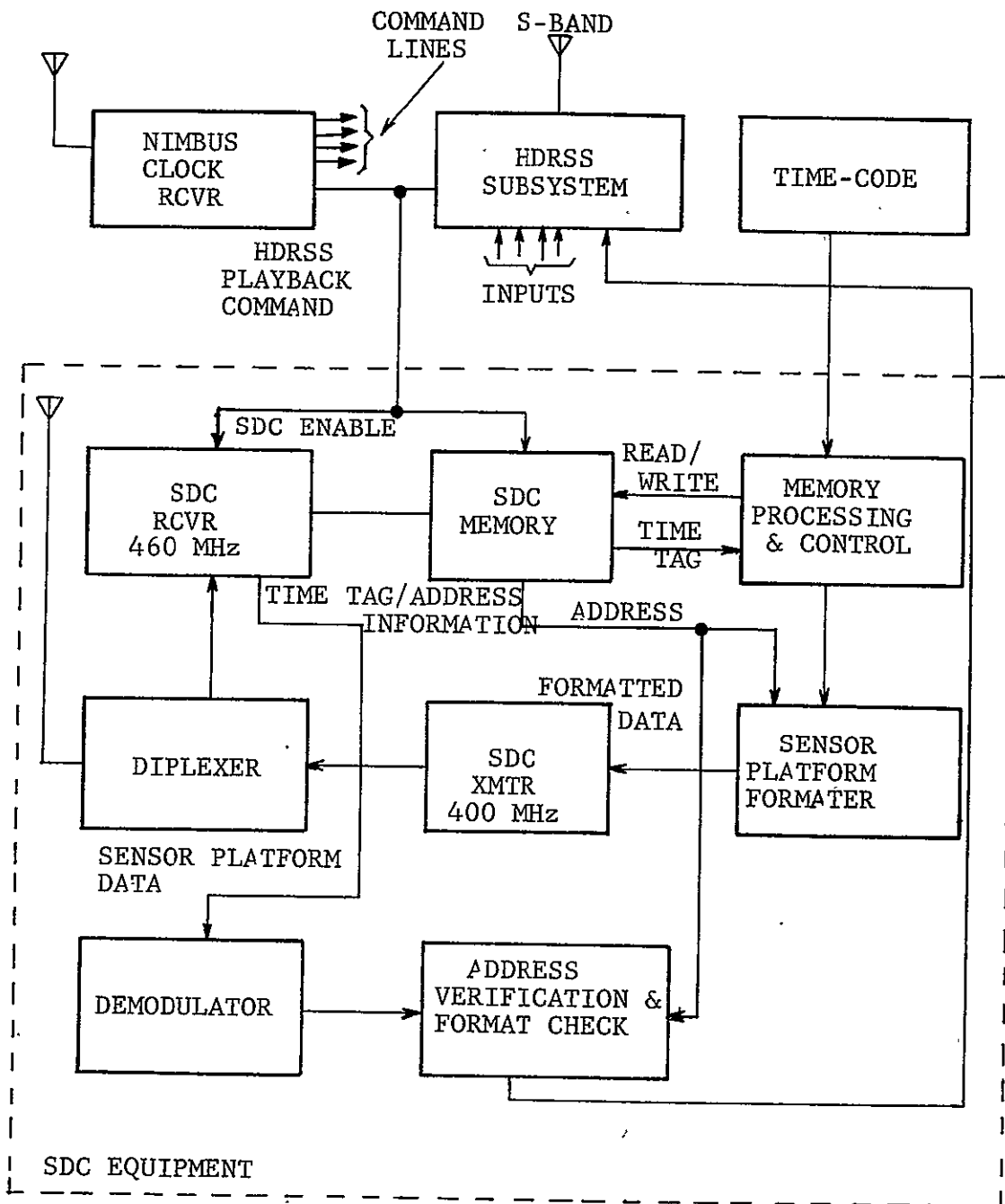


FIGURE 4.6-1

SPACECRAFT DATA COLLECTION BLOCK DIAGRAM

TABLE 4.6-1

EXPERIMENT 26 SIMPLIFIED DATA COLLECTION  
EXPERIMENT CHARACTERISTICS

TRANSMITTER		RECEIVER	
FREQUENCY	460 MHz	FREQUENCY	460 MHz
BANDWIDTH	100 KHz	BANDWIDTH	RF
MODULATION	FM		IF 100 KHz
POWER	5 Watts	SENSITIVITY	-120dBm
LOCATION	Earth	LOCATION	Nimbus
ANTENNA GAIN	3dB	ANTENNA GAIN	3dB
		NOISE FIGURE	4dB
		S/N	+17dB

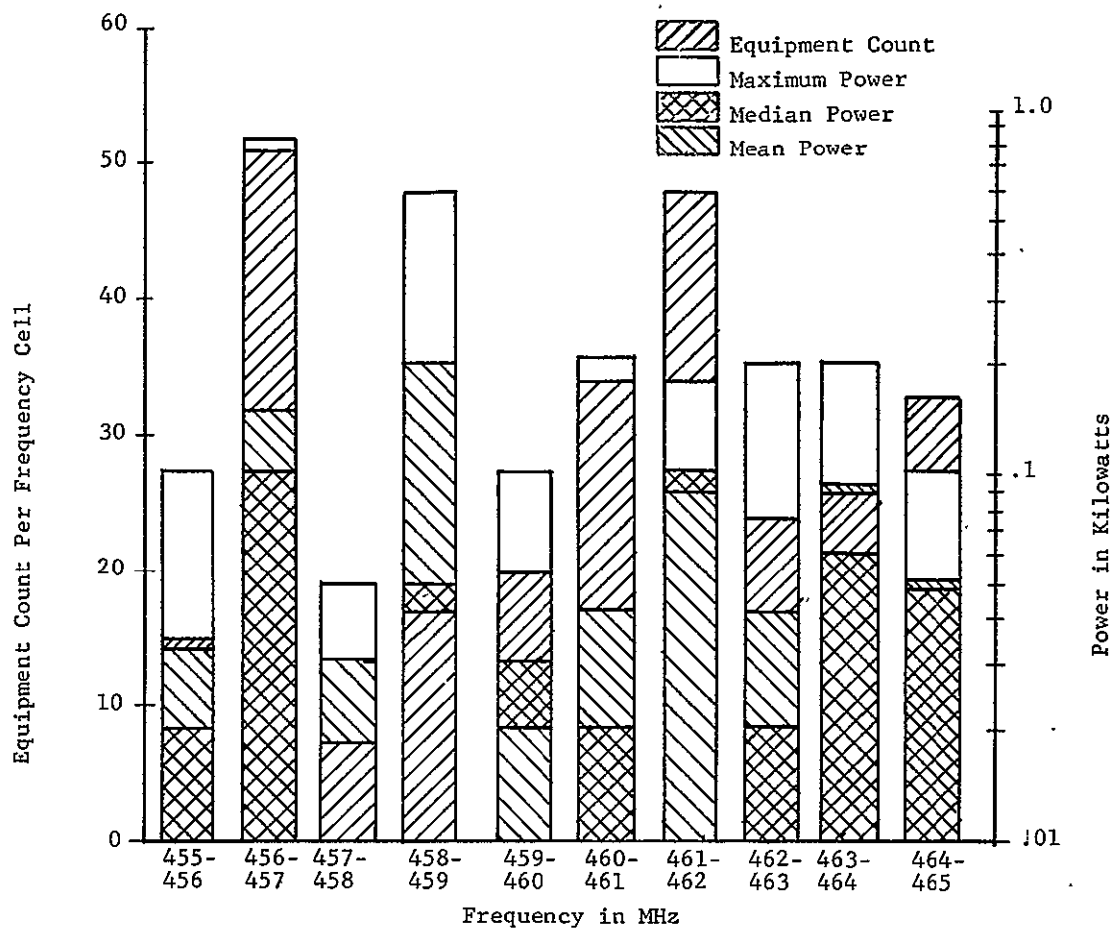


FIGURE 4.6-2

EXPERIMENT NO. 26 PRE-CULL SPECTRUM OCCUPANCY AND  
EFFECTIVE RADIATED POWER SUMMARY

### 4.6.3 Interference Evaluation and Analysis

The analysis technique of Section 3.4 was applied to each of the 695 emitters and 30 remained as potential sources of interference after this culling process (Table 4.6-2). Applying the orbit considerations of Section 3.5 of this report, the noise threshold interference regions were obtained as plotted in Figure 4.6-3. The solid lines show the regions for which the DACOL receiver could experience interference at levels above the noise threshold during satellite fly-over. However, the desired signal level is expected to be 17dB above the noise threshold of the DACOL receiver at the satellite. Using a margin of 3dB for desired signal above interference, the regions in which the S/I could be less than 3dB during a satellite pass were calculated. The 3dB margin selected for the S/I means that for a desired signal of 17dB above threshold, only those emitters capable of producing an interference level  $\geq 14$ dB above noise threshold (at 690 nautical miles) should be considered as a serious threat. Of the 30 emitters remaining after the analysis cull only 12 can cause the S/I to be 3dB or less. The regions over which the satellite could pass and experience this level of interference are shown by the dotted lines in Figure 4.6-3. The primary sources of potential interference are five 90 watt stations at 459.95 MHz located in Georgia, Penna., N. Y., N. J. and Virginia. These stations can produce a signal 6dB above the desired signal in the DACOL receiver. Therefore a reduction of at least 9dB in the interference level is desirable. An additional 12dB of isolation could be achieved for the five U.S. stations above by selecting a frequency 100 KHz above 459.95, at 460.05 MHz. However, such a frequency change is not recommended since the probability is high that a similar problem would be encountered at any selected frequency in the crowded land mobile band between 450 and 470 MHz.

Considering the intermittent type of emissions normally encountered in this band and more importantly the fact that FSK modulation will be utilized for the data collection, the possibility of interference is greatly reduced. For example, FSK being interfered with by an AM voice signal (6 KHz) can operate at an S/I = -12dB with only a bit error probability of 1%. Similarly, FSK against FM voice (12 KHz) can maintain a 1% error rate at an S/I = -6dB.<sup>1</sup> Obviously, the choice of FSK modulation is an excellent one for operation in the environment at 460 MHz.

---

<sup>1</sup>JTAC Report, "Spectrum Engineering - The Key to Progress", EMC Analysis Techniques, Supplement 8, Table 6, On-Tune Performance Threshold.

TABLE 4.6-2  
ENVIRONMENTAL SIGNAL LEVEL SUMMARY FOR DADOL EXPERIMENT

ASSIGNED FREQUENCY MHz	STATE/ COUNTRY	STATION CLASS	CLASS OF EMISSION	EFFECTIVE RADIATED POWER, kW	dB ABOVE NOISE THRESHOLD
459.9	Alaska/USA	Fixed Station	60F9	.02	5
459.9	USA	Aircraft Station	3JF3	.02	5
459.95	USA	Aircraft Station	36F3	.02	17
460.0	USA	Aircraft Station	HSA9	.2	10
460.0	Australia	Aeronautical Fixed Station Station Open To Official Corres- pondence Exclu- sively	550F3	.005	6
460.01	New Zealand	Fixed Station Station Open Ex- clusively To Cor- respondence of A Private Agency	36F3 6A3	.005	6
460.1	India	Base Station Land Mobile Station Station Open To Official Corres- pondence Exclu- sively	36F3	.01	2
459.95	USA Georgia Penn New York New Jersey Virginia	Fixed Station Base Station Land Mobile Station Station Open Exclusively To Operationally Traffic of The Service Con- cerned	36F3	.03	23
460.0	Canada	Fixed Station Station Open To Public Cor- respondence	54F9	.01	14
460.0	Cuba	Fixed Station Station Open Ex- clusively To Cor- respondence of A Private Agency Station Open To Official Corres- pondence Exclu- sively	40F3	.05	21
460.15	Argentina	Land Mobile Station Station Open Ex- clusively To Cor- respondence of A Private Agency	20F3	.1	6
460.0	Algeria	Fixed Station Station Open To Official Corres- pondence Exclu- sively	1000F9	.05	11
460.0	Spain	Fixed Station Station Open To Public Corres- pondence	6000P3F	.08	5
460.0	France	Fixed Station Station Open To Official Corres- pondence Exclu- sively	1000F9	.05	11
460.0	Norway	Fixed Station Station Open Ex- clusively To Cor- respondence of A Private Agency	36F3	.015	16
460.0	Yugoslavia	Fixed Station Station Open To Public Corres- pondence	3600F3	.025	2
460.0	Yugoslavia	Fixed Station Station Open To Public Corres- pondence	3600F3	.025	2
460.0	Yugoslavia	Fixed Station Station Open To Public Corres- pondence	3600F3	.025	2
460.0	Yugoslavia	Fixed Station Station Open To Public Corres- pondence	3600F3	.025	2
460.0	Yugoslavia	Fixed Station Station Open Public Corres- pondence	36F3	.025	18
460.05	Denmark	Land Mobile Station Station Open To Exclusively To Correspondence of A Private Agency	6A3 36F3	.05	21
460.05	Norway	Fixed Station Station Open Ex- clusively To Cor- respondence of A Private Agency	36F3	.02	17
460.05	Switzerland	Base Station Station Open To Public Corres- pondence	40F3	.02	17
460.1	Norway	Fixed Station Station Open Ex- clusively To Cor- respondence of A Private Agency	36F3	.02	5
460.1	Portugal	Fixed Station Station Open Ex- clusively To Cor- respondence of A Private Agency	110F3	.1	12
460.1	Switzerland	Base Station Station Open To Public Corres- pondence	40F3	.02	5

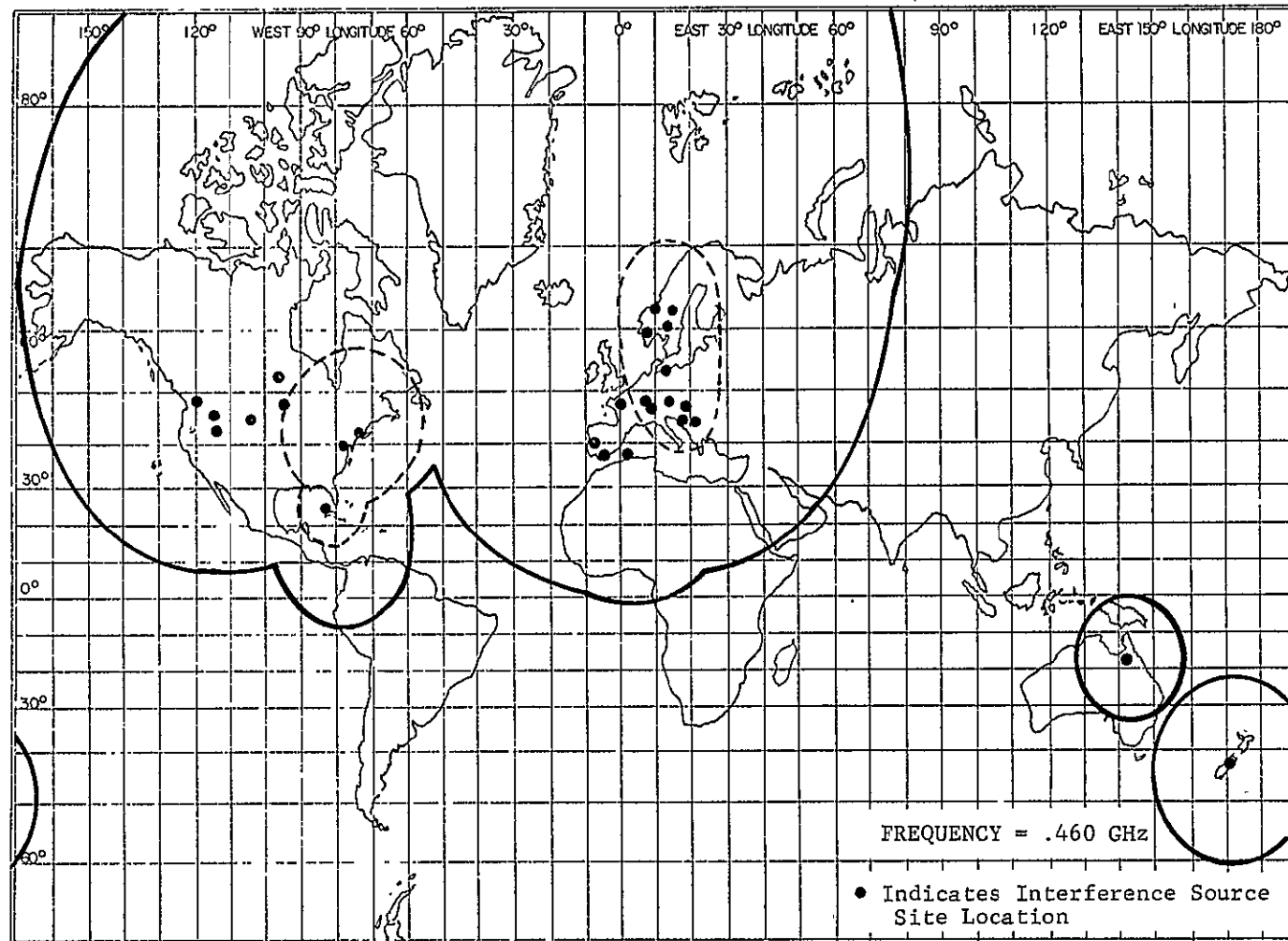


FIGURE 4.6-3  
PLOT OF INTERFERENCE REGION FOR SIMPLIFIED DATA COLLECTION (DACOL) EXPERIMENT

It is concluded that a minimum of degrading interference will be encountered for the DACOL experiment.

The maximum single orbit time in the solid line noise threshold regions on the map of Figure 4.6-3 is 32 minutes versus 11.6 minutes for the dotted line regions of  $S/I \leq 3\text{dB}$ . The maximum percent of time the Nimbus would be over the noise threshold regions (solid lines) in a 24 hour period is 26% and for the smaller  $S/I \leq 3\text{dB}$  regions (dotted) is 2.85%.

## 4.7 Nimbus-E Data Relay Links Through ATS-F (DARELI)

### 4.7.1 Purpose and Scientific Basis

This experiment is designed to establish a real-time relay link between Nimbus-E and a data acquisition facility in the U. S. through the ATS-F synchronous satellite. The purpose of this experiment is, 1) to define and resolve the technological problems imposed by a Data Relay Link on the Nimbus spacecraft as well as on the ATS satellite, and 2) to demonstrate the technological utility of a command link and of two-way data transmission at S-band over approximately 70% of the Nimbus orbit.

The essential elements of the proposed experiment are shown in Figure 4.7-1, as, 1) and ATS Data Acquisition Facility (DAF), 2) the ATS-F synchronous satellite operating as a repeater/relay, and 3) the Nimbus-E earth orbiting satellite. An additional aspect is that the repeater placed on board Nimbus will permit data acquisition and range and range-rate measurements directly by any STADAN station equipped with the Goddard range and range-rate (GRARR) system which is in radio view of Nimbus. Three separate functions can be performed over the DAF-ATS Nimbus links. These are: 1) real-time transmission of data originating at Nimbus over an S-band link to the ATS and hence relayed to the DAF over another S-band link; 2) simultaneous or independent range and range-rate (R and R) tracking of Nimbus by the DAF through the ATS to Nimbus S-band link and returning to the DAF by sharing the data link and; 3) real-time Nimbus command over a VHF link through the ATS.

Figure 4.7-2 is a system block diagram showing nominal link parameters between ground stations, the ATS-F relay satellite and the Nimbus-E target satellite. Figure 4.7-3 shows the spectrum for the critical 2253 MHz link from Nimbus to ATS. The range and range rate sidebands at  $\pm 3.2$  MHz and  $\pm 2.4$  MHz are also shown in this figure. The system characteristics are given in Tables 4.7-1 through 4.7-4.

The various links and frequencies involved in the Data Relay Experiment will be referred to as follows to avoid confusion in the environment and analysis discussions.

- 28-1 ATS to Nimbus Link at 1.8 GHz
- 28-2 ATS to Nimbus Link at 149 MHz
- 28-3 ATS to Earth at 1.8 GHz
- 28-4 Nimbus to ATS at 2253 MHz (Data)
- 28-5 Nimbus to ATS at 2253 MHz (Sidebands)



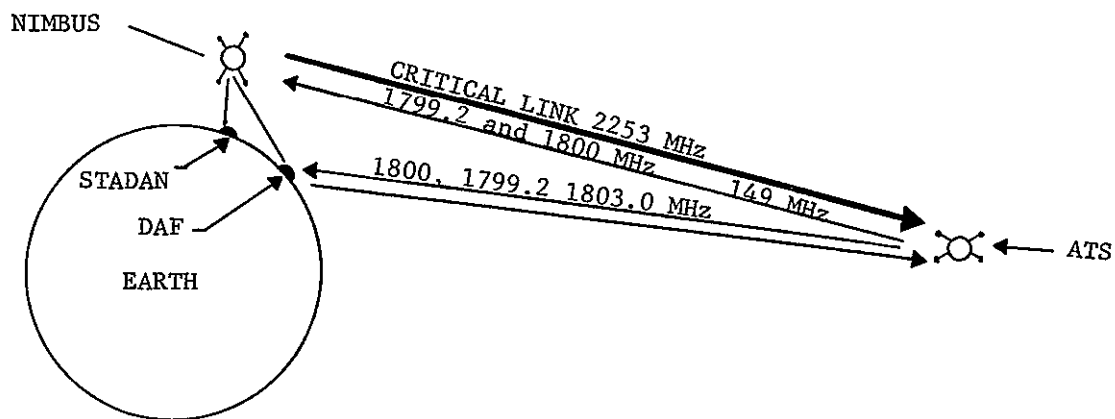


FIGURE 4.7-1

NIMBUS DATA RELAY LINK THROUGH ATS

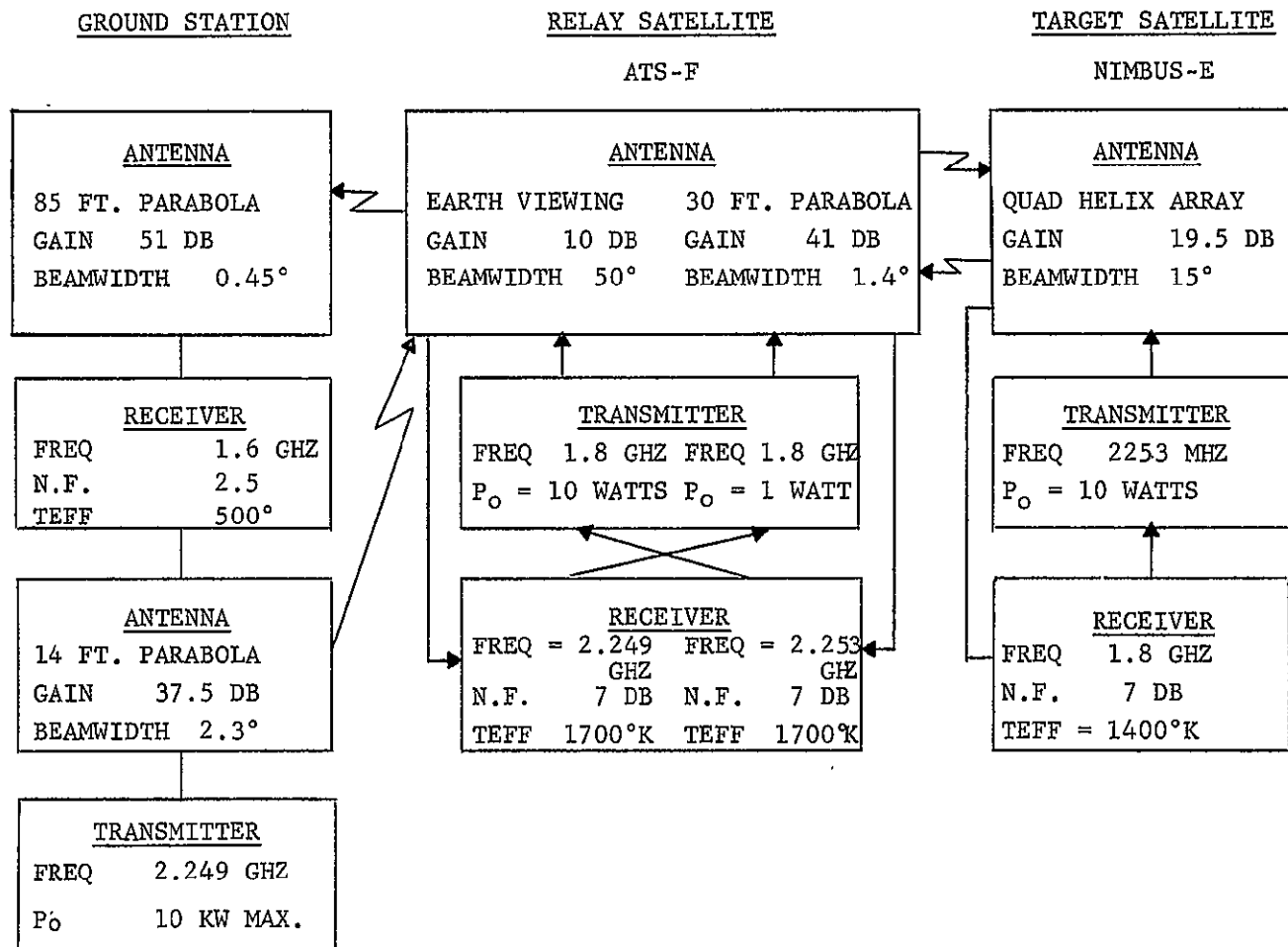


FIGURE 4.7-2

RELAY SATELLITE SYSTEM BLOCK DIAGRAM

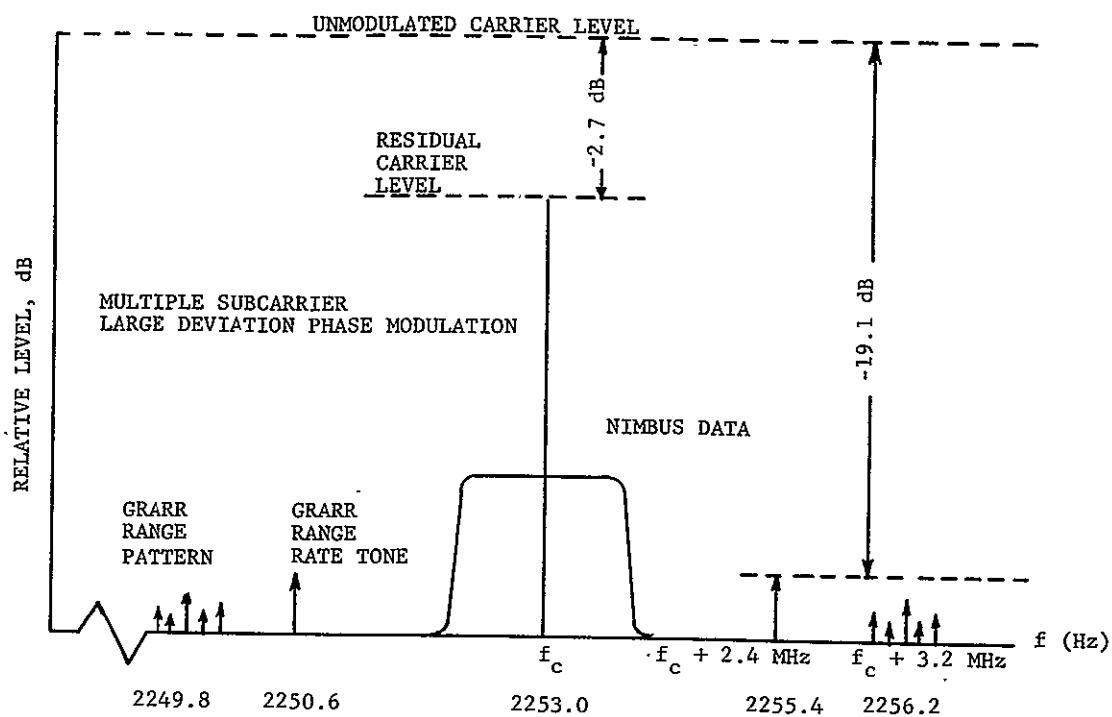


FIGURE 4.7-3  
SIGNAL SPECTRUM FOR NIMBUS-ATS LINK

TABLE 4.7-1

EXPERIMENT 28-1, DARELI, ATS TO NIMBUS LINK AT 1-8 GHz

TRANSMITTER		RECEIVER	
FREQUENCY	1799.2 MHz 1800.0 MHz	FREQUENCY	1799.2 MHz 1800.0 MHz
BANDWIDTH	.1 MHz	BANDWIDTH	RF 2 MHz IF .1 MHz
MODULATION	cw	SENSITIVITY	-117.1 dBm
POWER	1 Watt each	NOISE FIGURE	6.8 dB
ANTENNA GAIN	39 dB	LOCATION	Nimbus
LOCATION	ATS	ANTENNA GAIN	19.5 dB

TABLE 4.7-2

EXPERIMENT 28-2, DARELI, ATS TO NIMBUS LINK AT 149 MHz

TRANSMITTER		RECEIVER	
FREQUENCY	149.0 MHz	FREQUENCY	149.0 MHz
BANDWIDTH	50 KHz	BANDWIDTH	RF
MODULATION	AM		IF 500 Hz
POWER	16 dBW	SENSITIVITY	138.1 dBm
LOCATION	ATS	NOISE FIGURE	8.5 dB
ANTENNA GAIN	20 dB	LOCATION	Nimbus
		ANTENNA GAIN	0 dB

TABLE 4.7-3

EXPERIMENT 28-3, DARELI, ATS TO EARTH AT 1.8 GHz

TRANSMITTER		RECEIVER	
FREQUENCY	1800.0 MHz 1799.2 MHz 1803.0 MHz	FREQUENCY	1799-1803 MHz
BANDWIDTH	50 KHz each	BANDWIDTH	RF 4 MHz IF 50 KHz
MODULATION	cw	SENSITIVITY	-119 dBm
POWER	3.3 Watts each	NOISE FIGURE	8 dB
LOCATION	ATS	LOCATION	Earth
ANTENNA GAIN	18 dB	ANTENNA GAIN	51 dB

TABLE 4.7-4

EXPERIMENT NO. 28-4 and 28-5; DARELI, NIMBUS TO ATS AT 2253 MH

TRANSMITTER		RECEIVER	
FREQUENCY	2253.0 MHz	FREQUENCY	2253 MHz
BANDWIDTH	7 MHz	BANDWIDTH	RF 10 MHz
MODULATION	cw	Data	IF 2 MHz
POWER	10 Watts	Sideband	IF .8 MHz
LOCATION	Nimbus	SENSITIVITY	Data -103 dBm
ANTENNA GAIN	19.5 dB		Sideband -107 dBm
		LOCATION	ATS
		ANTENNA GAIN	41 dB
		NOISE FIGURE	Data 8 dB
			Sideband 8 dB

#### 4.7.2 Environmental Signal Level Summary

Link 28-1, ATS to Nimbus at 1.8 GHz. The 209 emitters found in the frequency range of 1794 to 1810 MHz are shown in Figure 4.7-4.

Link 28-2, ATS to Nimbus at 149 MHz. The 1484 emitters found in the frequency range of 148.5 to 149.5 MHz are shown in Figure 4.7-5.

Link 28-3, ATS to Earth at 1.8 GHz. The 209 emitters shown in Figure 4.7-4 (also applicable to 28-1) were evaluated against the earth receiver.

Link 28-4 and 28-5, Nimbus to ATS at 2253 MHz. The 133 emitters found between 2248 and 2258 MHz are shown in Figure 4.7-6.

#### 4.7.3 Interference Evaluation and Analysis

Link 28-1, ATS to Nimbus at 1.8 GHz. The interference threshold evaluation procedure of Section 3.4 was applied to the environment of 209 known emitters and only 1 emitter survived this cull as being a source capable of creating an interference signal above the noise threshold of the Nimbus 1.8 GHz receiver. This potential interference source is located in the state of Colorado with a power of 100 KW at a frequency of 1800.00 MHz. The emission bandwidth is 5 MHz and the modulation is F9. This transmitter could create a signal 21dB above noise threshold at the Nimbus receiver for a direct flyover, dropping to 0dB above noise threshold for an orbit approximately 37° away from the emitter location at 105° W longitude and 40° N longitude. The desired signal from ATS to Nimbus will be about 19dB above noise threshold and the Nimbus 19.5dB antenna will be oriented towards the ATS 39dB gain transmitting antenna. Considering that the worst case S/I is 19-21 or -2dB for direct flyover of Colorado and further that the Nimbus high gain receiving antenna is pointed away from the earth towards the ATS at synchronous altitude the probability of desired signal degradation is minimal.

The analysis technique of Section 3.5 resulted in the plot of the interference region shown on the map of Figure 4.7-7. The area within the oval shape is the region for which a threshold or higher interference level will exist for a Nimbus orbit. The maximum exposure time for one orbit is 19.8 minutes and the maximum percent of

IIT RESEARCH INSTITUTE



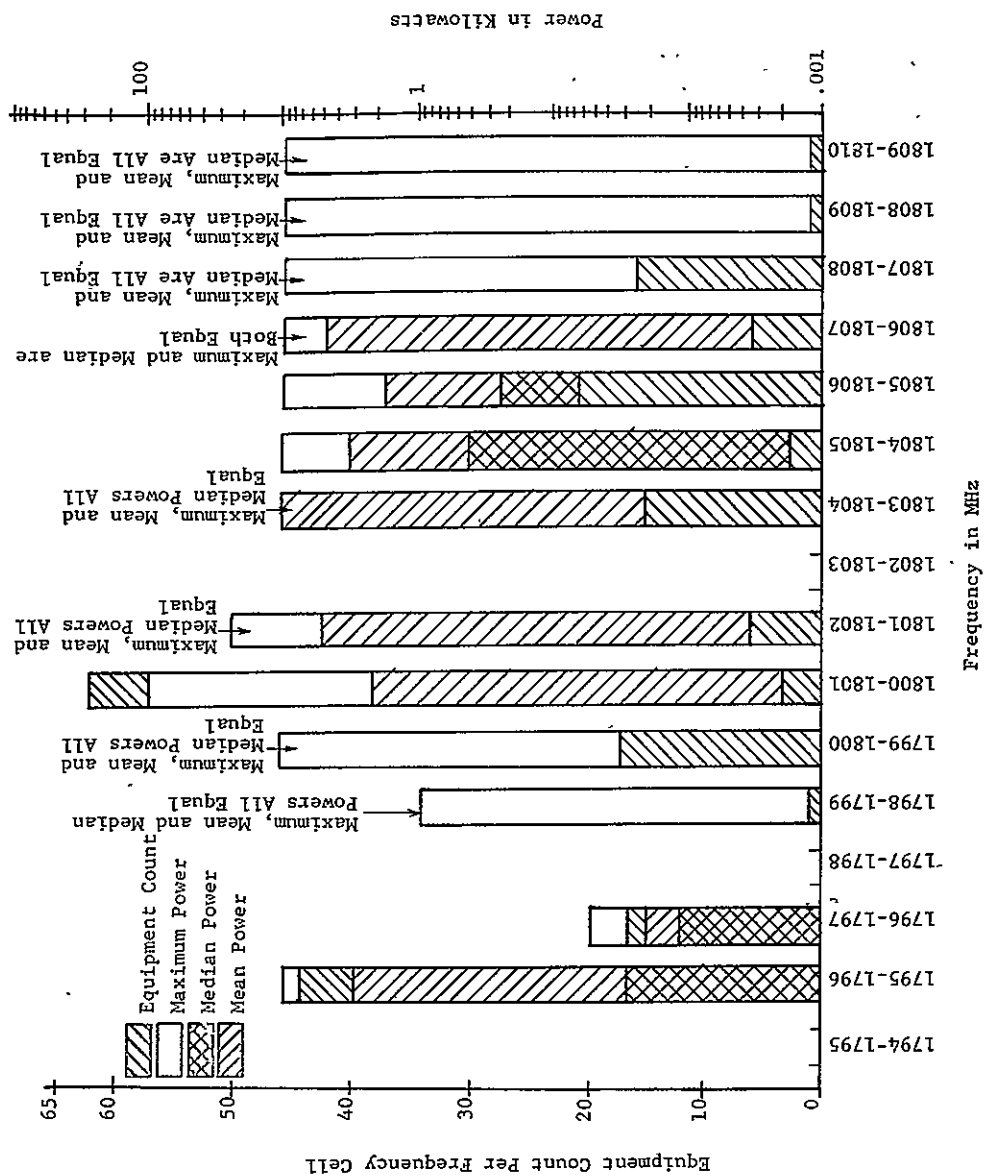


FIGURE 4.7-4  
EXPERIMENT NO. 28-1 and 28-3 PRE-CULL SPECTRUM OCCUPANCY AND EFFECTIVE  
RADIATED POWER SUMMARY

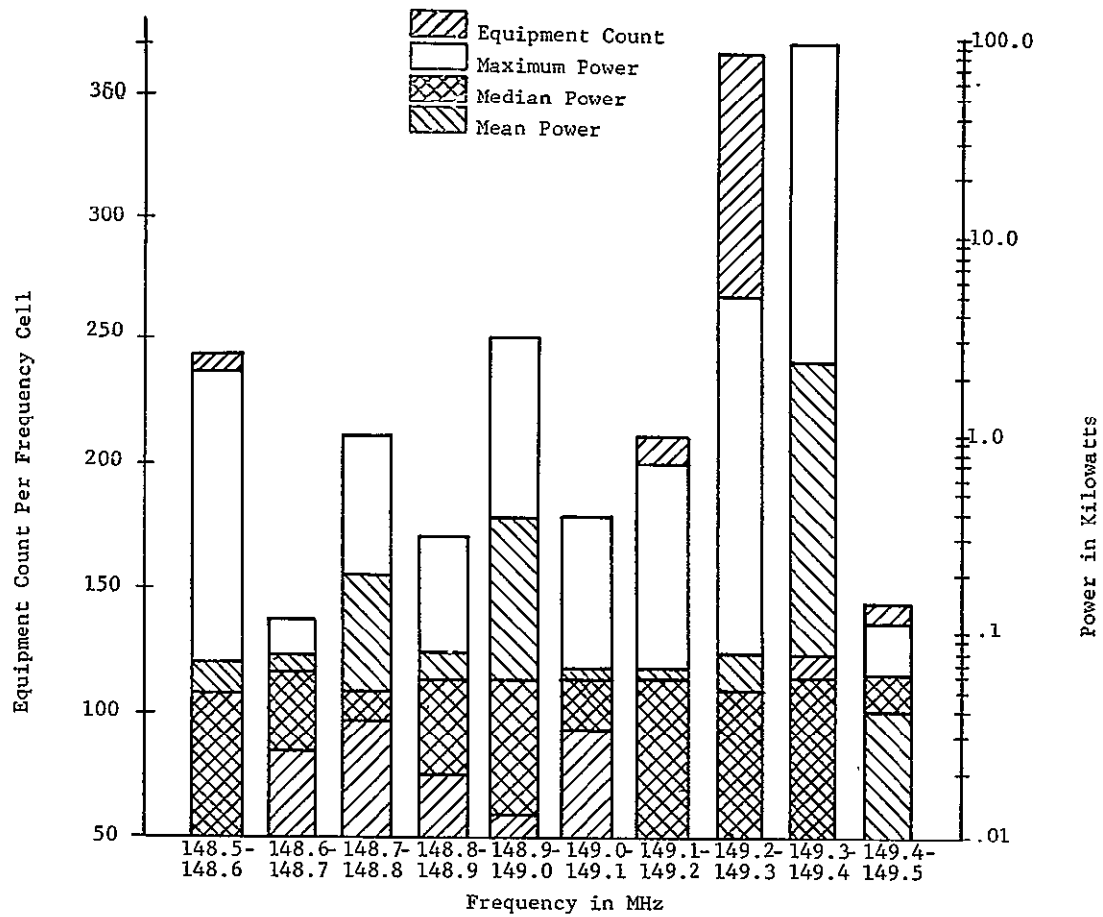


FIGURE 4.7-5

EXPERIMENT NO. 28-2 PRE-CULL SPECTRUM OCCUPANCY AND EFFECTIVE  
RADIATED POWER SUMMARY

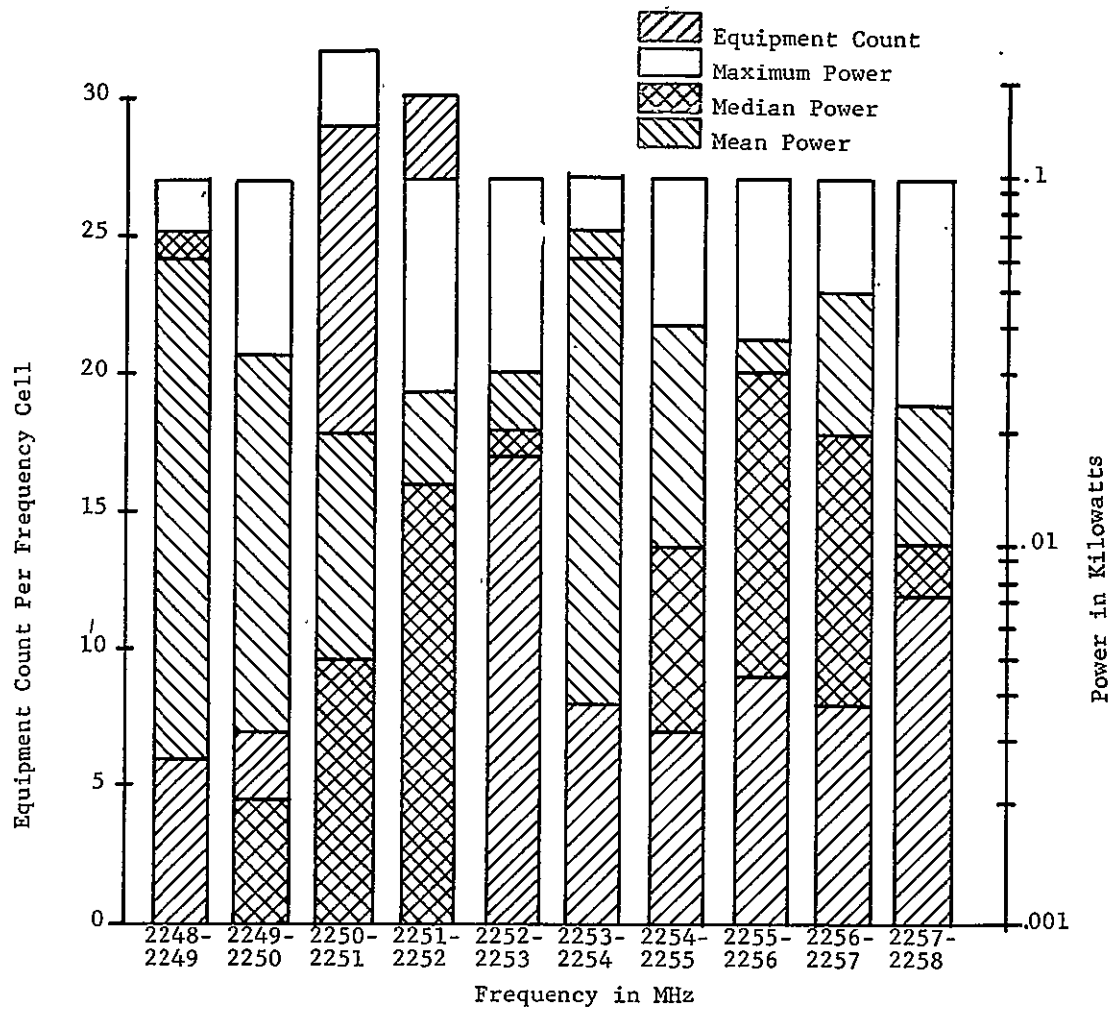


FIGURE 4.7-6

EXPERIMENT NO. 28-4 and 28-5 PRE-CULL SPECTRUM OCCUPANCY AND EFFECTIVE  
RADIATED POWER SUMMARY

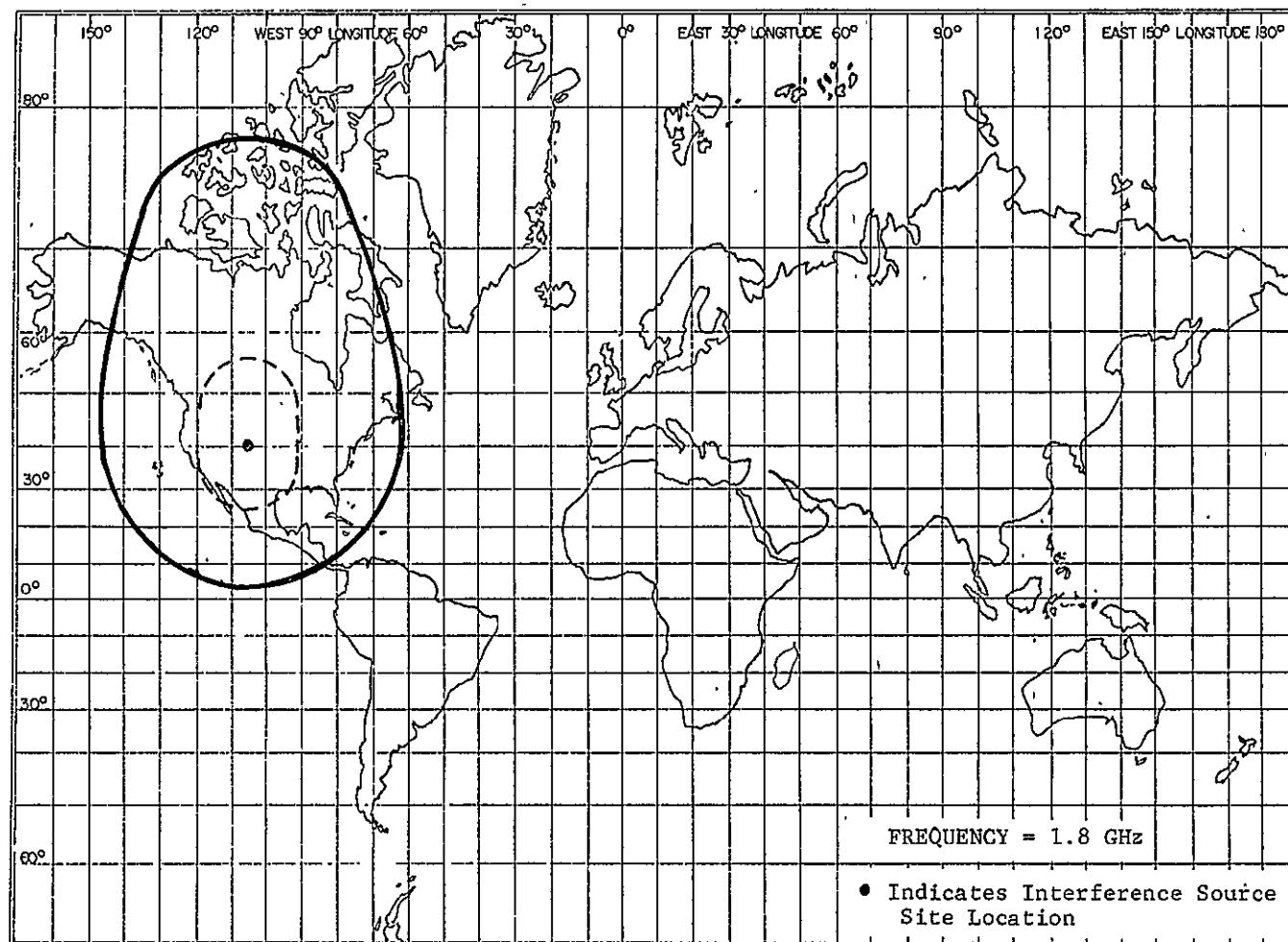


FIGURE 4.7-7

EXPERIMENT 28-1 PLOT OF INTERFERENCE REGION FOR NIMBUS-E DATA RELAY LINK THROUGH ATS-F (DARELI)

time that interference is above noise threshold for a 24 hour period is 7.1%. The area enclosed by the dotted line on the map of Figure 4.7-7 shows the fly over region where the interference level ranges from 3dB below the desired signal to 2dB above the desired signal. The region between the outer solid line and the inner dotted line represents the range for  $S/I = 19\text{dB}$  to  $S/I = 3\text{dB}$ . Due to the fact that phase-lock loop receivers will be used for this link, it is expected that an  $S/I = 3\text{dB}$  would ensure that lock would be maintained on the desired signal, which would be anywhere outside of the dotted line. It is concluded that the 1.8 GHz link from ATS to Nimbus will operate successfully in the given environment based on the IRAC and ITU files.

Link 28-2, ATS to Nimbus at 149 MHz. The interference threshold evaluation procedure of Section 3.4 was applied to the environment of 1484 known emitters and only 7 emitters remained as potential sources of interference. However, these 7 emitters are on the exact frequency, 149.0 MHz. The desired link calculation indicates that the transmission from ATS will be 37dB above noise threshold at the Nimbus receiver. None of the 7 emitters will produce a level greater than that of 37dB for the desired signal. Five of the emitters produce a level which is 7 or more dB below the desired signal. The 2 remaining emitters produce interference at the same level as the desired signal. These emitters are a 250 watt station in Thailand and a 400 watt station in Mexico, both with 36 KHz emission of F3 modulation. The command link is an important one and the degradation criteria extracted from the on-tune performance threshold table<sup>1</sup> for F3 interference versus A1 desired signal for a 1% probability of error is  $S/I = 7\text{dB}$ .

The analysis technique of section 3.5 resulted in the plot of interference region shown on the map of Figure 4.7-8. The maximum exposure time to noise threshold or higher level interference for one orbit of Nimbus is 47.5 minutes and the maximum percent of time that interference is above noise threshold for a 24 hour period is 26.5%. The dotted regions plotted on the map of Figure 4.7-8 represent the flyover area for which the interference would be equal to or less than the desired signal. The interference would be equal to the signal only directly over the emitters in India and Mexico and the interference would decrease to 7dB below the desired signal at the outer edge of the area denoted by the dotted lines. The

---

<sup>1</sup> JTAC Report, "Spectrum Engineering - The Key to Progress", EMC Analysis Techniques, Supplement 8, Table 6, On-Tune Performance Threshold.

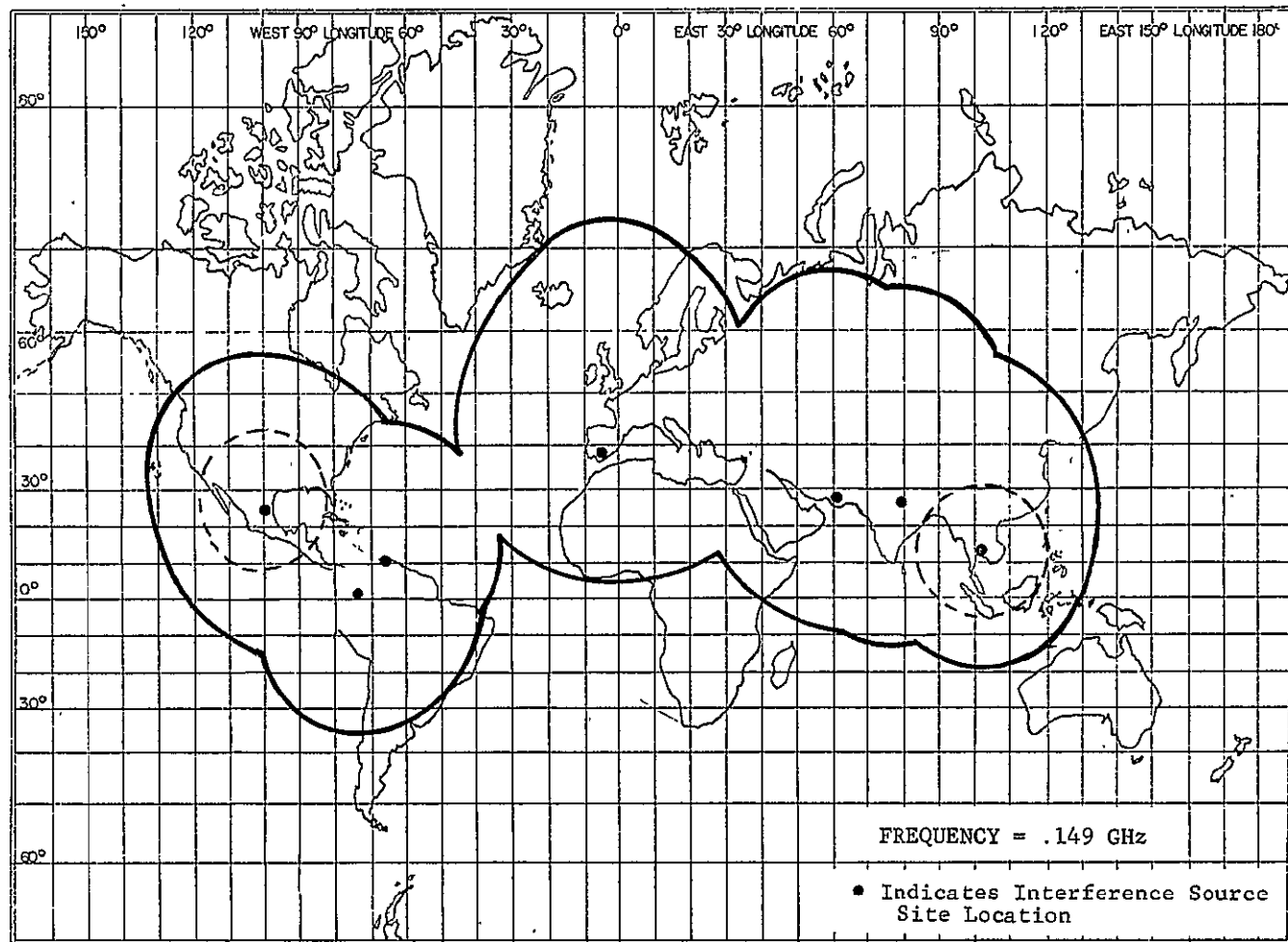


FIGURE 4.7-8  
EXPERIMENT 28-2 PLOT OF INTERFERENCE REGION FOR NIMBUS-E DATA RELAY LINK THROUGH ATS-F (DARELI)

maximum time Nimbus would be over these areas for one orbit is 20 minutes and the maximum percent of time in a 24 hour period would be 8.0%.

Link 28-3, ATS to Earth at 1.8 GHz. The interference threshold evaluation procedure of Section 3.4 was applied to the same 1.8 GHz environment of experiment 28-1, the difference being that the minimum distance is no longer orbital height, but the distance between an earth emitter and an earth receiver at 1.8 GHz. Of the 209 potential sources of interference only 37 are capable of causing an above noise threshold signal at a distance of six miles or less. Beyond six miles only the 100 KW station in Colorado discussed in experiment 28-1 can cause interference, and then only to a distance slightly beyond the radio line of sight (RLOS). The RLOS for a transmitting antenna at a height of 20 feet and a receiving antenna at the same height is 12.6 miles at which distance the interference is still 57dB above the 1.8 GHz receiver noise threshold. At a distance of 52 miles from the emitter the interference level is diminished to the receiver noise level due to the additional diffraction region propagation loss.

Siting in an interference free location for the 1.8 GHz receiver on the earth will pose no problem based on the analysis of the 209 potential interferers found in the environment.

Link 28-4 and 28-5, Nimbus to ATS at 2253 MHz. The interference threshold evaluation procedure of Section 3.4 was applied to each of the 133 emitters found between 2248 and 2258 MHz and all of these sources were eliminated as potential interferers.

Although all of the known emitters have been eliminated by analysis as potential interferers, it is possible that some other emitters may exist and the following comments are provided to show that a high probability of interference free operation exists in any event. The 41dB gain antenna at the ATS receiver has a half power beamwidth of  $1.5^\circ$  which is 572 miles across at a distance of 23,000 miles. When this beam is centered on Nimbus at an altitude of 690 miles, it does not intercept the earth for about one half of the Nimbus orbits in any 24 hour period. When the ATS orbit is at right angles to the Nimbus orbit, the ATS antenna will not see the earth, but when the ATS is located in the plane of the Nimbus orbit it will have to orient its antenna towards the earth to follow Nimbus in orbit. For that portion of time during which the ATS receiving antenna beam does not intercept the earth the probability of receiving interference is extremely slight. The use of 2253 MHz for the Nimbus to ATS link is predicted to be interference free with a high probability.

IIT RESEARCH INSTITUTE

## 4.8 Wide-Band Real-Time Data Transmission (DATRAN)

### 4.8.1 Purpose and Scientific Basis

This experiment is designed to implement both a wide-band and narrow-band data readout to small, (even portable) ground stations. An increase in transmission system bandwidths is necessary to accomodate new, wide-band sensors.

Spectrum is available at S-band and higher frequencies but the cost of S-band ground stations can be high, especially as local readout becomes necessary. This experiment consists of a solid state, S-band self-focusing phased array on the spacecraft to increase the effective radiated power, thus reducing the size of ground antennas. The proposed phased array is a self-focusing, phase conjugating retro-directive antenna which will automatically point its beam in the direction of a distant ground station which is radiating a CW pilot of the correct frequency.

The ground station antenna would be approximately 10 to 15 feet in diameter. The ground beacon transmitter power would be approximately 100 watts. A wide-band receiver demodulator, and a wide-band processor would be used to provide hard copy readout. Narrow-band data would be processed through the existing demods to be used on Nimbus-B and D. Operation of this ground station with the satellite phased array will prove out the feasibility of the overall problems, and provide a firm basis for the design and production of low cost, portable terminals for operational use in both meteorology and the earth sciences.

In looking ahead to the use of wide-band sensors on future earth-orbit spacecraft, a new problem in data transmission is foreseen. Given base-bandwidths of the order of 4 MHz, the RF bandwidth becomes about 20 MHz, placing the carrier at S-band in the vicinity of 2200 MHz. Consideration would have to be given to a new S-band transmitter, since present Nimbus transmitters are in the 1700 MHz band. Counting the two currently on-board, the total would come to three (or four if a back-up is desired).

A second aspect of the S-band transmission problem is that local users may wish to receive wide-band information in real-time if they could implement ground stations at a cost within their reach. In this respect, wide-band data transmission might enjoy some of the same national and world-wide participation as APT.



A third aspect is the need to back-up on-board data storage and provide real-time readout for low-data-rate as well as wide-band information.

These three factors, the anticipation of wider bandwidth systems, the advantage of unifying S-band transmission functions, and broadening the user market for data, have suggested a new look at the S-band transmission problem.

The use of a satellite retro-directive antenna array leads to an S-band transmission philosophy with significant advantages in all of the above areas. The most immediate advantage is seen in affording local users real-time access to wide-band data. This is because a phased array, with higher effective radiated power, leads to smaller-antenna and lower-cost ground stations.

But a phased-array, being a highly redundant set of low-power transponders, is inherently very reliable and degrades gracefully. A catastrophic failure in one of its elements diminishes power only slightly, in contrast to a bulk-power conventional transmitter. This fact suggests the wisdom of combining several S-band transmission functions into one (at most, two) transmitters to serve all spacecraft S-band transmission needs.

In one mode, a pilot tone from the user ground station steers the phased array antenna beam in the direction of the station. The transmit and receive frequencies are close but not identical. In the other mode two ground stations at different locations in the field of view send pilot tones at different frequencies to the satellite. Upon reception and processing of such signals, the satellite phased array antenna transmits to both ground stations by means of two different beams but at the same frequency in order to conserve spectrum. The transmit frequency is also different from the pilot frequencies. In either mode of operation, the spacecraft receiver is pre-programmed to turn on whenever suitable and when a ground station is available for read-out. The transmitter is turned on either by the same command that turns the receiver on or by means of a threshold detector that senses the presence of a signal in the receiver. The transponder is programmed to turn off after read-out is accomplished. Figure 4.8-1 shows the system arrangement of the self-focusing Nimbus antenna and a local ground station. Table 4.8-1 shows the system characteristics.

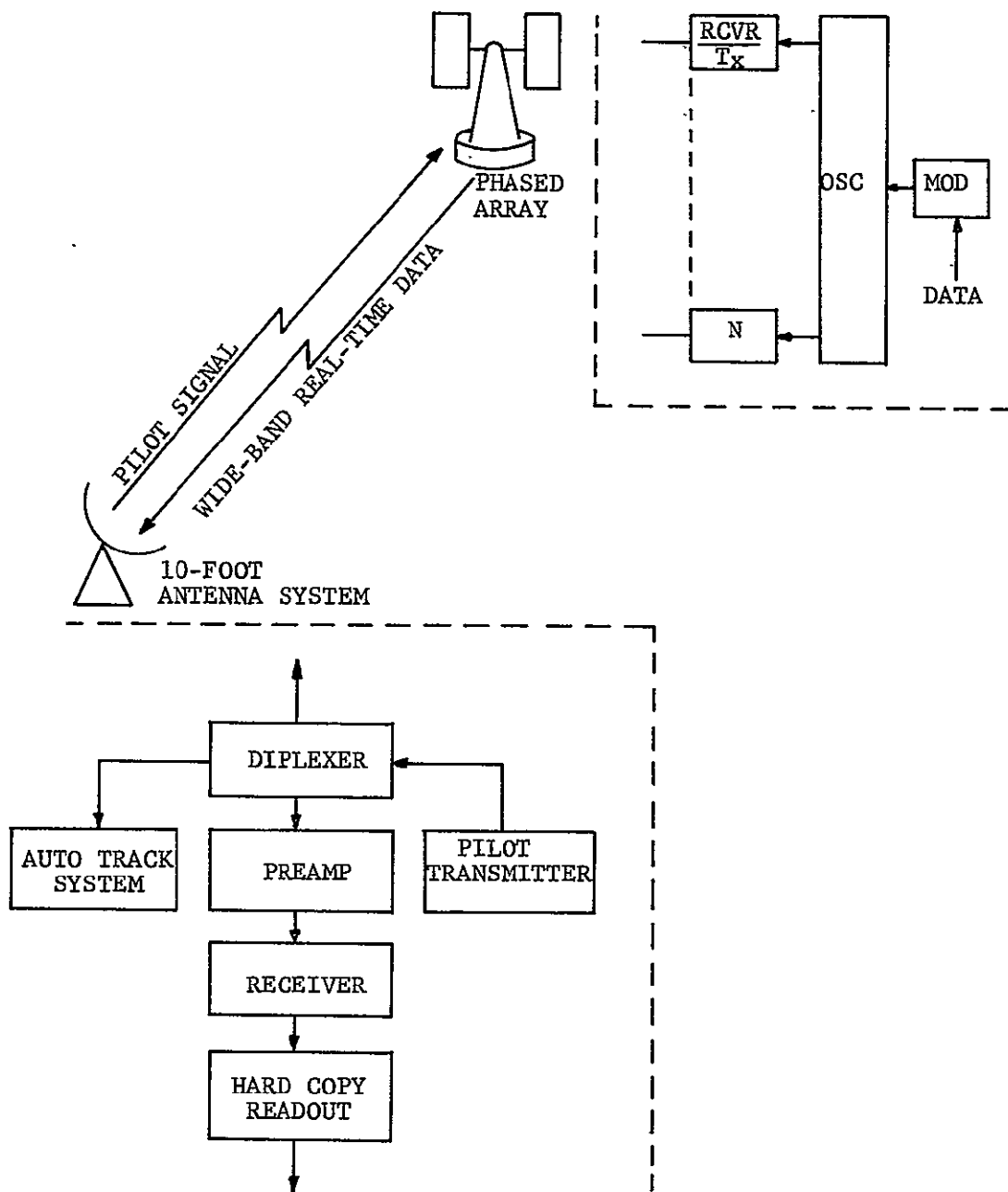


FIGURE 4.8-1

SELF-FOCUSSING NIMBUS ANTENNA AND LOCAL GROUND STATION

TABLE 4.8-1

EXPERIMENT NO. 29 WIDE-BAND REAL-TIME DATA TRANSMISSION CHARACTERISTICS

RECEIVER		ANTENNA	
FREQUENCY	2199.5 to 2200.5 MHz	TYPE	Phased Array
BANDWIDTH	RF IF 1 MHz	GAIN	15dB
SENSITIVITY	-104dBm	BEAMWIDTH	30°
NOISE FIGURE	10dB		

#### 4.8.2 Environmental Signal Level Summary

The environment determined from the ITU and IRAC frequency lists for the range 2100 to 2310 MHz is shown in Figure 4.8-2. A total of 953 emitters were found in that range with 168 between 2190 and 2210 MHz.

#### 4.8.3 Interference Evaluation and Analysis

The majority of the emitters in the environment were eliminated as potential interferers by use of the power cull and on tune rejection function technique explained in Section 3.4. The 67 remaining emitters were eliminated by use of the receiver selectivity model for Experiment 29, shown in Figure 3.4-1. Relatively narrow band emitters 10 MHz removed from 2200 MHz are 52dB down on the receiver selectivity skirts and most of the higher power emitters were more than 10 MHz away. It is concluded that reception of the relatively narrow band beacon signal from various ground stations prior to data transmission to earth will have a high probability of being accomplished without detrimental interference.

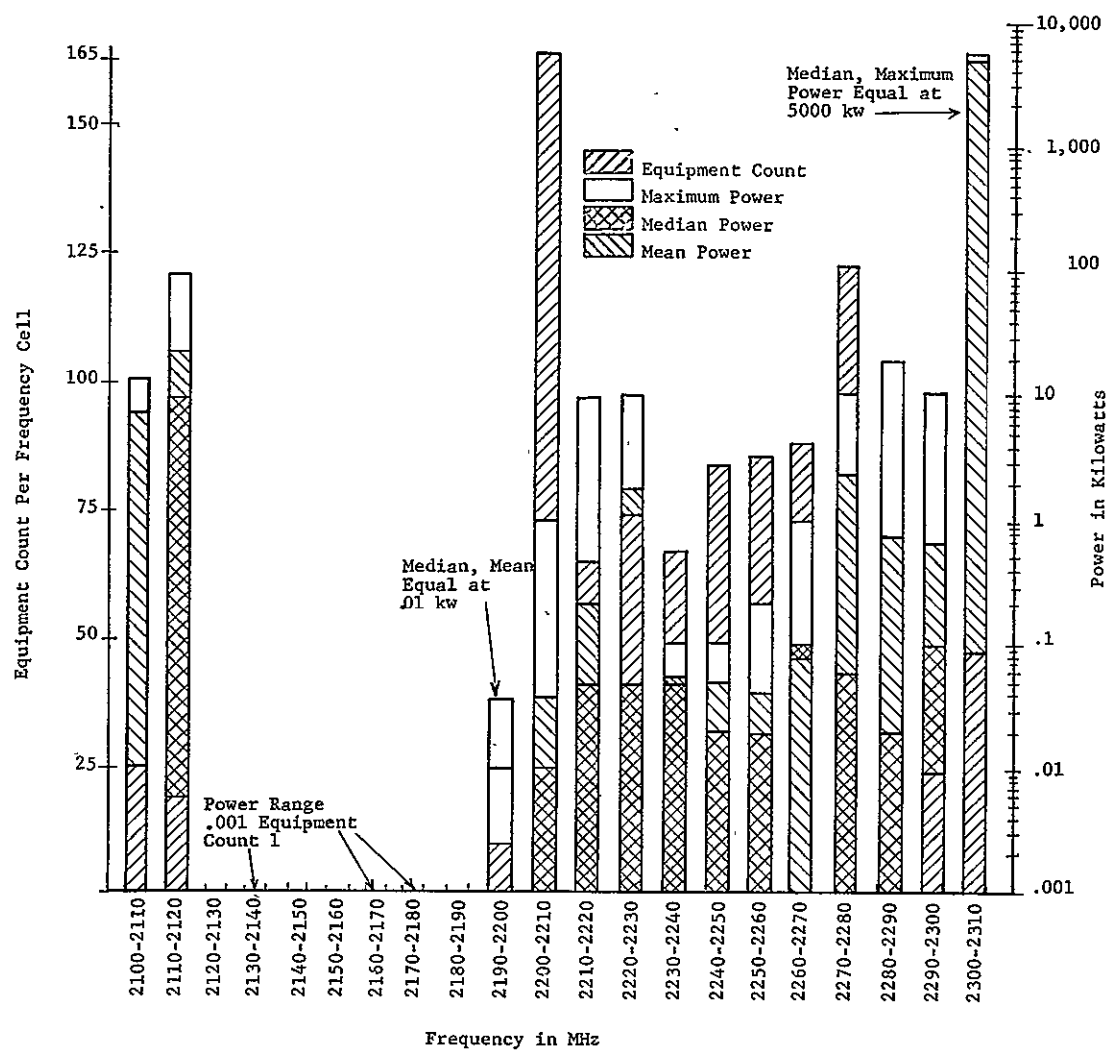


FIGURE 4.8-2  
EXPERIMENT NO. 26 PRE-CULL SPECTRUM OCCUPANCY AND  
EFFECTIVE RADIATED POWER SUMMARY